CHALMERS

Advanced Cooling of Electric Machine in a Hybrid Vehicle Application

Master of Science Thesis

Johan Fröb
Odyssefs Lykartsis

Department of Energy and Environment
Division of Electric Power Engineering
Chalmers University of Technology
Göteborg, Sweden 2014
Report No. 1

Advanced Cooling of Electric Machine in a Hybrid Vehicle Application
JOHAN FRÖB
ODYSSEFS LYKARTSIS
Department of Energy and Environment
Division of Electric Power Engineering
Chalmers University of Technology

The work is a collaboration with Johan Fröb, Sustainable Energy engineer student at Luleå University of Technology. Fröb has published the work at Luleå University. The work was carried out on behalf of the Volvo Group Truck Technology in the spring of 2014.

Göteborg, Sweden

Abstract

Transportation sector is consuming a large portion of the total energy used by the humans. Today, most of the commercial vehicles are driven by internal combustion engines. Replacing them with electrical machine could have a large impact in the environment. But there is still room for improvement in the electric machines in order to replace the internal combustion engines.

The electrical machines that are used in the automotive industry use permanent magnets in their rotors. They have a number of advantages such as very good efficiency and high power density. On the other hand, sensitivity of the magnets in high temperatures and their price is the major drawbacks of permanent magnet machines. The magnets cannot operate in high temperatures because they suffer from demagnetization. To deal with this problem, today, high temperature grade magnets with a lot of segments are used.

In this thesis an oil spraying technique is used to cool the magnets in a safe operating temperature, increase their performance and also reducing their manufacturing cost. The analysis is based on theoretical calculations and experimental results from a test rig that was designed and constructed within the thesis.

The oil-spraying cooling system, was designed to spray oil on the inside of the rotor of the electrical machine. Due to the high rotational speed the oil forms a thin film that absorbs the heat generated by the magnets. In the thesis a cylinder with an external heat source that simulated the actual rotor was used for evaluation.

The actual losses of the magnets in an electrical machine was calculated for different operation points and segmentation of the magnets. Then the temperature of the magnets was calculated, by developing a thermal model, with and without oil spraying. The results showed significant drop in the temperature of the magnets as well as reduction in the number of segments.

Acknowledgements

This work has been carried out at Volvo Group Trucks Technology in Chalmers Technical Park. A lot of people have contributed and supported during the duration of that project. More specifically we would like to thank:

- our *mothers*, *father* and *friends* for their encouragement
- our supervisors *Dan Hagstedt* and *Zhe Huang* for making this project possible and for their support and patience
- our examiners *Yujing Liu* and *Lars Westerlund*
- Volvo Group Trucks Technology, department of Advanced Technology & Research for allowing us to use their equipment and laboratories
- *Rickard Blanc*, *Jens Groot*, *Martin West*, *Pär Ingelström* from Volvo GTT for their help and patience

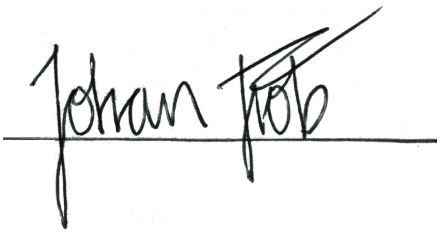

Johan Fröb
Göteborg, Sweden, 2014

Odyssefs Lykartsis
Göteborg, Sweden, 2014

Contents

List of Figures

List of Tables

List of Symbols

B_r Remanent Magnetic Flux Density. 12

B_{sat} Saturation Magnetic Flux Density. 12

H_c Coercive Field Strength. 12

H_{sat} Saturation Magnetic Field Intensity. 12

I_m Amplitude of phase current. 6

γ Form Factor of the Demagnetization Curve. 14

ω_{max} Maximum Magnetic Energy per unit of a magnet. 13

${}_iH_c$ Intrinsic Coercivity. 12

$(BH)_{max}$ Maximum energy density point on the demagnetization curve of the magnet. 13

A Area. 15, 18, 26, 32, 61

A_c Cross-section Area. 25, 62, 71

B Magnetic flux density. 10, 32, 71

B_i Inherit magnetization. 10, 12

D Diameter of the pipe. 45

D_h Hydraulic diameter. 20, 24–26

E Electric field intensity. 32, 93

E_r Radiative Power. 18

F_c Centripetal force. 23

F_g Geometrical factor. 37

F_{12} View factor from surface 1 to surface 2. 39

Fr Freude number. 24

H Magnetic field intensity. 10, 72

I Coil current. 72

K_L The sum of the coefficient of the minor losses h_L. 46

K_n Kinetic Coefficients. 94

L Depth of the fluid. 24

L Length of the pipe. 45

N Number of turns of the coil. 72

N_{ph} Series turns per phase. 6

P_w Wetted perimeter of the cross-section. 25

Pr Prandtl number. 19, 20, 25

Q Heating Energy. 61

Re Reynold's number. 19, 20

S Surface bounded by the closed loop C. 32

S Seebeck coefficient. 93, 94

$S - S_0$ Equivalent slope. 24

S_0 Slope of the surface. 24

S_{AB} Relative Seebeck coefficient. 94

T Respective temperature of the bodies. 39

T_s Surface temperature of the body. 18

Ta_m Taylor's number. 37

Ω_a Rotational speed in radians per second. 37

$\Omega_{a,cr}$ Critical rotational speed. 37

Φ Magnetic flux. 32, 71

δ Skin Depth. 74

$\dot{V}$ Average oil velocity. 26, 61

$\dot{m}$ Mass flow. 61

ϵ Respective emissivity of the bodies. 39

ϵ Roughness height. 46

$\frac{du}{dy}$ Derivative of the velocity component, parallel to the direction of shear. 17

$\mathbf{B_R}$ Magnetic Flux Density in the rotor. 8

$\mathbf{B_s}$ Magnetic Flux Density in the stator. 8

$\mathbf{J}$ Current Density. 93

μ Chemical Potential. 94

μ Dynamic Viscosity. 17, 20

μ Relative permeability. 8, 25, 45

μ_0 Magnetic Permeability of free space $\mu_0 = 4\pi \cdot 10^{-7}\ H/m$. 12, 72

μ_r Relative permeability of ferromagnetic materials. 12

μ_{rec} Recoil permeability. 10, 13

ω_e Angular frequency of the applied electrical excitation. 6

$\overline{Nu}$ Nusselts number. 19, 20

$\overline{h}$ Average heat transfer coefficient. 26

ρ Density. 20, 25, 26, 46, 61

σ Boltzmann's constant. 18, 39

τ Tear Stress. 17, 28

θ_{ae} Initial angle of the axis of phase α. 6

c_p Specific heat capacity. 20, 26

dT Temperature difference. 15, 18

dx Thickness of the material. 15

e elementary charge. 94

fV Friction factor. 24, 25, 45

g Acceleration of gravity. 24, 46

h Convective heat transfer coefficient. 18, 20

h_L Head losses coefficient. 46

k Thermal Conductivity Coefficient. 15, 74

k Emissivity constant. 18

k Thermal conductivity of the material. 15, 20, 26

k_1 Flux leakage outside the gap. 71

k_2 Compensation factor for the finite permeability of iron. 72

k_w Winding Factor, typically between 0.85 and 0.95 for most machines. 6

l Characteristic length. 20

m Mass. 23

q Thermal Power. 18, 26

r Radius. 23

r_m Mean radius. 37

u_m Kinematic viscosity. 20

u_m Mean velocity of oil. 25

v_{avg} Average value of the velocity profile. 45

$v_{tangential}$ Tangential speed of the oil. 23, 46

Chapter 1

Introduction

1.1 Background

Permanent magnet (PM) machines are commonly used in automotive applications. The reason for this is it's high efficiency in most operating points, high power density due to high magnetic flux density in the air gap and low maintenance cost due to the absence of brushes.

However the permanent magnet machines also have a number of drawbacks. Most of them are related to the magnets used in the rotor because they are expensive, especially rare earth magnets and also sensitive to overheating due to possible demagnetization of them.

Generally, the losses caused by the eddy-currents induced in the rotor magnets are relatively small compared to the other losses generated in the electric machine. But due to the relatively poor heat dissipation of the rotor, these losses can cause significant heating of the magnets. Especially, in rare earth magnets the eddy-current loss can be quite significant due to their relatively high electrical conductivity. Increased temperature in the magnets may result in partial irreversible demagnetization of them.

Better cooling performance of the machine's rotor will result in higher power density, better field weakening capability and reduced cost. Reduced cost will emerge from less permanent magnet material used and from bigger segments of the magnets that are easier to manufacture and place on the rotor.

1.2 Thesis Problem

The eddy-current losses that occur in the magnets of a permanent magnet motor are very often neglected in the motor design. The reason is that the rotor rotates synchronized with the fundamental stator magnetomotive force (MMF). As a result, the absolute value of the losses are relative small compared to other losses inside the motor, for example copper losses in the windings or eddy current losses in the stator.

However, due to slotting, non-sinusoidal stator MMF distribution and non-sinusoidal phase current waveforms, harmonics are produced in the motor's air gap field and therefore eddy-currents are induced in the rotor magnets. Newer machine designs use the reluctance torque produced by the interaction of the space-harmonic MMF with the permanent magnets. This

employs concentrated windings. Furthermore, alternate teeth winding is used in machine designs to enhance fault tolerance. All those result in non-fundamental MMFs which in turn induce eddy-currents in the rotor magnets. Eddy-current losses become quite significant in high speeds [1]. In brushless DC motors due to commutation effects the harmonic content is higher thus resulting in more eddy-current losses compared to brushless AC motors [1].

In Figure 1.1, a cross-section of a permanent magnet motor can be seen. The presence of an air gap between the rotor and the stator and the small temperature difference between those, results in poor heat dissipation and even the small eddy-current losses occurred in the magnets can result in relatively high temperatures.

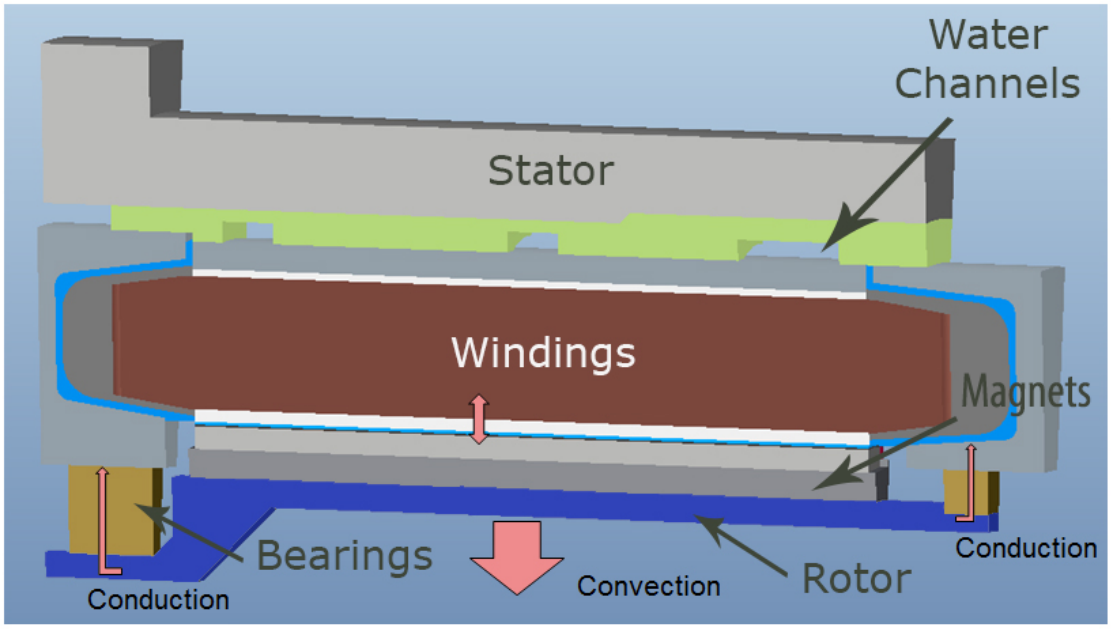

Figure 1.1: Stator Sectional View. Different parts of the motor are visible: the stator, the rotor, the water channels, the windings, the bearings etc. The heat transfer phenomena inside the motor are also visible with the arrows.

To solve the rotor overheating problem in permanent magnet motors different strategies are followed. One strategy is to reduce the losses in the permanent magnets and another is to improve the poor heat dissipation from the rotor.

The eddy current losses of the magnets can be reduced by segmenting the magnets, in the same way stator is being laminated. Then the motor can run in higher speed which usually results in higher power density but also in high cost.

Another alternative is to enhance the heat dissipation from the rotor. An example, which will be investigated in this thesis, is by creating an oil film on the interior surface of the rotor. This can be done with nozzles on co-axial oil lance inside the rotor. The oil film will effectively dissipate the heat from the rotor and will cool the magnets in a safe operating temperature.

Then possible reduction in the thickness of the magnets, and in the number of segments will be investigated. By keeping the magnets in lower temperature they are more resistant to demagnetization, which either means that higher field weakening possibilities or the possibility

for less magnet material.

In a real electric machine a lot of phenomena take place simultaneously and it would be very difficult to separate those phenomena. In this thesis two coaxial cylinders will be used to simulate the real rotor. The inner cylinder will have the oil inlet in the center and through some axial nozzles the oil will be sprayed to the outer cylinder as can be seen in Figure 1.2.

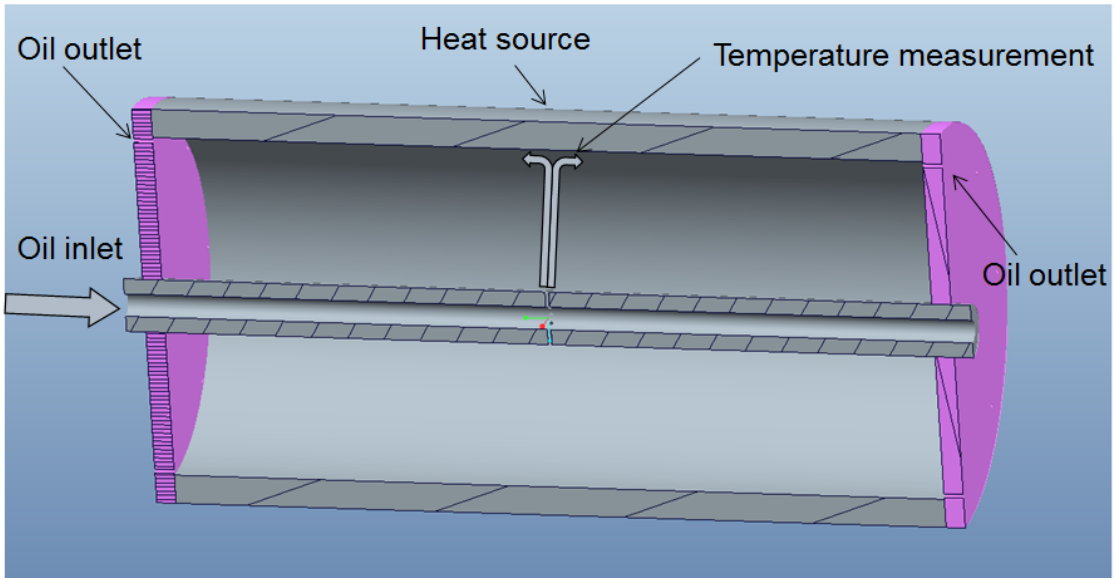

Figure 1.2: Test rig Visualization. A heating element will heat up the bigger cylinder. The oil will be inserted from the lance and sprayed into the center of the cylinder. Then the centrifugal force will push it outwards through the oil outlet. Temperature sensors will be in the surface of the cylinder to monitor the temperatures.

1.3 Thesis Aim

The thesis will focus on improving the performance of a permanent magnet electrical machine, in the means of increasing its power density and reducing its cost.

To achieve that, this thesis will investigate a cooling technique based on oil spraying, to cool the rotor magnets and study its effects in the design of the electric motor: the effects in the size of the rotor's magnets as well their segments size will be investigated. The temperature distribution along the rotor and heat transfer coefficients for a number of cases are to be investigated.

1.4 Thesis Scope

The scope of this thesis is to calculate the losses of a PM machine in a number of operating points and for different segmentations of the magnets. Additionally, to calculate the heat transfer coefficient of the oil spraying technique and to estimate the temperature of the magnets for a different cases. Finally to investigate possible improvements in the machine design due to the addition of the cooling of the rotor.

1.5 Thesis Outline

Chapter 2 presents the theory about the concepts that this thesis deals with. It is divided mainly in two parts: electric machines and heat transfer. In Chapter 3 the thermal model of the cylinder is being analyzed and a simplified theoretical model is being developed. The Nusselts number is being calculated for the studied geometry along with heat transfer coefficient maps for different oil flows. Chapter 4 is about the experimental part of the thesis. In the beginning of the chapter the investigation before the test rig is being discussed. Next, the test rig is presented and the post process treatment of the data is being discussed. Lastly the results are presented with a short discussion. In chapter 5 the losses in the permanent magnets for different segmentation is calculated. A thermal model of the rotor is being constructed and temperature maps of the magnets for different segmentation are created. In the last chapter, the discussions are being summarized and future work is proposed.

Chapter 2.1, 4.2, and 5 is documented by Odyssefs Lykartsis while chapter 2.2, 3, 4.1.2, 4.1.3 and 4.4 is documented by Johan Fröb. Other prarts was done together. Regarding the workload the work was divided by subject. The thermal calculations except for the induction heating analysis was conducted by Johan while the simulations regarding electrical machines and electrical effects was conducted by Odyssefs. The experimental work was done by both authors.

Chapter 2

Theory

2.1 Electric Machines

2.1.1 Introduction to AC Machines

AC machines can be generally categorized into two categories: *synchronous* and *asynchronous*. The main difference between those two categories is that in the first, the rotor currents are supplied from the stationary frame through a rotating contact. In the latter, the rotor currents, are induced in the rotor windings due to the relative movement of the rotor compared to the produced Magneto-motive Force (MMF) by the stator windings.

The Rotating Magnetic Field

In Figure 2.1, a simple three-phase stator can be seen. The three phase windings consist of three separate circuits that are placed with distance of 120 electrical degrees one from the other around the surface of the stator.

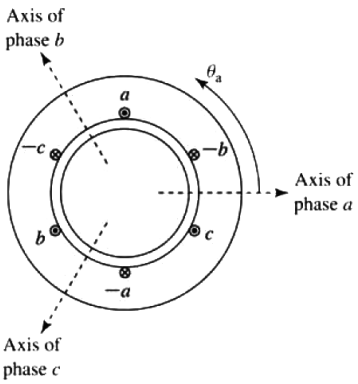

Figure 2.1: Simplified two-pole, three-phase stator winding.

Each phase is excited by an alternating current whose magnitude varies sinusoidally with

time. Thus, the instantaneous currents for every phase are

$$i_a = I_m cos\omega_e t \tag{2.1}$$

$$i_b = I_m cos(\omega_e t - 120^\circ) \tag{2.2}$$

$$i_c = I_m cos(\omega_e t + 120^\circ) \tag{2.3}$$

where
I_m is the amplitude of the phase current
ω_e is the angular frequency of the applied electrical excitation.
The time $t = 0$ *sec* is taken when phase-A is at its maximum value, and the sequence of the phases is assumed to be *abc*. The MMF produced by phase-A F_{a1} has proved to be [2]

$$F_{a1} = F_{a1}^{+} + F_{a1}^{-} \tag{2.4}$$

where

$$F_{a1}^{+} = \frac{1}{2} F_{max} cos(\theta_{ae} - \omega_e t) \tag{2.5}$$

$$F_{a1}^{-} = \frac{1}{2} F_{max} cos(\theta_{ae} + \omega_e t) \tag{2.6}$$

and

$$F_{max} = \frac{4}{\pi} \left(\frac{k_w N_{ph}}{poles} \right) I_m \tag{2.7}$$

where k_w is the winding factor of the machine typically in the range of 0.85-0.95, N_{ph} is the number of series turns per phase. Thus the product $k_w N_{ph}$ is the effective series turns per phase. The θ_{ae} is the initial angle of the axis of phase α.

In a similar way the MMF produced by phases B and C are delayed 120 and 240 degrees respectively [2]:

$$F_{b1} = F_{b1}^{+} + F_{b1}^{-} \tag{2.8}$$

$$F_{b1}^{+} = \frac{1}{2} F_{max} cos(\theta_{ae} - \omega_e t) \tag{2.9}$$

$$F_{b1}^{-} = \frac{1}{2} F_{max} cos(\theta_{ae} + \omega_e t + 120^\circ) \tag{2.10}$$

and

$$F_{c1} = F_{c1}^{+} + F_{c1}^{-} \tag{2.11}$$

$$F_{c1}^{+} = \frac{1}{2} F_{max} cos(\theta_{ae} - \omega_e t) \tag{2.12}$$

$$F_{c1}^{-} = \frac{1}{2} F_{max} cos(\theta_{ae} + \omega_e t - 120^\circ) \tag{2.13}$$

The total MMF of the stator is the sum of the contributions of each phase

$$F(\theta_{ae}, t) = F_{a1} + F_{b1} + F_{c1} = \frac{3}{2} F_{max} cos(\theta_{ae} - \omega_e t) \tag{2.14}$$

The rotating MMF can be seen also in Figure 2.2 for different time moments. For $\omega_e t = 0$, in Figure 2.2(a), the current in phase-A has its maximum value I_m while the MMF produced by phase-A is also at its maximum $F_a = F_{max}$. At this moment, the currents in both phases B and

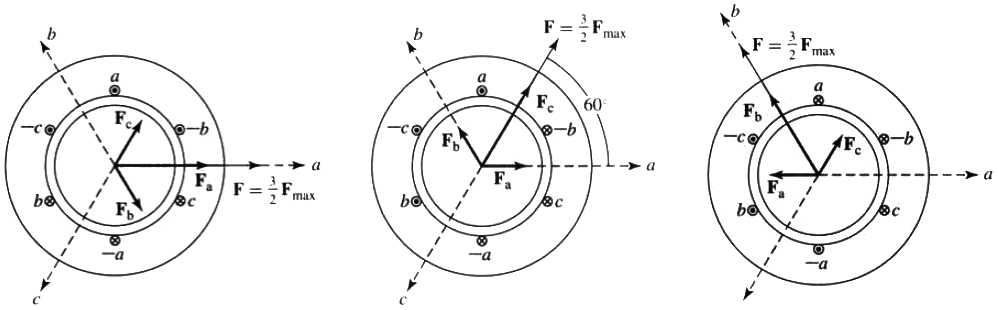

(a) MMF at $\omega_e t = 0$ (b) MMF at $\omega_e t = \pi/3$ (c) MMF at $\omega_e t = 2\pi/3$

Figure 2.2: The production of rotating magnetic field F by three-phase currents. F_a, F_b, F_c is the MMF produced by phase A, B and C respectively.

C are $i_b = i_c = -\frac{I_m}{2}$ and thus the produced MMF is $F_b = F_c = F_{max}$ in the *negative* direction. The resulting MMF, obtained by adding all the individual contributions is in the direction of axis of phase-A and has a vector magnitude of $F = \frac{3}{2}F_{max}$.

In Figure 2.2(b), the individuals and the resultant MMF in a later time moment $\omega_e t = \pi/3$ can be seen. At this time moment the currents of phase A and B are $i_a = i_b = \frac{I_m}{2}$ and the current of phase C is at its maximum negative value $i_c = -I_m$. The resultant MMF compared to Figure 2.2(a) is now rotated 60 degrees counter clockwise.

In a similar way, in Figure 2.2(c) the resultant and individual MMF at $\omega_e t = 2\pi/3$ can be seen. In this time moment, the resultant MMF is rotated 120 degrees counter clockwise compared to $\omega_e t = 0$ and is now aligned with the axis of phase-b.

Induced Torque

In an AC machine there are always two magnetic fields present: one from the stator circuit and another from the rotor. The interaction of those two magnetic fields is what produces the torque in an AC machine. The two magnetic fields will always try to align. Since the stator's field is rotating the field from the rotor will try to align with it, thus creating a constant torque. In order to understand the torque production in an AC machine, a single wire loop inside the stator can be examined. In order to find the induced torque, the loop will be divided into two wires, as seen in Figure 2.3.

The induced forced $\mathbf{F}$ in conductor 1 is given by the expression

$$\mathbf{F} = i(\mathbf{l} \times \mathbf{B}) = ilB_s sin\ a \tag{2.15}$$

where i is the current flowing through the conductor, l is the length of the conductor and the direction of the force as seen in Figure 2.3. The torque for conductor 1 is

$$\tau_{ind,1} = (\mathbf{r} \times \mathbf{F}) = rilB_s sin\ a \tag{2.16}$$

In a similar way, the induced force and torque on conductor 2 are the same in magnitude with different directions, as shown in Figure 2.3.

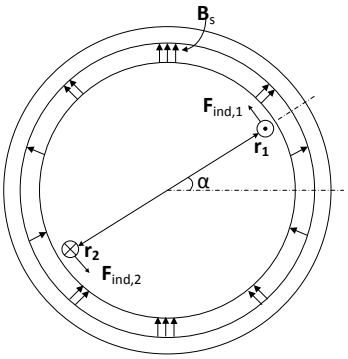

Figure 2.3: Simplified version of AC machine with sinusoidal stator flux distribution and a single wire loop mounted into the rotor.

Finally, by considering that the magnetic field of the rotor is produced by the current of a single coil, then the magnitude of the magnetic field intensity $\mathbf{H_R}$ is directly proportional to the current flowing in the rotor:

$$H_R = Ci$$

where C is a constant.

Then the torque produced by the AC machine is given by the expression

$$\tau_{ind} = K\mathbf{H_R} \times \mathbf{B_s} = k\mathbf{B_R} \times \mathbf{B_s} \tag{2.17}$$

where $k = K/\mu$ where μ is the relative permeability which generally varies due to the magnetic saturation of the machine, $\mathbf{B_s}$ is the flux density in the stator and $\mathbf{B_R}$ is the flux density in the rotor.

2.1.2 Permanent Magnet Machines

Synchronous Machines in General

Synchronous motors operate in absolute synchronism with the stator's electrical frequency [2–5]. In general synchronous motors are categorized according to their design, their construction and their materials to the following categories [5]:

- Electromagnetically excited motors. These motors use an excitation circuit to produce the rotor's magnetic flux.
- Permanent magnet (PM) motors, which use permanent magnets embedded to the rotor to create constant flux.
- Reluctance motors, that their operation is based on inducing non-permanent poles on a ferromagnetic rotor. They use the phenomenon of magnetic reluctance to produce torque.
- Hysteresis motors, whose rotor consists of a central nonmagnetic core. On the top of this core there are mounted rings of magnetically "hard" material. This type of motor takes advantage of the large hysteresis loop of this material to create a almost ripple free constant torque.

PM motors

Permanent Magnet machines have a number of advantages compared to the ones with electromagnetic excitation [5]:

- no electrical energy is used to create the rotor flux, meaning that there are no resistive losses in the excitation circuit, substantially increasing efficiency.
- higher power density and torque
- better dynamic performance due to higher flux density
- lower maintenance cost
- simpler design

however, there are two major disadvantages

- the price of magnets are high, especially rear earth magnets, which electrical machines mostly use.
- the magnets are sensitive to temperature because of demagnetization. In Table 2.1, for example, the maximum continuous service temperature is $120°C$ for Neodymium-Iron-Boron (NdFeB) magnets which have the highest operating temperature. Higher temperature NdFeB magnets also exist, but they are more expensive and typically they have smaller energy product.

Construction Permanent magnet (PM) motors can be constructed by using different rotor configurations, as can be seen in Figure 2.4.

Interior-Magnet Rotor An Interior-Magnet rotor can be seen in Figure 2.4(a). This type of rotor has radially magnetized and alternately poled magnets. The reactance in d-axis on those PM machines is smaller than the q-axis, since the flux can pass through the steel core without crossing the magnets that have permeability of 1. An advantage of this type of rotor configuration is that the magnets are buried inside the rotor and is therefore very well protected against centrifugal forces. As a result, this rotor configuration is suitable for high-speed motors.

Surface-Magnet Rotor A Surface-Magnet rotor is shown in Figure 2.4(b). It has also its magnets usually radially magnetized. Sometimes, an external high conductivity non-ferromagnetic cylinder is used to protect the magnets from the centrifugal forces. In this configuration the synchronous reactance on d and q axis are practically the same.

Inset-Magnet Rotor In Inset-Magnet rotor configuration the magnets are also radially magnetized and placed inside shallow plots Figure (2.4(c)). The q-axis synchronous reactance is greater than the one in d-axis. In general the EMF induced by the magnets is lower compared to the Surface-Magnet rotor configuration.

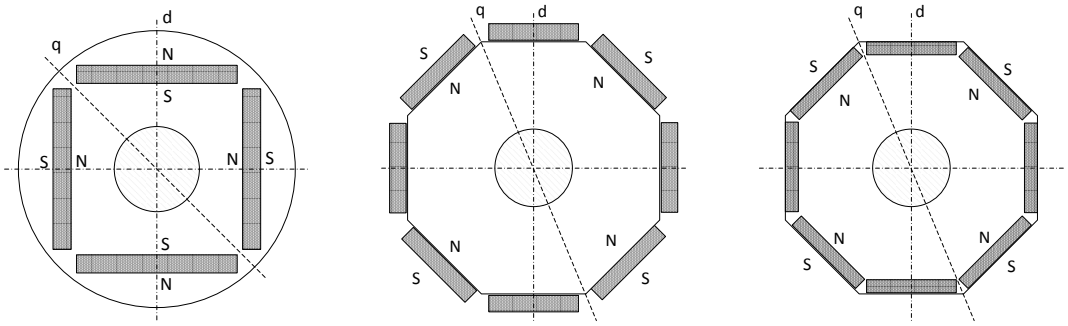

(a) Interior Magnet Rotor (b) Surface Magnet Rotor (c) Inset Magnet Rotor

Figure 2.4: Rotor configurations for PM synchronous motors

2.1.3 Permanent Magnets

A permanent magnet (PM) is an object made from a material that is magnetized and creates its own persistent magnetic field without the need of excitation and with no electric power dissipation. As every other ferromagnetic material, permanent magnets are described by their B-H *hysteresis loop*. A typical hysteresis loop can be seen in Figure 2.6.

Ferromaterials are categorized into three big categories: soft, semi-hard and permanent magnets. These categories are illustrated in Figure 2.5. Permanent magnets in each category offer different magnetic properties, with the largest differences being their stability against opposing magnetic field, remaining magnetism and hysteresis losses.

Demagnetization Curve

Demagnetization curve, a portion of the materials hysteresis loop, is often the basis for evaluating a permanent magnet.

A typical demagnetization curve can be seen in Figure 2.6, where the point L represents the *remanence* or *remanent magnetism*. Point K represents the magnetic flux of a previously magnetized material when a reversed magnetic field intensity is applied. As a result the presence of the reverse field has reduced the remanent magnetism, and when the reverse field is removed, the flux density will return through the small B-H loop to the point L again. Instead of using this small B-H curve usually a straight line is used, called the *recoil line*, which introduces a small error. The slope of this line is called recoil permeability μ_{rec} [5].

The magnets can be considered reasonably permanent as long as the negative value of field intensity is not exceeding the maximum value corresponding to point K. In case of a higher field intensity H, the flux density will be lower than point K, but when the field is removed, a new and lower recoil line will be created and the magnet will be partially demagnetized.

A general relationship between the magnetic flux density B, inherent magnetization B_i and applied magnetic field intensity H is [5]:

$$B = \mu_0 H + B_i = \mu_0(H + M) = \mu_0(1 + \chi)H = \mu_0\mu_r H \tag{2.18}$$

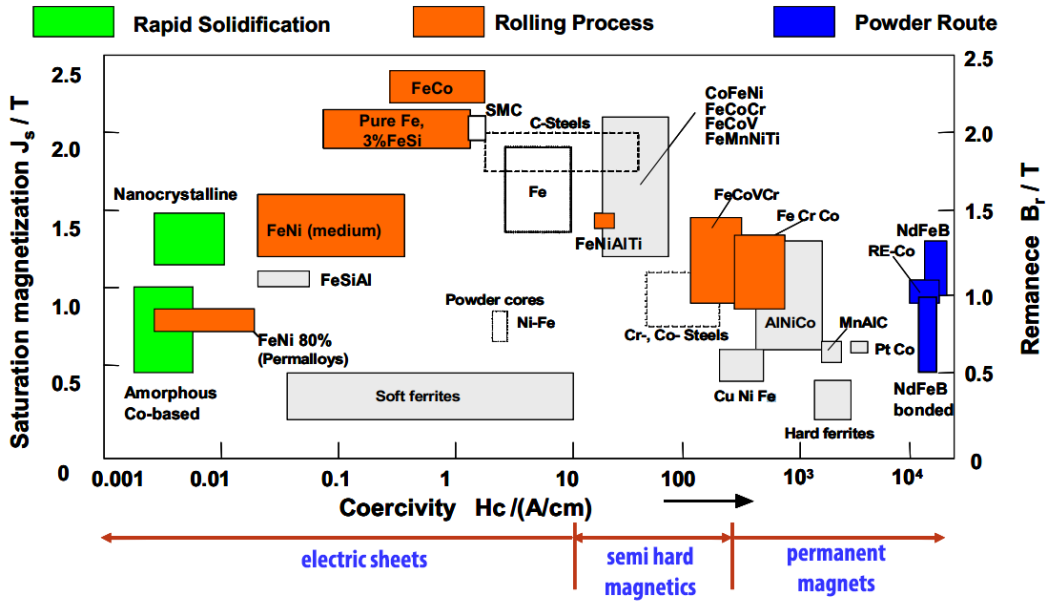

Figure 2.5: Overview of magnetic materials. The magnets are categorized based on their coercivity and their remanece. [6].

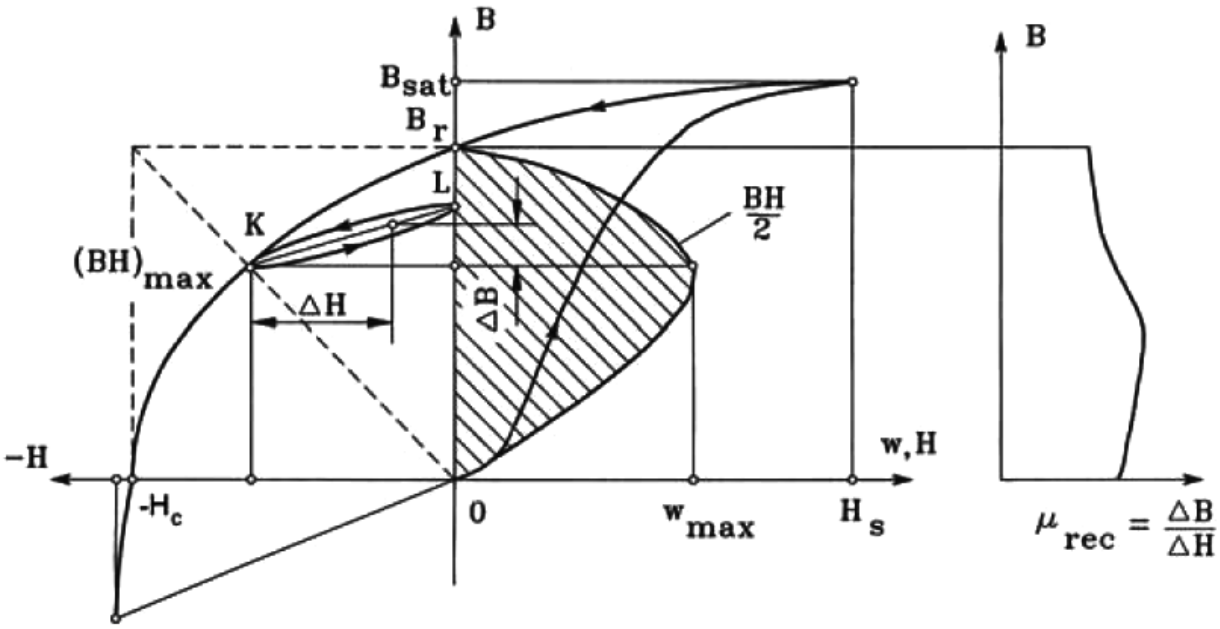

Figure 2.6: Demagnetization curve, recoil loop, energy of a PM, and recoil magnetic permeability [5].

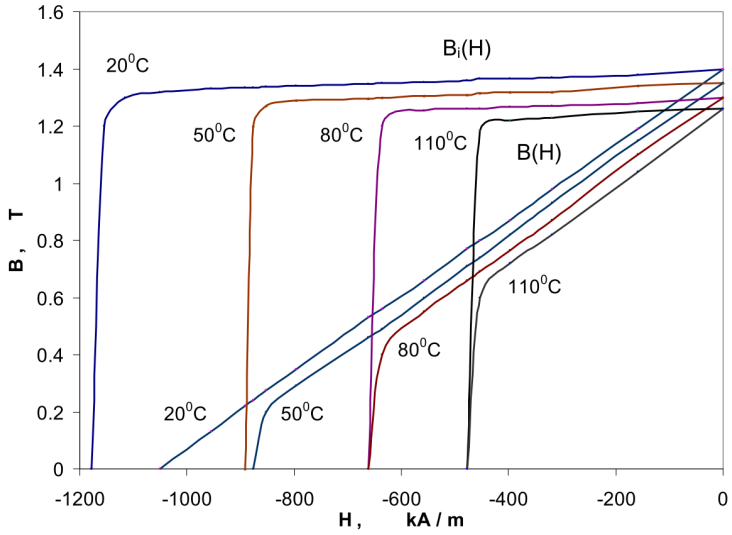

Figure 2.7: Comparison of B-H and B_i-H demagnetization curves and their variations with the temperature for sintered N48M NdFeB PMs [5].

where μ_0 is the magnetic permeability of free space, μ_r is the relative permeability of ferromagnetic materials and $M = B_i/\mu_0$.

Demagnetization curve is also *temperature dependent* for the same material as can be seen from Figure 2.7.

Magnetic Parameters

Permanent Magnets are characterized by the following parameters [5]

- *Saturation Magnetic Flux Density* B_{sat} and *Saturation Magnetic Field Intensity* H_{sat}. At this point the alignment of all *magnetic moments of domains* is in the direction of the externally applied magnetic field.
- *Remanent Magnetic Flux Density* B_r or *remanence*. Is the magnetic flux density corresponding to no externally applied magnetic field. The higher this value the higher magnetic flux density in the air gap of the electric machine.It corresponds to point L in Figure 2.6.
- *Coercive Field Strength* H_c or *coercivity*. This property is the value of magnetic field intensity required to make the field density zero in a previously magnetized material. High coercivity means that the magnet can withstand higher demagnetization field.
- *Intrinsic Demagnetization Curve*. It is the upper-left quadrant of the $B_i = F(H)$ curve where $B_i = B - \mu_0 H$ is according to eq. (2.18).
- *Intrinsic Coercivity* ${}_iH_c$. It is the required magnetic field strength in order the intrinsic magnetic flux B_i of a magnetic material to become zero. For permanent magnets typically ${}_iH_c > H_c$.

Table 2.1: Properties of NdFeB permanent magnet materials at 20°C [6].

Property	Vacodym 633 HR	Vacodym 362 TP	Vacodym 633 AP
Remanent flux density, $\mathbf{B_r}$ $[T]$	1.29 to 1.35	1.25 to 1.30	1.22 to 1.26
Coercivity, $\mathbf{H_c}$ $[kA/m]$	980 to 1040	950 to 1005	915 to 965
Intrinsic coercivity ${}_{\mathbf{i}}\mathbf{H_c}$ $[kA/m]$	1275 to 1430	1195 to 1355	1355 to 1510
$(\mathbf{BH})_{\mathbf{max}}$ $[kJ/m^3]$	315 to 350	295 to 325	280 to 305
Relative recoil magnetic permeability $\mu_{\mathbf{r,rec}}$	1.03 to 1.05		1.04 to 1.06
Temperature coefficient $\alpha_{\mathbf{B}}$ of $\mathbf{B_r}$ at 20°C to 100°C [%/°C]	-0.095	-0.115	-0.095
Temperature coefficient $\alpha_{\mathbf{iH}}$ of $\mathbf{B_r}$ at 20°C to 100°C [%/°C]	-0.65	-0.72	-0.64
Temperature coefficient $\alpha_{\mathbf{B}}$ of $\mathbf{B_r}$ at 20°C to 100°C [%/°C]	-0.105	-0.130	-0.105
Temperature coefficient $\alpha_{\mathbf{iH}}$ of $\mathbf{B_r}$ at 20°C to 100°C [%/°C]	-0.55	-0.61	-0.54
Curie Temperature [°C]	approximately 330		
Maximum Continuous service temperature [°C]	110	100	120
Thermal conductivity $[W/(m\ °C)]$	approximately 9		
Specific mass density $\rho_{\mathbf{PM}}$ $[kg/m^3]$	7700	7600	7700
Electric conductivity $\times 10^6$ $[S/m]$	0.62 to 0.83		
Coefficient of thermal expansion at 20°C to 100°C $\times 10^6$[/°C]	5		
Young's modulus $\times 10^6[MPa]$	0.150		
Bending stress $[MPa]$	270		
Vicker's hardness	approximately 570		

- *Recoil Magnetic Permeability* μ_{rec} . Is the ratio of the magnetic flux density to magnetic field intensity at any point of the demagnetization curve:

$$\mu_{rec} = \mu_0 \mu_{r,rec} = \frac{\Delta B}{\Delta H}$$

  where the $\mu_{r,rec}$ typically in the range of $\mu_{r,rec} = 1....3.5$.

- *Maximum Magnetic Energy per unit*, ω_{max}, produced by a permanent magnet is equal to

$$\omega_{max} = \frac{(BH)_{max}}{2}\ [J/m^3]$$

  where the product $(BH)_{max}$ corresponds to the maximum energy density point on the demagnetization curve with coordinates B_{max} and H_{max}.

- *Form Factor of the Demagnetization Curve*, γ which characterizes the shape of the demagnetization curve
$$\gamma = \frac{(BH)_{max}}{B_r H_c} = \frac{B_{max} H_{max}}{B_r H_c}$$
and $\gamma = 1$ corresponds to square demagnetization curve while $\gamma = 0.25$ corresponds to a straight line.

All the parameters are visible in Figure 2.6.

Losses in the magnets of PM machines

In an ideal PM machine with perfectly distributed windings only the fundamental MMF component exists in the air-gap. The rotor of a PM machine is rotating with the fundamental frequency of the MMF wave and thus the field that the magnets experience over time is constant [2–5].

After the verification that concentrated windings are capable of producing sinusoidal electromotive force (EMF) the usage of those machines increased significantly [7, 8]. Machines with concentrated windings offer a lot of advantages. The most important is the possibility of shorter end windings. This results in smaller motor size, less amount of copper used and in turn copper losses [9–11].

The main disadvantage compared to motors with distributed windings is the high harmonic content of the MMF generated in the air gap. Those high frequency components rotate at the stator of the electrical machine with a non synchronous speed. The magnet of the machine experience those harmonics as time and space varying fields [12, 13].

According to Faraday's Law eq. (4.1), eddy current losses are only created due to time varying flux over a closed surface.

Additionally to those harmonics that created due to slotting [14], harmonics are also introduced in phase current waveforms because of PWM [15] or six-step operation [16].

Due to poor heat dissipation from the rotor those eddy-current losses can cause significant heating of the permanent magnets and rise their temperature significantly changing their characteristics as explained in Section 2.1.3. Increased temperature in the magnets also reduces their coercivity to opposing magnetic fields, as seen in Table 2.1, reducing the capability of field weakening, a technique widely used in high speed drive applications.

Even the highest temperature graded permanent magnets, NbFeB have maximum continuous working temperature of about $200°C$. Lower temperature magnets offer better flux density and can withstand higher opposing fields. The problem becomes worse in NdFeb magnets because of relative high electrical conductivity, which enhances eddy current losses.

Currently the rare earth magnets are cut into small, insulated pieces in a similar way as laminations in the iron core, to reduce eddy currents[17–21].

2.2 Heat transfer mechanisms

One of the fundaments of this thesis is thermodynamic and heat transfer specifically. This section of the report will explain the main mechanisms behind the heat transfer. The initial section will give a brief background to the different modes of heat transfer.

2.2.1 Heat transfer

The definition of heat transfer proposed by P. Incropera et al. in [22] is: Heat transfer (or heat) is thermal energy in transit due to a spatial temperature difference. This means that whenever there is a temperature gradient or difference in a medium heat transfer will occur. The temperature or thermal energy of a substance is in reality vibration and movement, of a large and adjacent group of molecules in a micro scale. The heat transfer occurs because of differences of the movement and vibration of the molecules in the medium.

Three different modes that heat can be transfered in are Conduction, Convection and Radiation. Conduction occurs whenever there is a temperature difference in a substance. The mechanism is independent of the phase of the substance.

Convection is a collective name for two mechanisms, namely diffusion and advection. Convection is used as a model when a fluid is in motion on a macroscopic scale.

The last mode of heat transfer is radiation. Every surface with a finite temperature emits energy in form of electromagnetic radiation.

Conduction

The conduction heat transfer has the difference in magnitude of vibration and motion of molecules as a driving force. Molecules collide or resonate and thereby transfer the energy between each other. The heat transfer occurs from the more energetic to the less energetic molecule.

A good example of conduction would be considering a gas with a temperature gradient without internal motion. As can be seen in Figure 2.8 the molecules will all move randomly within the space that they are limited to. If a molecule or a group of molecules has higher speed and vibration that any other their interaction (collision and vibration) with each other will in the end eliminate this difference. Since molecule motion is analogue to its temperature this would mean that the transit of heat would occur from the warmer part to the cooler part of the medium. The interaction between molecules is called diffusion of heat.

The equation for the conductive heat transfer in steady state in one dimension is:

$$q_x = -kA\frac{dT}{dx} \tag{2.19}$$

where q_x is the power transferred in the x-direction, k is the thermal conductivity coefficient, A is the cross sectional area, dT is the temperature gradient in the direction being evaluated and dx is the distance between in the material. This equation is usually referred to as furiers law within the conditions mentioned above.

where k is the thermal conductivity of the material, A is the conduction area, is the temperature difference dT= $T_{hot} - T_{cold}$ and dx is the thickness of the material.

The same mechanisms occur in liquids. However, the spacing between the molecules in liquids is much smaller than in gases and therefore the interaction will be much stronger and occur more frequently.

When it comes to diffusion of heat in solids it is also caused by vibrations of the molecules. Heat transfer can only occur between adjacent molecules since they are stationary and immobile. Another mechanism that takes place in conduction is the exchange of energy through free electron movement. Apart from the interaction of molecules, the free electrons or -holes transfer energy

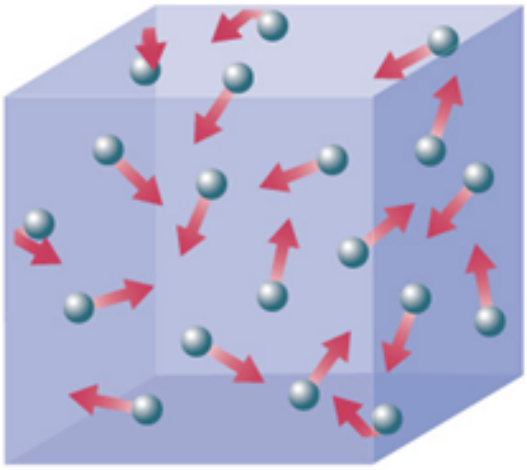

Figure 2.8: Heat transfer by conduction in a gas at rest.

through the substance. This mechanism is much faster than the molecule interaction, generally making a good electrical conductor a good heat conductor as well.

Convection

Convection is the sum of both the random molecule movement and interaction between each other,which is called diffusion, but also the bulk movement or the fluid movement on a macroscopic level. The later mechanism is called *advection*. Convection between a fluid over a surface is a common situation in engineering applications and an example is a radiator, which can be seen in Figure 2.9.

There is a variety of different scenarios when it comes to convection. Often the relations are empirical meaning that they are achieved from experimental data. Therefore there is a number of standard cases for different geometries.

Another fact to be considered is the different flow patterns. Across a surface, the fluid viewed in profile going from side-to-side, two types of distributions along the surface normal direction will develop. Firstly, hydrodynamic profile or boundary layer develops, which is the velocity distribution along the normal direction of the plane. In this profile, closest to the wall the fluid stands still and the velocity increases in the normal direction of the plane.

The other distribution is the thermal profile or boundary layer. Depending on the bulk temperature of the fluid, if it is higher or lower than the surface, the profile will look different. The temperature of the fluid is always the same as the wall's or the surface's temperature. This due to the no slip condition: the fluid layer closest to the wall will have the same speed as the wall. Due to infinite residence time the fluid layer adjacent to the wall eventually will have the same temperature as the wall.

The heat transfer is very much dependent on the velocity distribution and there are a number of different cases and situations. There are three types of flow patterns over a surface. All three can occur within the same flow in different parts of the stream in respect to the flow direction. The

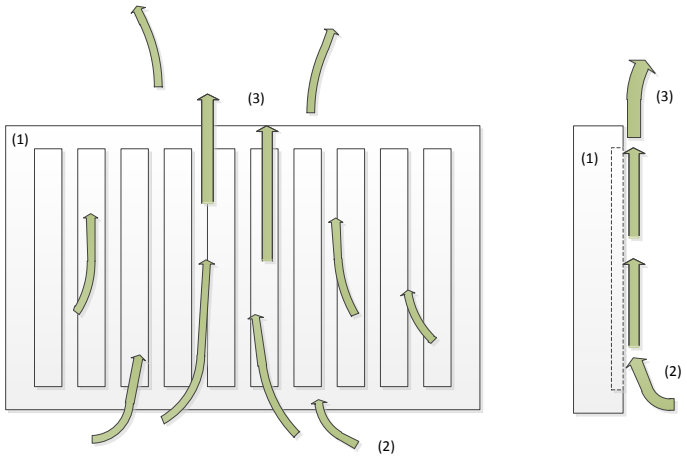

(a) Front view (b) Side view

Figure 2.9: Convection between cooler air and a warmer radiator. The radiator (1) heats the air in (2) which, due to buoyancy effects, makes the air travel upwards along the surface of the radiator (3). This is an example of convection and this specific case is called natural since no external forces influences the air.

laminar flow is harmonious and particles of the fluid are said to move predictably. By predictable means that the particles of the fluid does not move in the direction that is perpendicular to the flow.

The second pattern, the turbulent flow, is stochastic and hard to predict. Small vortices occurs everywhere in the stream which disrupts the boundary layer, both thermal and velocity. Turbulent flow increases the heat transfer since the temperature distribution will be more homogeneous.

The last flow pattern is a combination of laminar and turbulent flow. In certain conditions the flow will shift between laminar and turbulent randomly. This flow pattern is called transition flow region. Flow disturbances occurs due to the shear stress introduced in the fluid originating from the wall. The shear stress is directed both in the opposite direction of the flow on the fluid and in the flow direction on the surface. With higher velocity gradient in the fluid the shear stress becomes higher if the fluid can be assumed to be Newtonian. A Newtonian fluid will behave as the linear expression:

$$\tau = -\mu \cdot \frac{du}{dy} \tag{2.20}$$

where μ is the dynamic viscosity,τ is the tear stress and $\frac{du}{dy}$ is the derivative of the velocity component, parallel to the direction of shear. It is a measure of how much a fluid deforms when it is exposed for a tensile or shear stress. u is the fluid velocity and y is the distance of point of measurement relative to the wall.

Beside from the flow pattern there is another classification of the flow, forced and natural convection:

Convection is said to be forced if the bulk moves due to an external force. The force can for example be a fan or pump which drives the flow. It can also be the wind or velocity difference

between the surface and the fluid because of propulsion.

Natural convection takes place when a fluid is heated and starts to flow because of the buoyancy due to the change in density.

Usually the convective heat transfer coefficient h is introduced to simplify the phenomena taking place. It is defined as:

$$h = \frac{q}{A\ dT} \tag{2.21}$$

where q is the thermal power, A is the area and dT is the temperature difference. The convective heat transfer coefficient describes the heat transfer capability of in a certain situation depending on the temperature difference and the area for the heat transfer for a certain power.

Radiation

All surfaces at non-zero temperature emit energy independent of the medium they are in and regardless of their phase. Radiative heat transfer, is most effective in vacuum because no particles are blocking the irradiated energy. An example is the heated piece of metal, seen in Figure 2.10. The thermal radiation is manifested in a visual way because the metal emits thermal radiation in the visible part of the electromagnetic spectra.

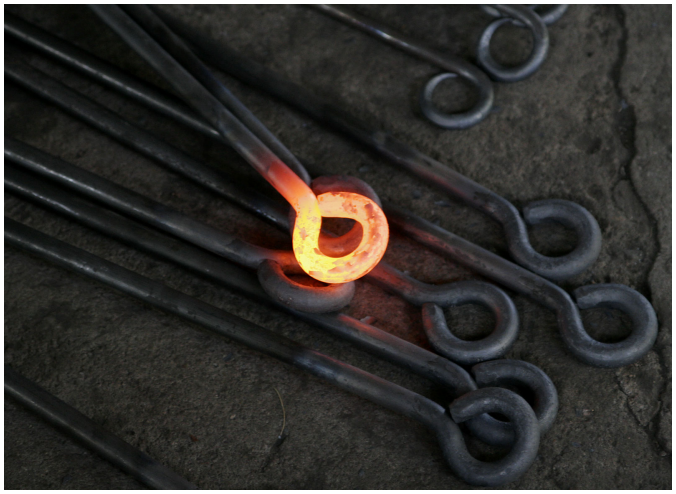

Figure 2.10: Hot metal glowing red. The eye perceives the heat since the metal is heated to the point where the thermal radiation it emits is within the spectra wavelengths that the human eye can intercept. [23]

In radiative heat transfer the energy is transported through *electromagnetic waves* or *photons*. The radiation power for an ideal emitter or a black body is:

$$E_r = k \cdot \sigma \cdot T_s^4 \tag{2.22}$$

where E_r is the radiative power,k is the emissivity constant, σ is Boltzmann's constant and T_s is the surface temperature of the body.

To compensate for the materials inability to emit energy perfectly the emissivity factor k is introduced. Emissivity ranges from zero to one, where 1 is the emissivity for a black body.

Another factor used in radiation calculations is the view factor. It also spans from zero to one. View factor is used to estimate the radiation distribution regarding different directions as well as the fraction of the irradiated energy compared to the total energy emitted by the body.

2.2.2 Empirical relations

Due to the nature of some phenomena , it is difficult to be described by an analytical relation. To make the analysis easier, another approach is taken by introducing dimensionless numbers.

Dimensionless numbers are combinations of variables that affect the sought variable. The combination of the numbers should be dimensionless, thereby the name, and the reason for that is that they are not meaningful by themselves. However, they are a powerful tool when combining them in empirical relations that are found by experiments.

Empiricism is a philosophic science where theory is purely constructed by the observed occurrences and proven by sampled data. For example, a test rig is constructed for a certain experiment. A set of variables is chosen beforehand and the test rig is constructed so that these variables can be varied. A number of series tests are conducted and the dependent variables are varied one at the time. During every run, everything is monitored and sampled. By combining the dimensionless numbers and plotting the data relations can be made. One of the numbers will contain the desired parameter and the theory is proven if the test can be repeated. The relation will be case specific and valid in a certain range of the dimensionless numbers.

Empirical convection relation

Empiricism is used widely to describe heat transfer by convection. To understand how empiricism is applied to describe convection one basic case will be examined: fluid flow over a flat plate.

The plate is heated to maintain a constant temperature or a constant heat flux. The temperature of the surface of the plate, the bulk temperature of the fluid, the input electrical power , the velocity of the fluid, the geometry of the plate and the properties of the fluid are all measured or are known. One at the time these variables are varied, for example the length or width of the plate, the fluid that is used, the electrical power that is heating the plate or another parameter and the data is used to achieve the dimensionless numbers. Then they are plotted and studied to find the dependence between them.

The relation between Nusselt and Reynolds then often appear as a straight line when plotted on a log-log scaled plot, for one given fluid (constant Prandtl). This indicates an exponential relation between these numbers on the form of

$$\overline{Nu} = C \cdot Re^m \cdot Pr^n \tag{2.23}$$

C, m and n are the sought constants that defines the dependence between Nusselt's number $\overline{Nu}$, Reynolds' number Re and Prandtl number Pr.

They are often independent of the fluid properties and thereby the family of lines that appear due to different Prandtl numbers can be merged into one by plotting the ratio between the Nusselt number and the Prandtl number :

$$\frac{\overline{Nu}}{Pr^n} = CRe^m \tag{2.24}$$

Nusselt number $\overline{Nu}$ is defined as

$$\overline{Nu} = \frac{hl}{k} \tag{2.25}$$

h being the convective heat transfer coefficient, l being the characteristic length and k being the thermal conductivity of the fluid.

Reynolds number Re is defined as

$$Re_D = \frac{\rho u_m D_h}{\mu} \tag{2.26}$$

where ρ is the density of the fluid, u_m is the kinematic viscosity of the fluid, D_h is the hydraulic diameter and μ is the dynamic viscosity of the fluid.

Prandtl number Pr is defined as

$$Pr = \frac{c_p \mu}{k} \tag{2.27}$$

where c_p is the specific heat capacity, μ is the dynamic viscosity and k is the thermal conductivity.

Assuming a constant Prandtl number however can introduce major errors if the temperature variation over the entire plate is large or if there is a major difference between the temperature of the fluid and the temperature of the surface. To cope with these variations two different methods are used.

The first is by defining the film temperature that is the average of the surface and the free stream temperature. The second method is to evaluate all the properties at fluid temperature and multiply the empirical relation with a correction factor on the form of

$$\frac{Pr_b}{Pr_s}^r$$

or

$$\frac{\mu_b}{\mu_s}^r$$

where b is bulk and s is surface.

As mentioned earlier, these kinds of relations are case specific and also limited to a certain range of dimensionless numbers. Relations of similar structure can be formed for cases with other geometries or conditions.[22]

Chapter 3

Heat Transfer in the cylinder

One of the outlines of this thesis is to measure the convective heat transfer coefficient between the inner wall of a rotating cylinder and the applied coolant, which is oil. The oil is sprayed on the inside of the cylinder. To have a first approximation of what is to be expected the situation has been simplified to match a existing empirical relation. To be able to use an empirical relation the situation needs to be justified by some assumptions.

3.1 Assumptions

The assumptions that were made are summarized in that the oil:

- is distributed evenly on the inside of the cylinder
- absorb heat only due to its movement in the axial direction
- move frictionless against the air inside the cylinder
- has constant properties over the entire temperature span
- forms incompressible flow

It is also assumed that:

- the radiation effect is negligible
- the oil film can be approximated with infinitely long square duct

3.1.1 Even distributed oil film

This assumption is necessary to enable calculation of the oil film as a continuous geometry. For more advanced situations with variation of the cross section geometry a CFD program would be used. This assumption is adequately correct for the speeds used in the test rig.

Another parameter to be considered for this assumption is the contact angle between the fluid and wall. With small contact angle the fluid will tend to distribute evenly over the surface. On the other hand, a large contact angle will prime the fluid to form streams. This will make the

distribution of the fluid on the surface jagged. Oil to a stainless steal surface has a low contact angle.[24]

3.1.2 Oil movement

The oil flow in radial direction is assumed to have little or no impact to the heat flow. This because the relative speed between the wall and oil in radial direction is near zero. The oil film is assumed to be very thin and this combined with the no slip condition means that the average speed of the oil is almost the same as the speed of the wall.

Also the drag force that the oil experience, from the air inside the cylinder, is very small according to the calculations that are made following the empirical relation in Principle of Heat and Mass Transfer by P. Incropera et al. [22]. The MATLAB code can be seen in appendix B.2

3.1.3 Constant oil properties

Oil properties like density, viscosity, thermal conductivity and some other properties are all functions of the temperature. Since the wall and the oil is in different temperatures heat will transfer between these two elements. The temperature of the oil and the wall will converge until they are the same. Since the oil moves over the surface, there will always be a temperature gradient. The temperature change will yield a change in the properties of the oil.

To compensate for this the oil properties are evaluated at the mean of inlet- and outlet temperature[22]. This assumption can be made for relatively small temperature changes but might not be applicable when the temperature difference of the oil at inlet and outlet is above a couple of degrees. The reason for this is that some of the oil properties is not linear and vary differently from each other over different temperature intervals. The errors for higher temperature differences might strongly affect the result.

3.1.4 Incompressible flow

This assumption is valid when the pressure drops are relatively small. This can generally be assumed for liquid fluids. The change in flow work can then be neglected.

3.1.5 Negligible radiation effect

If high temperatures occur, radiation effect between the fluid and wall might be considerable large. In the specific case however, the temperatures are comparably small and the effect will be negligible compared to the convection power.

3.1.6 Infinite square duct

Because the ratio between the circumference of the cylinder and the thickness of the oil film is between 300 and 10000 this approximation is valid:[22]

$$\frac{a}{b} = \frac{\pi \cdot r_c}{t_O} \tag{3.1}$$

The criteria for the geometrical approximation was evaluated but since the thickness of the oil film was so small compared to the length of the circumference of the cylinder the calculation

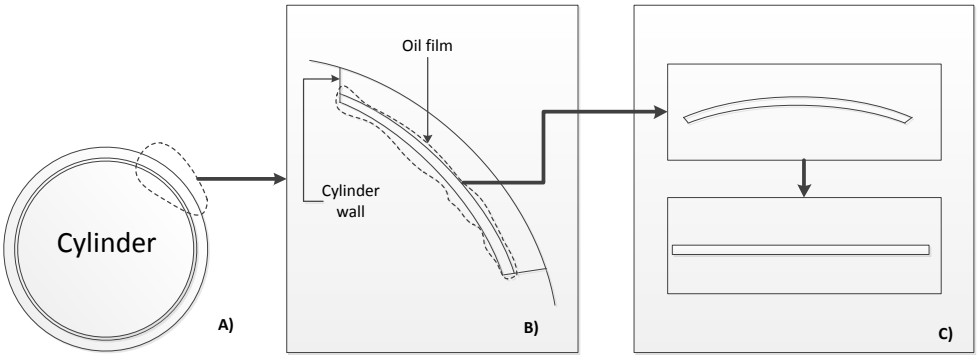

Figure 3.1: An illustration of the simplification that is made geometry wise for a small section of the oil film. In the calculations the entire section is used.

is not shown. The result of this is that the ratio between the inner and outer circumference of the cross section of the oil film will approximately be 1. Figure 3.1 shows the approximation stepwise. In A) the entire cylinder is shown and in B) a section is magnified to visualize the cylinder wall and oil film more clearly. In the last part C) the figure illustrates the shape of the duct that is made up from the oil film. The oil film in the entire circumference was used to form the square duct and not just a part as shown in the figure.

Thickness estimation

Since the heat transfer is so strongly dependent on the film thickness of the oil it will have a significant impact on the cooling performance of the system. While the relevance of it was discovered too late to measure it experimentally it became important to estimate it numerically. The thickness of the oil layer was also used to improve the theoretical analysis as it formerly was based on an approximation.

Generally when an object is rotating inside a cylinder or an annulus it is exposed to a force. This force is called the centripetal force and acts upon the object to make it stay in its given trajectory. Within the experiment a normal force from the wall gives the oil an acceleration towards the center of the cylinder. When entering the cylinder the oil forms a layer on the cylinder wall. This layer or "film" will have a certain thickness which will be strongly dependent on the force acting upon the oil according to [25]. The force in turn is dependent of the rotational speed of the cylinder since the centripetal force F_c is calculated according to:

$$F_c = \frac{v_{tangential} m_{obj}}{{r_{path}}^2} \tag{3.2}$$

where m is the oil's mass, r is the effective radius and $v_{tangential}$ is the tangential speed of the oil.

One dimensional layer thickness evaluation has been made according to [25]. The analogy is made between an open channel flow driven by gravity and the flow over the inner surface in an rotating annulus driven by the by the centripetal force.

In the one dimensional case it was assumed that the oil moved with the wall perfectly. This is however a simplification of reality. The oil film will move in multiple layers. Further away from

the wall will move slightly slower than the layers closer to the wall. The magnitude of the effect culminates at the wall surface where the fluid have the exact same speed as the wall. This will effect the thickness of the oil film since it is depending on the rotational speed of the layers. Thereby the thickness will be underestimated. The speed was readily appreciated to be :

$$v_{tangential} = n_{rps}\pi D_{annulus} \tag{3.3}$$

with n_{rps} beeing the rotatonal speed in revolutions per second

In the end of the cylinder the oil was assumed to be allowed to fall freely over the edge of the cylinder. At this point the thickness of the film would correspond to the critical height:

$$h_c = \left(\frac{Q^2}{b^2 g}\right)^{1/3} \tag{3.4}$$

where b is equal to the circumference of the cylinder inner wall and g is the acceleration of gravity.

This height was used as an initial value to calculate the film thickness upstreams according to equation

$$\frac{dh}{dx} = \frac{S_0 - S}{1 - Fr^2} \tag{3.5}$$

where Fr is the Freude number, $S - S_0$ is the slope equivalent and S_0 corresponds to the slope of the surface.

The Freude number is the ratio between the speed of the flow compared to the speed of propagation of a small disturbance according to :

$$Fr = \frac{V}{\sqrt{gL}} \tag{3.6}$$

where L is the depth of the of the fluid. For the test rig this was the inner wall slope of the cylinder.

$$S = \frac{fV^2}{D_h 2g} \tag{3.7}$$

where fV is the friction factor, V is the velocity of the oil, g is the gravity acceleration, D_h is the hydraulic diameter and L is the depth of the fluid.

The cylinder was divided into 17000 small segments and the thickness of the oil film was calculated stepwise starting in the far end of the cylinder going upstream. The number of elements was decided by trial and the number of elements was adequate when the thickness profile remained constant upon increasing number of elements furhter. The code can be seen in the Appendix B.5 .

3.2 Calculation

All the properties of oil was obtained from equations, which are dependent on the temperature. For that reason they were evaluated before each iteration with the average temperature, for the oil at inlet and outlet, as base. To determine the convective heat transfer coefficient the flow had to be categorized. The characteristic of the flow was evaluated according to the condition:

$$Re_{D,c} < 2300$$

where Re is the Reynolds number which is determined as:

$$Re_D = \frac{\rho u_m D_h}{\mu} = \frac{\rho u_m D_h}{\nu} \tag{3.8}$$

where ρ beeing the density of oil, u_m beeing the mean velocity of oil and μ beeing the kinematic viscosity of oil.

Since the cross section of the geometry is non-circular the diameter is replaced with the hydraulic diameter D_h, which is defined as:

$$D_h = \frac{4A_c}{P_w} \tag{3.9}$$

where A_c is the cross-section area and P_w is the wetted perimeter of the cross-section.

Depending on the Reynolds number the next step for all situations with $Re < Re_{D,c}$ is the distance for the thermal boundary layer to develop. This had to be determined according to equation :

$$L_h = 0.05 Re D_h \tag{3.10}$$

$$L_t = 0.05 Re Pr \tag{3.11}$$

where Pr is the Prandtl number, which is based on the fluids properties and is evaluated in eq. (2.27).

Next, the length of the entrance region was compared to the actual length of the tube. If flow did not reach fully developed condition before the end of the pipe eq. (3.12) was used, and if the flow was fully developed before the end of the pipe eq. (3.13) was used instead.

$$\overline{Nu}_{entrance\ region} = 8.24 + \frac{0.03\ \frac{Dh}{l}\ Re\ Pr}{1 + \left[0.016\ \frac{Dh}{l}\ Re\ Pr\right]^{2/3}} \tag{3.12}$$

$$\overline{Nu}_{tot} = 8.24\frac{L_h}{l} + \overline{Nu}_{entrance\ region}\left(1 - \frac{L_h}{l}\right) \tag{3.13}$$

When Reynolds number on the other hand satisfied the condition $Re > 10000$ the Nusselt number was calculated by considering the friction factor of the wall. The friction factor fV was calculated from eq. (3.14) and can be seen together with eq. (3.15) for $Re > 10000$.

$$f = (0.790\ ln(Re) - 1.64)^{-2} \tag{3.14}$$

$$\overline{Nu}_{turbulent} = \frac{\frac{f}{8}\ (Re - 1000)\, Pr}{1 + 12.7\ \sqrt{\frac{f}{8}}\ \left(Pr^{2/3} - 1\right)} \tag{3.15}$$

When the Re number satisfied the condition $2300 < Re < 10000$ the flow was considered to be in the transient flow region. The Nusselt number then was calculated according to eq. (3.16) that is a combination between the turbulent relation and the laminar entrance region relation.

$$\overline{Nu}_{transient} = \left\{ \overline{Nu}_{entrance\ region} + e^{\left[\frac{a - Re}{b}\right]} + \overline{Nu}_{turb}^{c} \right\}^{c} \tag{3.16}$$

When the Nusselt number was found the procedure became the same regardless of the characteristic of the flow.

The average heat transfer coefficient was then found with:

$$\overline{h} = \frac{\overline{Nu}\ k}{Dh} \tag{3.17}$$

where k is the thermal conductivity and D_h is the hydraulic diameter.

With the new heat transfer coefficient a new more accurate oil outlet temperature could be estimated with as:

$$q = \overline{h}\ A\ \left(T_{surface} - \overline{T}_{oil}\right) \tag{3.18}$$

where $\overline{h}$ is the average heat transfer coefficient, T are the temperatures respectively, A is the area and q is the heat flux. The change of the oil temperature ΔT_{oil} is:

$$\Delta T_{oil} = \frac{q}{c_{p,oil}\ \dot{V}\ \rho} \tag{3.19}$$

where ρ is the density of the oil, c_p is the thermal capacity, q is the heat flux and $\dot{V}$ is the average velocity of the oil.

When the new oil outlet temperature was evaluated the procedure was repeated all the way from eq. (3.8) but now with the new oil properties. This procedure is repeated until the evaluation temperature of oil does not change with more than $0.001°C$ between iterations.

3.3 Results

The resulting heat transfer coefficient for 10 different volumetric flows and 20 rotational speeds can be seen in Figure 3.2. It spans from 1000 W/m^2K to about 6000 W/m^2K which is a reasonable magnitude for convection in fluids which is up to around 10000 W/m^2K for the thinnest layer of the fluid that is evaluated. The heat transfer coefficient seems to be strongly related to the thickness of fluid film in contact with the cylinder wall.

The Reynolds number for all the different volume flows and rotational speed can be seen in figure 3.3. The Reynolds number does not vary more than 25% over the span of different conditions that is evaluated. In addition to this, the Nusselt number is nearly constant regardless of Prandtl and Reynolds for the analogy of choise. This is valid while the flow is within the laminar regions. The Matlab script that have been used can also be found in Section B.2 of the Appendix.

As seen in Figure 3.3 the Reynolds number occurs in the range of 0-10 for the conditions that have been evaluated.This is well inside the laminar flow region, which means that the flow will be laminar all the time.

The Prandtl number is also used and therefore plotted against the same variables in the same fashion as the Reynolds number seen in Figure 3.4

The Prandtl number has no effect on the characteristic of the flow and is solely a parameter to evaluate the heat transfer. The Prandtl number is usually proportional to the heat transfer

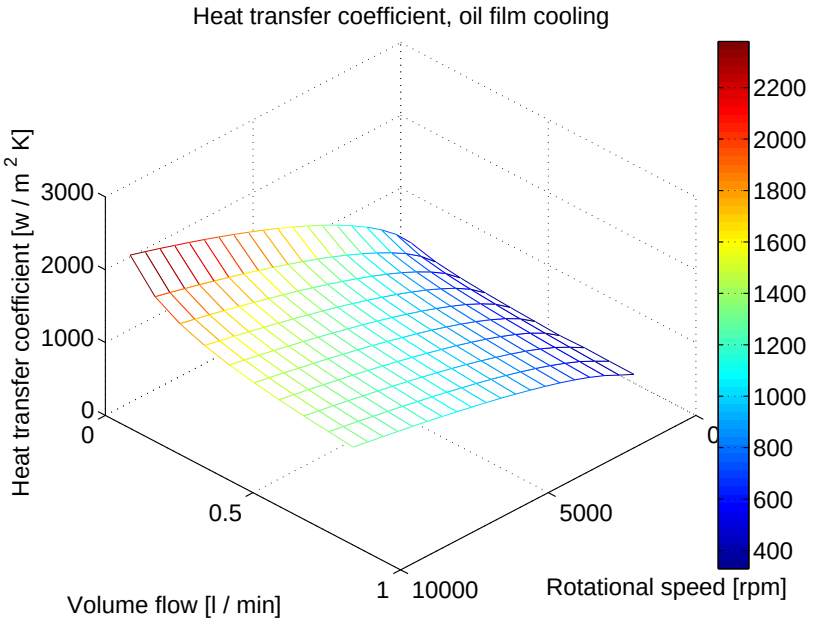

Figure 3.2: The heat transfer coefficient as a function of the volume flow and rotational speed. The curve considers all types of flow characteristics.

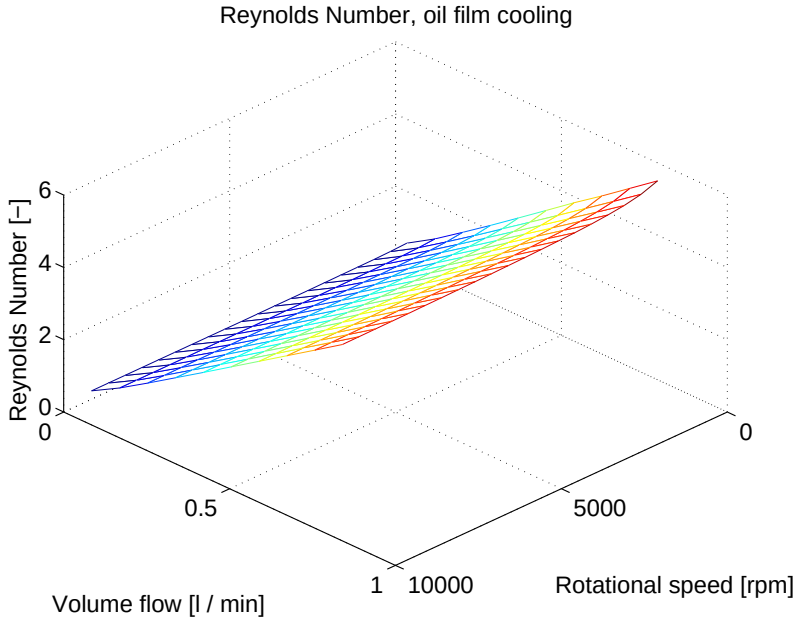

Figure 3.3: Reynolds Number as a function of the volume flow and rotational speed.

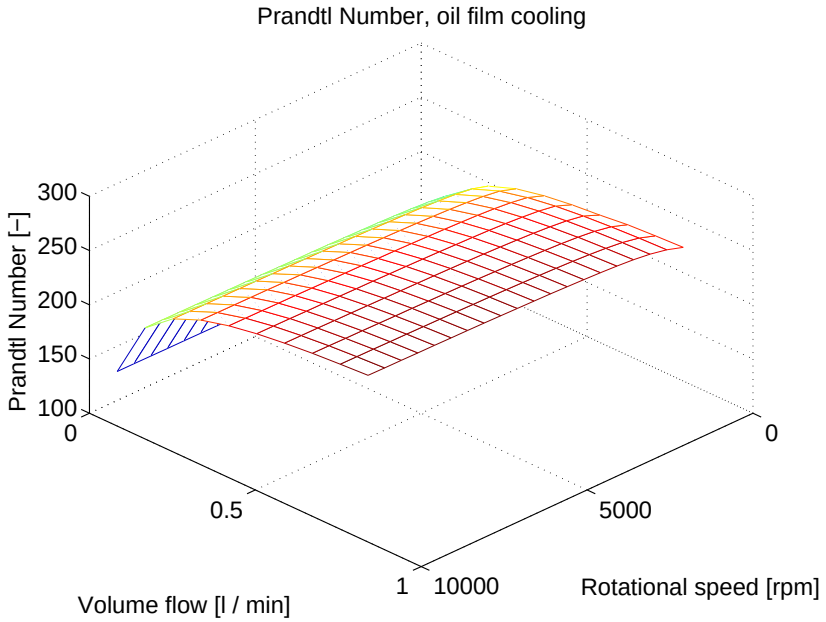

Figure 3.4: Prandtl Number as a function of the volume flow and rotational speed. This parameter can be strongly related to the temperature since it only is dependent of thermal properties of the fluid.

to some exponential but in the case of laminar flow the Nusselt number will reach a maximum and the high Prandlt number won't affect the heat transfer.

The assumption that the drag force experienced between the fluid and air surface inside the cylinder would be neglected is confirmed by the Matlab calculations. The results are displayed in in Figure 3.5. The calculation is based on the emperical relation [26]:

$$\tau = \frac{2 \cdot 0.332}{3v\sqrt{\rho\mu v l}} \tag{3.20}$$

where τ is the shear stress.

With the heat transfer coefficient an approximate average surface temperature was calculated. The results can be seen in figure 3.6. This is the average temperature of the surface and not a temperature distribution along the surface of the cylinder. The characteristics of this is strongly related to the volume flow within the ranges that are of interest as can be seen in the figure.

The magnitude of the heat transfer coefficient is strongly dependent of the thickness as seen in eq. (3.2). This is because the heat transfer coefficient is reversely proportional to the hydraulic diameter, which is proportional to the thickness of the film layer. Also when the hydraulic diameter goes toward zero the heat transfer coefficient goes towards infinity. The Prandlt number is also increasing due to temperature change but since the flow is laminar all the time for the system the Prandlt number has limited effect on the Nusselt number and thereby the heat transfer coefficient.

The analysis could also become more complete by dividing the cylinder into sections for the energy balance. The temperature of the oil could be evaluated for each section and used to minimize the error regarding same thermal properties along the entire length of the cylinder/rotor.

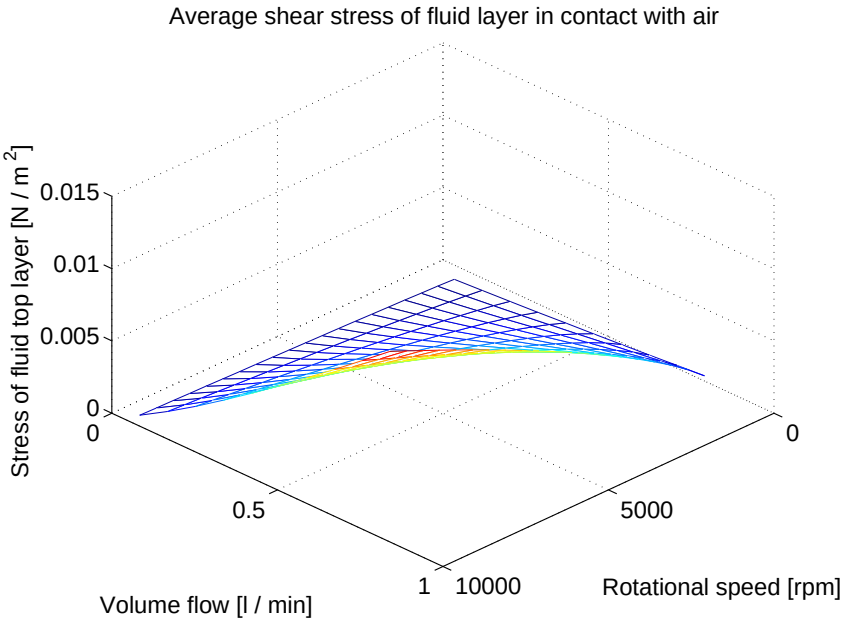

Figure 3.5: The average shear force per square meter as a function of the volume flow and rotational speed. This parameter can be strongly related to the temperature since it only is dependent of material properties.

One conclusion that can be drawn from this analysis regardless of its accuracy is that the cooling is strongly dependent on thickness of the oil film. The oil film thickness in turn is dependent on both the volume flow of the oil and the rotational speed of the cylinder.

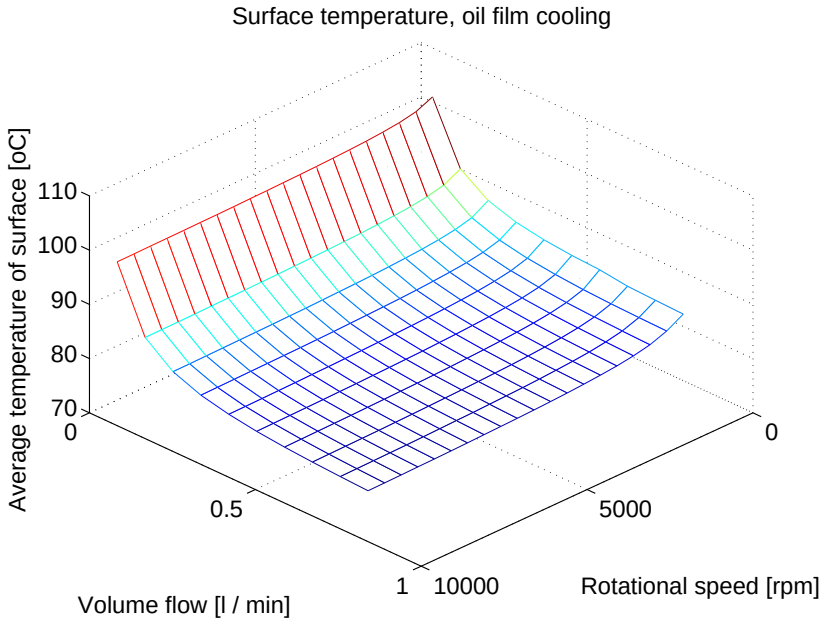

Figure 3.6: Average surface temperature of cylinder with respect to different flows and thickness of oil.

Chapter 4

Experiment

4.1 Experimental Investigation

4.1.1 Heating

The cylinder of the test rig has to be heated in order to simulate the losses of the permanent magnets and evaluate the cooling performance of the internal cooling. There are some requirements that the heating method preferably would comply with:

- Even Heat Distribution.
- Robust.
- Must heat the cylinder while rotating.
- The heating of the vicinity area must be minimal.
- Real heating power in the cylinder must be measured in an accurate way.
- Relatively high heating power.

A number of different solutions for heating the cylinder were examined: induction heating, stationary heating with airgap and radiative heating.

Induction Heating

Heating metals by induction is not something new: Michael Faraday discovered the basis for heating metals in 1831 while he was experimenting with two coils of wire wrapped around a common iron core. After the experiments, Faraday concluded the *Law of Induction*: "The electromotive force (EMF) induced in a circuit is directly proportional to the time rate of change of magnetic flux through the circuit":

$$\oint_C \mathbf{E} \cdot \mathbf{ds} = -\frac{d}{dt} \oint_S \mathbf{B} \cdot \mathbf{dA} \tag{4.1}$$

where S is the surface bounded by the closed loop C, E is the electric field intensity, B is the magnetic field intensity, and A is the area included by the surface S. Later Heinrich Lenz formulated the *Lenz's Law*:"The polarity of the induced EMF is such that it tends to produce a current that will create a magnetic flux Φ to oppose the change in magnetic flux Φ_B through the loop"[27]:

$$E = -\frac{\theta \Phi_B}{\theta t} \tag{4.2}$$

For several decades eq. (4.1) and eq. (4.2) were used to develop and design electrical machines and transformers to use electricity more efficiently. However, one by-product of this is the heat generated inside the machine's stator and the core of the transformers. To avoid the heating losses inside the transformers' core as well as inside the electrical machines' stator, they were made of laminated steel. In induction heating the exact opposite attempt is utilized: to take advantage of the above phenomena and heat metal parts by induction.

Two loss mechanisms are associated with time-varying fluxes through magnetic materials. The first mechanism is the "Joule Effect" I^2R heating which is associated to the induced currents in the core material. By looking at eq. (4.1) the time-varying magnetic fields create electric fields. These fields inside magnetic materials, which have relatively low resistance, create induced currents, commonly referred as *eddy currents*. The eddy currents circulate inside the magnetic material and oppose changes in the magnetic flux density.

The most common way to describe a magnetic material is through the *B-H curve* or *hysteresis* loop. A typical hysteresis loop can be seen in Figure 4.1 and it shows the relationship between the magnetic flux density B and the magnetizing force H. It can be observed that as the magnitude of H increases the magnetic flux B curve begins to flatten out. This is due to the occurring *saturation* of the material, and in very high magnitudes of H the material curve is almost flattened out meaning that the material is behaving like air.

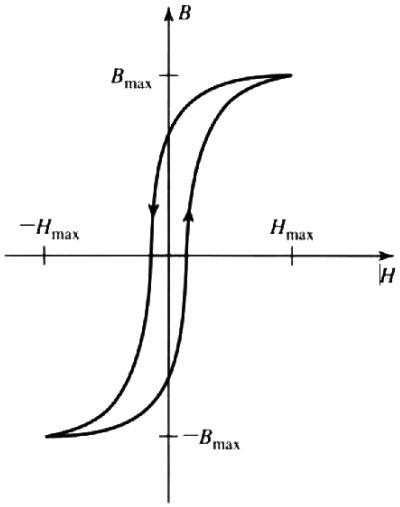

Figure 4.1: Hysteresis loop; hysteresis loss is proportional to the loop area.

The second mechanism is due to the *hysteresis losses* occurred in magnetic materials. The

energy input W to a magnetic core as the material undergoes a single hysteresis loop cycle is [2]

$$W_{hyst} = \oint i_\phi \, d\lambda = \oint \left(\frac{H_c I_c}{N} \right) (A_c N \, dB_c) = A_c I_c \oint H_c \, dB_c \tag{4.3}$$

where $A_c l_c$ is the volume of the core and the closed integral is the area of the hysteresis loop. Every time that the material undergoes a magnetizing cycle there is energy input inside the material. This energy is required to move the magnetic dipoles that exist in the magnetic core and is dissipated as *heat*. For a given flux level, from eq. (4.3) it can be observed that the corresponding hysteresis losses are proportional to the *area of the hysteresis loop* and the *volume* of the magnetic material. This is the energy that is lost in every magnetization cycle and the hysteresis loses are thereby proportional to the *frequency* of the applied excitation. When an electrically conductive part is exposed to a varying magnetic fields, the above mentioned mechanisms generate heat inside the material. If the generated heat is not dissipated, the temperature will increase.

Investigation The most important requirements for the heating methodology was to ensure that only the cylinder was heated and not the vicinity objects, and also that the power distribution was as uniform as possible along the length of the cylinder. The exact amount input power into the test object had to be known.

Metallic objects such as bearings, or the shaft of the cylinder that was located near the coil could have been heated as well by the varying magnetic field. Therefore, the magnetic flux leakage as well as the efficiency and the power factor (PF) had to be evaluated for different configurations of the induction coil. There was also a risk that the varying magnetic flux would interfere with the signal of the thermocouple. The problem could arise if a voltage was induced in the closed loop of the thermocouple.

For the reasons mentioned above the magnetic flux distribution in the area close to the coil was examined. During this thesis a number of different topologies for the induction coil were examined. Simulations with Finite Element Calculation (FEM) method were carried out to evaluate the magnetic flux distribution and heating uniformity. Simulations were carried out with FEMM software .

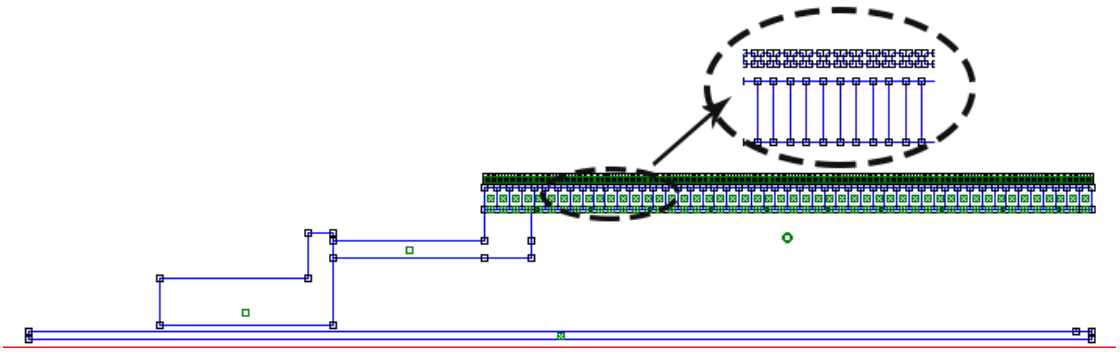

Figure 4.2: Simulation Topology for Solenoid Coil. The cylinder surface has been split into 50 segments. The induction coil is with black and it consists of 100 turns.

Topology 1 The first arrangement for the induction coil was to use a solenoid with the cylinder acting as a core. Since the problem is axis symmetric the simulation was done in a plane and the topology can be seen in Figure 4.2.

The cylinder was sliced in 50 different segments to be able to examine the uniformity of the heat generation. The coil is consisting of 100 square conductors of $A = 1.5\ mm^2$. The distance of the coil from the cylinder surface was set to be 2 mm. The most left part seen in Figure 4.2 is the telemetry system that is made of aluminium and the part in between that connects the telemetry system and the cylinder segments is the shaft that is made of steel.

The magnetic field distribution is visible in Figure 4.3 and it can be observed that a magnetic field line is quite close to the shaft of the cylinder and that there is quite high flux leakage in the vicinity area. This indicates a potential interference with the thermocouples and unwanted heating of the near component.

The FEM simulation showed that the unwanted heating of the steel shaft was retained to only 1.18 W while the total heating of the cylinder was 2.29 kW. The power distribution along the cylinder length can be seen in Figure 4.4. The heating of the other parts, such as the telemetry system and the oil lance was negligible.

The power calculations for this arrangement showed total Real Power $P = 2360\ W$, Apparent Power $S = 2568\ VA$ and a Power Factor $PF = 0.92$.

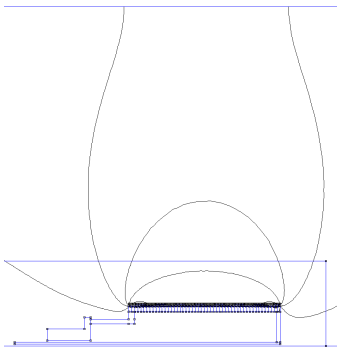

Figure 4.3: Resulting Magnetic Flux Distribution around the cylinder.

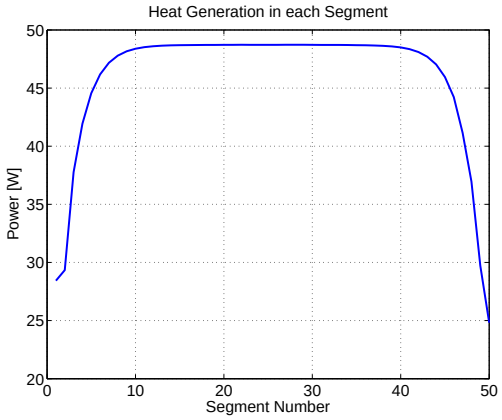

Figure 4.4: Power Distribution along the solenoid length. Every segment is 4 mm wide.

In order to improve the flux leakage of this topology the possibility of adding a core on top of the solenoid was examined. The purpose of this core was to guide as much flux as possible and to reduce the flux leakage with the lowest possible losses. For that reason SMC material was used in the simulation. The electrical resistivity value for that material was considered to be $200\mu\Omega \cdot m$ and the B-H curve can be found in the Appendix.

SM^2C offers relatively low permeability but on the other hand offers a three dimensional insulation, since it is composed of insulated metal powder particles that are pressed together and form a solid construction. A format that greatly reduces the eddy currents. The new configuration can be seen in Figure 4.5.

The new flux distribution around the cylinder can be seen in Figure 4.6 and the new power

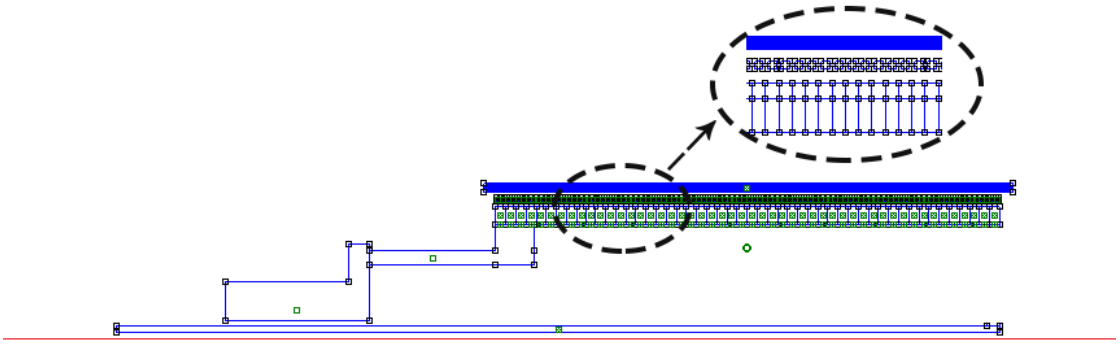

Figure 4.5: Simulation topology for solenoid coil with extra core. The cylinder surface has been split into 50 segments. The induction coil is with black and it consists of 100 turns.

distribution can be seen in Figure 4.7. Most of the flux is now going through the SM^2C material and flux leakage is reduced, compared to the case with no core.

The power calculation results of this arrangement is total Real Power $P = 4566\ W$, Apparent Power $S = 5642\ VA$ and Power Factor $PF = 0.81$. The power losses in the SM^2C material were calculated to be $P_{loss} = 503\ W$.

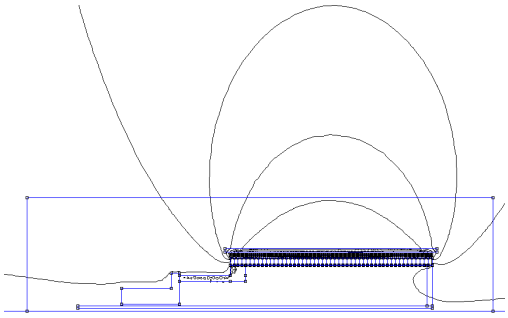

Figure 4.6: Resulting Magnetic Flux Distribution around the cylinder, Topology 1 extra core.

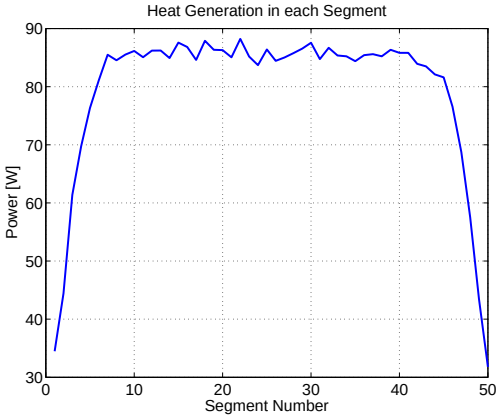

Figure 4.7: Power Distribution along the solenoid length, Topology 1 extra core. Every segment is 4 mm wide.

Topology 2 Another arrangement for the induction coil examined, was to twist the coil in one direction for 50 turns and then twist it in the opposite direction for another 50 turns. In that way, two "poles" will be created and the flux leakage will be reduced. The topology was similar to the one in Figure 4.2 except from the fact that half of the square wires was connected to a circuit with negative current.

Again, for comparison reasons a total number of 100 turns was used, 50 twisted in one direction and 50 twisted in the other, and the current through the coil was again 10 Amperes.

The magnetic field distribution can be seen in Figure 4.8, while the heat generation along the cylinder length can be seen in Figure 4.9.

It can be observed from Figure 4.8 that the field is more concentrated than in Topology 1, both with core and no core. However in this case the power distribution, as seen in Figure 4.9, is worse because there is a gap in the heat generation at the middle of the cylinder length.

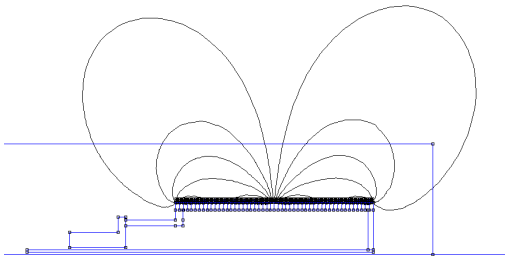

Figure 4.8: Resulting Magnetic Flux Distribution around the cylinder, Topology 2.

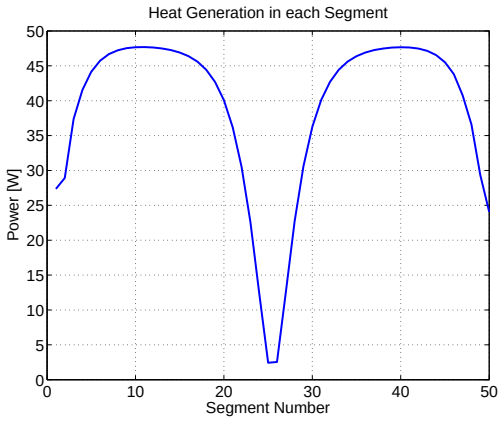

Figure 4.9: Power Distribution along the cylinder length, Topology 2. Every segment is 4 mm wide.

The power calculations of that circuit revealed total Real power of $P = 2012\ W$ and Apparent power of $S = 2320\ VA$, thus a Power Factor $PF = 0.87$.

Topology 3 The last arrangement that was examined for the induction coil was to create four "poles" by reversing the direction of twisting the coil every 25 turns. In that way an even more concentrated field could be created. The simulation results for this coil configuration can be seen in Figure 4.10 and the power distribution in the Figure 4.11.

The power calculations of this last configuration was: total Real power $P = 1440\ W$ and Apparent power of $S = 1908\ VA$, thus a Power Factor of $PF = 0.75$.

Heating with air gap

The second solution that was investigated was heating with resistive films in the stationary outer shell of the test rig. The heat would go through the outer cylinder, be transferred through the air by convection and then conducted through the inner cylinder wall. The basic idea is illustrated in Figure 4.12

To evaluate this heating method the heat transfer through air between two co-axial cylinders had to be considered. Howey, Childs, and Holmes made an empirical study of this in 2012 [28] and their empirical relations was used to evaluate the possibility of transferring heat as described in Figure 4.12.

First the hydraulic diameter was defined as $D_{Hydraulic} = 2g$ Where g is the distance between the two cylinders, length of air gap. Also the Reynolds Number was defined as:

$$Re_g = \frac{\Omega g R}{\nu} \tag{4.4}$$

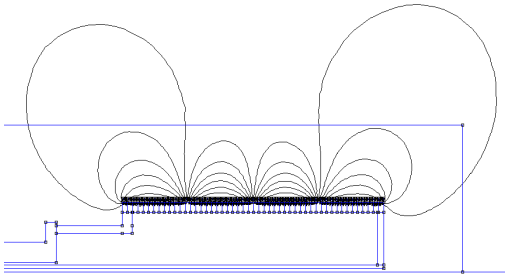

Figure 4.10: Resulting Magnetic Flux Distribution around the cylinder, Topology 3.

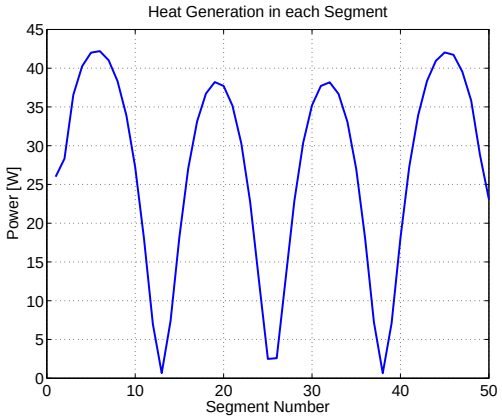

Figure 4.11: Power Distribution along the cylinder length, Topology 3. Every segment is 4 mm wide.

The Reynolds Number is proportional to the Nusselt number and the kinematic viscosity is reversed proportional to the Reynolds number. That indicates that with increasing temperature of air the heat transfer will increase. The Nusselt number is defined in eq. (3.17).

Another dimensionless number that was introduced here is the Taylor Number. It is a measure to see the behavior of the flow regarding formation of vortexes. The Taylor number Ta_m in the test rig set up is defined as:

$$Ta_m = \frac{\Omega_a r_m^{0.5} (b-a)^{1.5}}{\nu} \tag{4.5}$$

where Ω_a is the rotational speed in radians per second, a is the inner cylinder outer radius and b is the outer cylinder inner radius and r_m is the mean radius of a and b.

To determine the flow behaviour between the cylinders a geometrical factor F_g also needs to be introduced. It is defined as

$$F_g = \frac{\pi^2}{Ta_{m,cr}\sqrt{S}} \left(1 - \frac{b-a}{2r_m}\right)^{-1} \tag{4.6}$$

where $T_{m,cr}$ is calculated with the critical rotational speed $\Omega_{a,cr}$:

$$\Omega_{a,cr} = \pi^2 \nu \sqrt{\frac{a+b}{2S\,(b-a)^3\, a^2\, [1-(\Omega_b/\Omega_a)\, b^2/a^2]\,(1-\Omega_b/\Omega_a)}} \tag{4.7}$$

and S is

$$S = 0.00056 \left[\frac{1+\Omega_b/\Omega_a}{1-\Omega_b/\Omega_a} + 0.652\left(1-\frac{1}{x}\right)\right]^{-1} \tag{4.8}$$

This expression becomes simpler if the outer cylinder is stationary as in the case of the test rig. The expression can be simplified further if the air gap is considered to be small compared to the radius of the cylinders which it also is in the test rig so that $Ta_{m,cr} = \sqrt{1697} = 41.19$.

In cases where $Ta_m^2/F_g^2 < 1697 \approx 1700$ (or $Ta_m < 41.19$ since $F \approx 1$) the conduction mode is dominating in the heat transfer and therefore

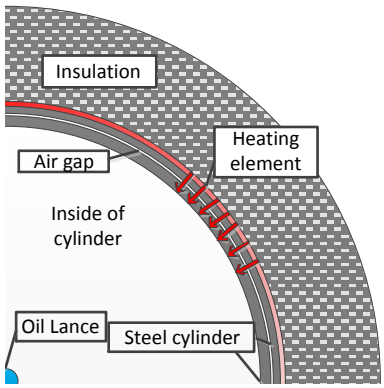

Figure 4.12: The heat is transferred through both the outer steel cylinder, which acts like a shell to make the structure stable, and the inner cylinder before it reaches the coolant. Except the conduction through the cylinders the heat also have to be conducted through the air gap between the two cylinders.

$$Nu = \frac{2\left[(b-a)/a\right]}{\left[1+(b+a)/a\right]} \tag{4.9}$$

In cases where $1700 < Ta_m^2/F_g^2 < 10^4$ with laminar flow and vortices, from Becker and Kaye [29]. Nusselt number becomes:

$$Nu = 0.128\left(Ta_m^2/F_g^2\right)^{0.367} \tag{4.10}$$

For turbulent flow where $10^4 < Ta_m^2/F_g^2 < 10^7$ eq. (4.11) is used also proposed by Becker and Kaye [29].

$$Nu = 0.409\left(Ta_m^2/F_g^2\right)^{0.241} \tag{4.11}$$

The temperature difference over the air gap spanned from about $35 - 80°C$ at its highest when the viscosity, ν, was evaluated for the air temperature $100°C$.

The temperature was set to $80°C$ to be conservative and not overestimate the possibility to heat the cylinder by this method. The temperature shifts with a few degrees when adding the conduction through the material into the consideration but maintains the behaviour of the temperature difference for different rotational speed of the cylinder as seen in Figure 4.13.

This indicates that the main cause to the poor heat transfer is the low convection over the air gap. Around 2200 rpm the temperature difference drops to about half. This is because of the vortices phenomenon discussed by Tzeng [30].

A number of different widths of the air gap was also examined. With a larger air-gap width the heat transfer became lower. The results displayed in Figure 4.13 are for an air gap of 2,5 mm and a heating power of 400 W. The curve with higher temperature gradient over gap considers the outer cylinder as a thermal resistance. This cylinder is to which the heating elements is glued or otherwise constricted.

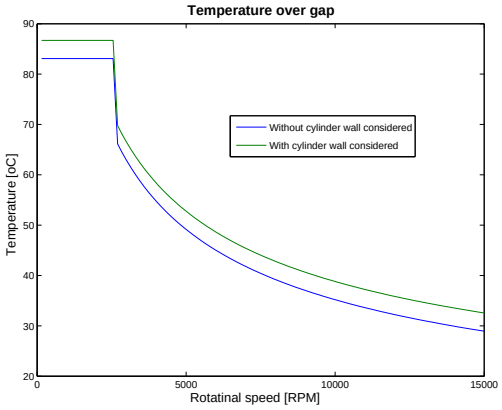

Figure 4.13: The temperature difference between the outer cylinder and the inner one when heating from the outside of the cylinder over the air gap. The heating power is 400 W and the air gap is 2,5 mm.

Radiative heating

Another alternative solution to heating the cylinder was with radiant heaters. The reason is that similar to inductive heating, the power would pass through the air gap and heat the cylinder without transfer losses to the air surrounding the cylinder. The heater could be located in a stationary part and directly heat the rotating cylinder.

The emissive power from the heater to the cylinder was calculated according to an analogy with special diffuse, grey, two-surface enclosures. The special case that was used is two infinite concentric cylinders. The infinite part of the equation means that the far ends of the cylinders are negligible which correspond to the set up for the test rig (adiabatic ends).

The equation for radiative heat transfer can be found in [26] and is:

$$q_{12} = q_1 = -q_2 = \frac{\sigma\left(T_1^4 - T_2^4\right)}{\frac{1-\epsilon_1}{\epsilon_1 A_1} + \frac{1}{A_1 F_{12}} \frac{1-\epsilon_2}{\epsilon_2 A_2}} \tag{4.12}$$

where T is the respective temperature of the bodies, ϵ is the respective emissivity of the bodies, σ is the Boltzmann's constant and F_{12} is the view factor from surface 1 to surface 2.

Since it is assumed that the model can be simplified to two long concentric cylinders the view factor becomes unity, $F_{12} = 1$ and eq. (4.12) may be simplified to:

$$q_{12} = q_1 = -q_2 = \frac{A_1\sigma\left(T_1^4 - T_2^4\right)}{\frac{1}{\epsilon_1} + \frac{1-\epsilon_2}{\epsilon_2}\left(\frac{r_1}{r_2}\right)} \tag{4.13}$$

Most of the radiative heaters of the market are either half cylindrical or a portion of a circle and the result of eq. (4.13) could be multiplied with the fraction between the arc width of the heater and its circumference to obtain the actual heating power, since only a fraction of the outer cylinder emits the heat:

$$frac = \frac{r_2 * \phi}{2 * r_2 * \pi} = \frac{\phi}{2 * \pi} = \frac{Arc\ Length\ of\ emmitter}{Outer\ Cylinder\ Perimeter} \tag{4.14}$$

where ϕ is the angle that the heater makes with it radius.

To be able to calculate the heat transfer it is important to know the emissivity of both the material. Since oxidized aluminum has a fairly low emissivity the aluminium was assumed to be spray painted with high temperature matt black paint if it was to be used. The exact emissivity of the paint is unknown but averages for oil and plastic paint, which is matt, is about 0.94. In calculations a value of 0.9 has been used to make sure that the emitted power is not overestimated.

The key factor for the evaluation of radiant heaters is the maximum power that can transmit in a certain temperature. The radiant heaters CRB10033 from Omega Engineering was chosen to be evaluated due to their availability, price and suitable dimensions. These radiant, curved faced, ceramic heaters with dimensions 245 $mm \times 60$ mm have a rated power $P = 1000$ W. Their nominal operating temperature is in $T_{nom} = 771$ $^{\circ}C$

The heaters was considered to be placed on a cylinder with diameter of $r_1 = 120$ mm and the heated cylinder diameter was considered to be $r_2 = 105$ mm.

If we consider nominal operating temperature for the heaters and room temperature for the inner cylinder and with $\epsilon_1 = \epsilon_2 = 0.9$ as discussed in section 4.1.1 eq. (4.13) becomes:

$$\begin{aligned} q_{12} = q_1 = -q_2 &= \frac{A_1\sigma\left(T_1^4 - T_2^4\right)}{\frac{1}{\epsilon_1} + \frac{1-\epsilon_2}{\epsilon_2}\left(\frac{r_1}{r_2}\right)} \\ &= \frac{\pi \cdot 120 \cdot 245 \cdot 10^{-6} \cdot 5.67 \cdot 10^{-8} \cdot (798^4 - 296^4)}{\frac{1}{0.9} + \frac{1-0.9}{0.9}(\frac{120 \cdot 10^{-6}}{105 \cdot 10^{-6}})} \\ &= 5.11 \ kW \end{aligned} \tag{4.15}$$

where

$$A_1 = \pi \cdot 120 \cdot 245 \cdot 10^{-6} \ m^2$$

and

$$\sigma = 5.67 \cdot 10^{-8} \ W \ m^{-2} \ K^{-4}$$

is the Stefan–Boltzmann's constant.
If only the fraction of the outer cylinder that corresponds to the arc that is cover by the heater is considered then from eq. (4.14):

$$fraction = \frac{67 \ mm}{\pi \cdot 120 \ mm} = 0.1777$$

and the actual heating power then becomes:

$$P = q_{12} \cdot fraction = 909 \ W$$

From this result it is shown that with nominal operating temperature and with conservative emissivity for the two bodies, the power that would be transferred is approximately 910 W.

During the experiment, the expected temperature of the inner cylinder would be maximum at $T_{max} = 150$ $^{\circ}C$ and in that case the radiative heat transfer for nominal operating temperature would be $P = 890$ W.

Heating evaluation

After this analysis not all the heating methods were found suitable for heating the test object.

Heating with a resistive element and having an air gap in between would create high temperature difference, seen in Figure 4.13. This temperature difference is deemed high when the heating element would be technically difficult to remove after the heating is done. The result would be a slow system. Furthermore, the thermal mass that will surround the inner cylinder will need to be compensated because it will exchange heat with the test object.

When it comes to induction heating, the uniformity of the generated heat could be questioned. The coil needs to be constructed and designed in a very complicated way with the highest cost of the three methods. Also controlling and measuring the actual heating power is highly questionable, because the flux leakage will heat objects in the vicinity. Controlling of the power is also complicated. Another issue that may arise is the magnetic field induces voltage to the thermocouples and alter the temperature measurements.

The third method that was analysed, radiative heating provides the possibility of much easier power control and monitoring. The heat generation will be homogeneous and have the desired power. The only consideration is the very high temperatures of the emitters and that the insulation will have to sustain those high temperatures. Because suitable insulation was found and the cost of the heaters was the least along with the other advantages, radiative heating was finally chosen as the method to heat the test object.

4.1.2 Insulation

One of the losses that were introduced in the setup was the losses from the cylinder to the surroundings. To limit this loss, insulation could be placed outside of the cylinder. There are some criteria, which the material that was to be used would have to meet.

Preferred properties of the insulation/Base material:

- Maximum service temperature of about $100 - 150°C$.
- High structural integrity between 10–$150°C$.
- High thermal resistance / Low thermal conductivity.
- Non health compromising.
- Ductile/applicable to a cylindrical geometry.
- Adequate price.
- Availability.
- Low thermal mass.

Insulation material

To meet all the above requirements a number of different insulation for insulating the cylinder were examined:

(a) Gypsum or thermoplaster which is applied to a wall for insulation and surface treatment.

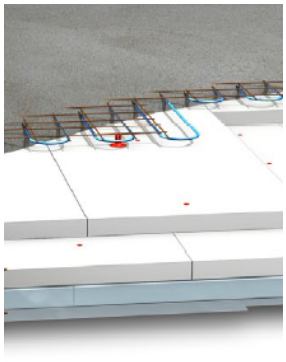

(b) Cell plastic or polystyrene often produced in blocks and used as insulation in the ground due to its resistance against cold and moisture.

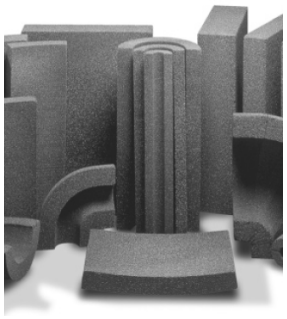

(c) Cell glass, produced in the same manner as cell plastic but with other materials. Often used to insulate pipes in the industry.

(d) Mineral wool, melted earth and glass material that is formed to fibres.

Figure 4.14: Four of the considered materials

Insulating Gypsum/Plaster This material is made up by different raw components.It mainly consists of clay, glass waste products or other sand-like materials [31]. The mixture is often bought dry in flour form and then mixed with water.

A drawback of this material is the restrictions in how thick the insulation layer can be made per layer. For a specific one, Thermopor, the maximum thickness allowed per layer is 40 mm [32]. A structure could be created thicker by a multiple-layer construction that would require more processing time. Another drawback is the high thermal mass and the difficulty to cast complex geometries.

Beside the above drawbacks its thermal properties meet the requirements for the test rig application [33].

Insulating cement This type of insulation is very similar to gypsum. The contents of this concrete is mineral wool, clay and some parts of other material, which gives the concrete its specific properties.

As the gypsum, it has the same drawbacks about insulation thickness, high thermal mass and difficulty to cast complex geometries. All other properties are suitable for the application of the test rig [34].

Cellular glass This material is widely used for a number of applications. Among them are insulating pipes. It is made by small pearls of glass. Cellular glass has excellent water resistance properties as well as strength and stability [35].

From a safety point of view the only concern is the hydrogen sulphide which through inhalation or contact with the eyes can compromise the health [36].

Polystyrene/Cellular plastics Similar to cellular glass polystyrene, a polymer, can be heated from pearls to make an insulation material by blocks. Cellular plastics however have a drawback and disadvantage compared to the cellular glass [37]: it can only sustain temperatures of about 80-90 degrees Celsius. After that point it loses its structural integrity. It is also flammable at very high temperatures [38].

Mineral fiber/Rock wool Mineral fiber or mineral wool is a generic name for fibers and wools made by raw stone and glass material melted.

It lacks structural strength and therefore, a framework or a stabilizing structure had to be constructed to encapsulate the insulation. Apart from this the rock wool material have suitable properties for the application: low thermal conductivity, high maximum service temperature and low thermal mass. The latter is because the low density of the material.

It is also available in-house so the price and time limitations does not apply to this material [39].

Selection

As shown in Table 4.1 most of the different polystyrene compounds does not sustain the temperature that would occur during the tests. The conduction of all the materials are acceptable even though some of them have significantly lower thermal conductivity than other. However, the thickness of the insulation could compensate for the lower conductivity.

All of the materials are safe to use under the right circumstances. The health risks are small and comprises irritated skin and some risks regarding respiration when produced.

Cellular glass or cement are clearly superior concerning the structural strength but the mineral wool could be used with a suitable framework.

For the above reasons insulating cement and cellular glass are the most suitable of all the materials that were examined.

Table 4.1: Table of different insulation materials that could be used in the test rig and the corresponding value of different important properties of the material

Material	**Maximum service temperature [°C]**	**Conductivity (@300 K) [w/mk]**	**Thermal mass**
Gypsum / Plaster	500	0.17	High
Insulating Cement	649 - 981	0.071 - 0.108	High
Cellular Glass	423	0.058	Low
Polystyrene	87	0.027	Low
Mineral fibre / Rock wool	1100	0.038 - 0.052	Low
Material	**Health compromising**	**Geometrically flexibility**	**Structural strength**
Gypsum / Plaster	None	Castable	High
Insulating Cement	Minor	Castable	High
Cellular Glass	Minor	Cylindrical	High
Polystyrene	None	Castable	Medium
Mineral fibre / Rock wool	Minor	Formable	porous and soft

However due to the availability and its high simplicity to further processing after it had been casted, *polystyrene* was used.

Since the fire foam has a very low thermal conductivity due to its porosity it was assumed that only a small portion of the material would be exposed to these kind of temperatures. The fact that the heater would be kept at a temperature of $700°C$ was underlining the importance of complete insulation from the fire foam since the material could not handle those temperatures.

Therefor the in-house available mineral fiber was used as an insulation later between the heaters and the fire foam. The idea was not to expose the fire foam to very high temperatures but still use its structural strength and excellent thermal properties.

4.1.3 Pump performance

To correctly evaluate the pump that had been provided by Volvo and see if it's capacity was sufficient for the test rig an investigation had to be made. The goal was to obtain a system curve with a calculation of the major losses obtained by the dimensions and properties of the tubes within some tolerance interval.

The pump

The manufacturer of the pump was MARCO and the specific model was the UP3/Oil. It is a gear pump driven by a 12 volt DC motor. The specifications and pump curve was obtained from the data-sheet [40]. The operating points where extracted the curve provided in the data-sheet and a polynomial fitting was performed.

The original graph can be seen in Figure 4.15(a) while the curve generated with polyfit on top of the original curve is visible in Figure 4.15(b) . The polynomial fit was used both to make the curve more smooth but mostly to be able to extend the curve in higher pressures and lower volumes flows.

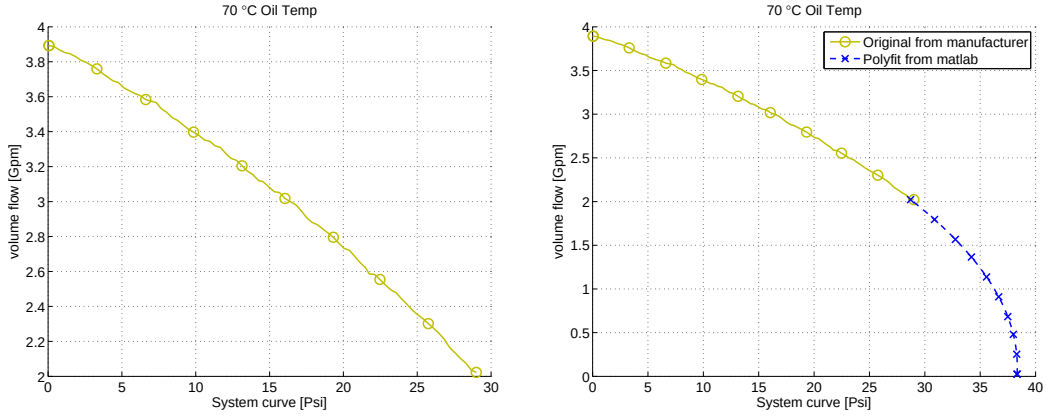

(a) Pump curve in matlab made from data series obtained via [40].

(b) Pump curve fitted with polyfit in matlab on top of the original pump curve.

Figure 4.15: Pump curve for the in house pump used in the experimental rig.

The System

Pressure loss The pipes in which the fluid that is pumped flows is defined as "The system". The losses introduced by the system can be categorized into two groups. The first group is the major losses which occurs in the straight part of the tubes due to friction between the wall and the fluid. The flow was considered to be fully developed in the whole system and for that reason no entrance region was considered. This assumption was justified by the ratio between the diameter of the tubing and the length of the tubes. The flow type is determined with the Reynolds number:

Laminar flow Losses are calculated with the average value of the velocity profile. It is calculated as [41]:

$$\Delta P = \frac{32\mu L v_{avg}}{D^2} \tag{4.16}$$

where v_{avg} is the average value of the velocity profile, μ is the dynamic viscosity, L is the length of the pipe and D is the diameter of the pipe.

The losses can be expressed with the friction factor as well. The later can be used for both laminar and turbulent flow and is therefore convenient to use. The friction factor fV for the laminar, fully developed flow is expressed as :

$$f = \frac{64}{Re} \tag{4.17}$$

Transient flow In this region, both laminar and turbulent flow may occur. This region is justified by a Raynold's number in the region of $2300 < Re < 4000$. Because the flow can be both laminar and turbulent in the value of the friction factor can be the value for both laminar and turbulent flow. The flow can also change back and forth between the two different flow characteristics. All this depends on the disturbances of the flow.

Turbulent flow In the turbulent case the equation for the friction factor is implicit which means that an iterative solution is required. Instead of the implicit relation a explicit approximation was used. The flow in the system is small and as a result the characteristics of the flow was assumed to be laminar. The friction factor is calculated as

$$\frac{1}{\sqrt{f}} = -1.8\ log\left[\frac{6.9}{Re} + \left(\frac{\epsilon/D}{3.7}\right)^{1.11}\right] \tag{4.18}$$

where ϵ is the roughness height of the pipe and ρ is the density of the fluid.

Regardless of flow characteristics, the friction factor can be used, to calculate the pressure drop ΔP with from

$$\Delta P_L = f\frac{L}{D}\frac{\rho v_{avg}^2}{2} \tag{4.19}$$

Minor losses Those loses are introduced by the system through deviation in the geometry of the pipe. Those deviations occure because of valves, area changes, bends and other deviations. Calculating minor losses has been standardized with the use of loss coefficients. The reason is that it is very hard to determine the loss over for example a knee, elbow or valve analytically. They are called minor losses since they in many cases are what the name suggests, minor, compared to the losses in the straight sections of the pipe, major losses. The pressure drop that these deviations from the straight pipe geometry causes is due to disturbance of the flow by flow separation and mixing.

The sum of the coefficient of the minor losses K_L is usually used to calculate the pressure drop or head loss h_L introduced by theses geometrical deviations:

$$K_L = \frac{\Sigma h_L}{V^2/2g} \tag{4.20}$$

where $v_{tangential}$ is the speed of the fluid and g is the acceleration of the gravity.

The major and minor head losses can then be summed as shown in eq. (4.21) and converted to pressure drop to obtain a system curve for different volume flows as done in eq. (4.22)

$$h_{L,tot} = h_{L,minor} + h_{L,major} \tag{4.21}$$

$$\Delta P_L = h_{L,tot}\rho g \tag{4.22}$$

The flow and pressure drop that will occur in the system combined with the specific pump can be found graphically by the intersection point of the two curves as shown in figure 4.16.

4.2 Measuring Equipment

4.2.1 Thermocouples

Laser Welded unshielded K-Type thermocouples from *Pentronic* were used for measuring the surface temperature of the cylinder. Further information can be found in Appendix A.

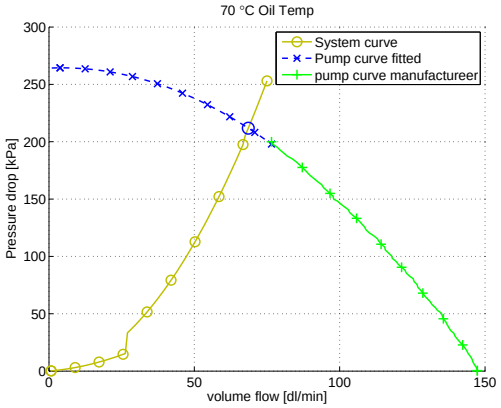

Figure 4.16: The pump fitted pump curve plotted together with the system curve. Intersection point determines flow and pressure drop for the system working together with the pump.

4.2.2 Telemetry system

A telemetry system was required to make the temperature measurements in the rotating cylinder because no physical connection in the thermocouples could be done.

The telemetry system used was manufactured by MANNER SensorTelemetrie and was found in-house. It is a custom build unit based on an existing model. It has 8 PCM channels, and it is calibrated for type K thermocouples with accuracy of 0.5 $°C$. Its output is analog with range from 0 to 10 V.

The telemetry system is made of three parts. One part which rotates with the rotating object. In the case of this thesis it was mounted on the shaft of the roller drum and then connected to the thermocouples. The second part of the telemetry system is a pickup constructed as a ring which was mounted in a base and placed in a way that the rotating part rotated inside it. Finally, the third part is the receiver unit which filters the signal and converts it to the desired interface. A schematic of the telemetry system can be seen in Figure 4.17.

4.2.3 Flow-meter

LSF80 by OVAL Instruments was used to measure the oil flow. It is a positive displacement flow-meter designed for the measurement of very small flow rates in applications requiring high accuracy.

The principle of operation is that two OVAL shaped gears which rotate when fluid passes through a fixed measuring chamber.Rotation of gears displaces a fixed volume of fluid. The sensor picks up gear rotation, which is proportional to fluid volume and flow rate.

4.2.4 Software

During the experiment a lot of different equipment had to be used for data measuring and therefore a software had to be developed to log all the signals and information in a efficient way. Then the data had to be stored so that it could be processed afterwards. For that purpose National Instruments Lookout software was used, because it was already available in-house.

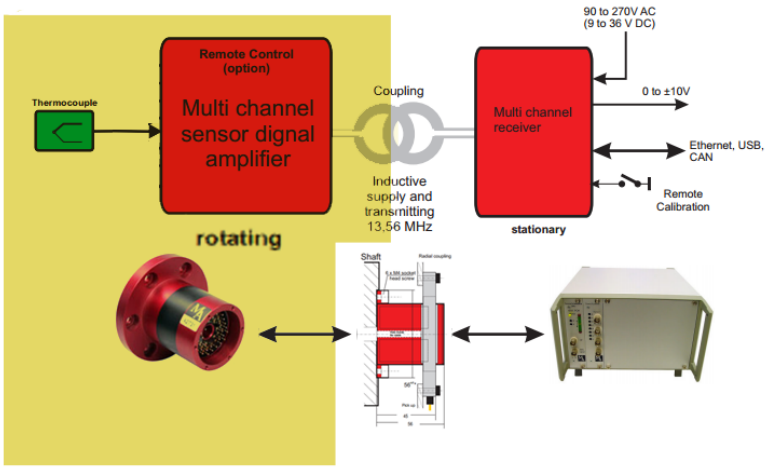

Figure 4.17: Schematic of the telemetry system. It consists of 3 parts, one rotating and two stationary. The signal amplifier along with the thermocouples are rotating. Then the signal is transmitted through the amplifier to the coupling unit and then the receiver converts it to the desirable interface.

By using NI Lookout an interface for monitoring the I/O Modules, converting and saving the signals was build. The final result can be seen in Figure 4.18.

4.2.5 I/O Modules

National Instruments FP-1600 unit was used to monitur Inputs and Outputs (I/O). It is a modular system that offers a wide variety of different input/output modules to meet different needs. Some of them are:

- 8 channel, Thermo-couple input, which offers inputs for all common types of thermo-couples as described in Section A.1.
- 8 channel, Resistance temperature detectors (RTDs) PT-100 input, which is also used for temperature measurement.
- 8 channel, Analog input which is a general analog input module, with range of -36 to +36 volts.
- 8 channel, Analog output which is a general analog output module, with output range of 0 up to +10.2 volts.
- 8 channel, Digital input which is a general purpose digital input module.
- 8 channel, Digital output which is a general purpose digital output module.
- 8 channel, 16-bit Counter Module which has eight independent counter circuits, with 4 gates as inputs and 4 outputs.

and they are connected to the PC by using an Ethernet network interface.

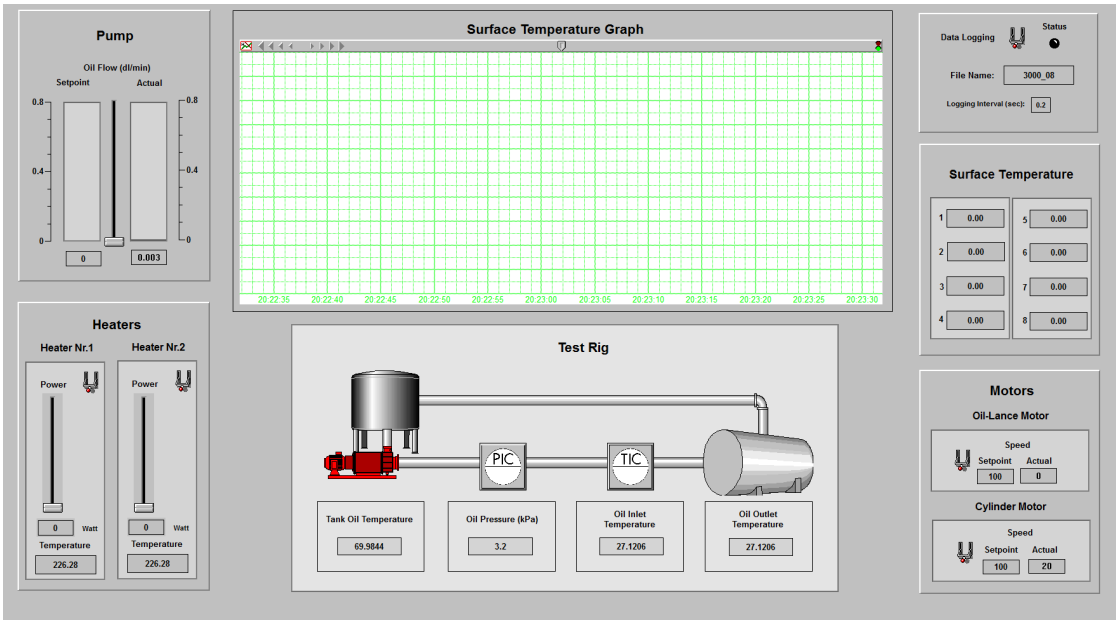

Figure 4.18: Overview of the logging interface custom build for the specific test-rig. It gathers the temperatures from the cylinder surface, as well as the heaters and the oil temperature. Also it implements the flow control by using an internal PID controller.

4.2.6 Frequency detection

To be able to monitor the oil flow and rotational speed of the cylinder through the Lookout software, a frequency meter had to be developed. This because of the outputs of the cylinder rotational speed sensor and flow meter which were varying frequency outputs.

Since there is no dedicated modules to detect the frequency of a signal, a frequency meter had to be constructed by using the existing modules. In order to detect the frequency of an input signal, the number of pulses in a certain time period had to measured and then the frequency would be

$$Frequency = \frac{No.\ of\ Pulses}{Time\ period}$$

.

Using digital input

Initially the digital input module was used to track the low and high signals from the sensors and the measurement of the pulses was done inside the software in the PC. But shortly after the implementation, measurements were incorrect. The reason was found to be in the module manual: there was an internal input low-pass filter with cutoff frequency of 50 Hz, and as a result signals with frequency of about 250 Hz and higher couldn't be measured with this specific module.

Instead of using the digital input module to track the signal of the speed sensors and the flow meters, it was then decided to use the counter module instead. The counter module has a bandwidth of 50 KHz and also has an optional input filter at 50 Hz which was disabled.

Using counter circuit

Method 1 The basic principle to be able to measure the frequency with a counter is to count the pulses which can be seen in Section 4.19. In order to measure the frequency the counter circuit is used to count the pulses for a certain period. After the end of the period the counter value is read and then the counter circuit is reseted. The the counter counts again for the next measure.

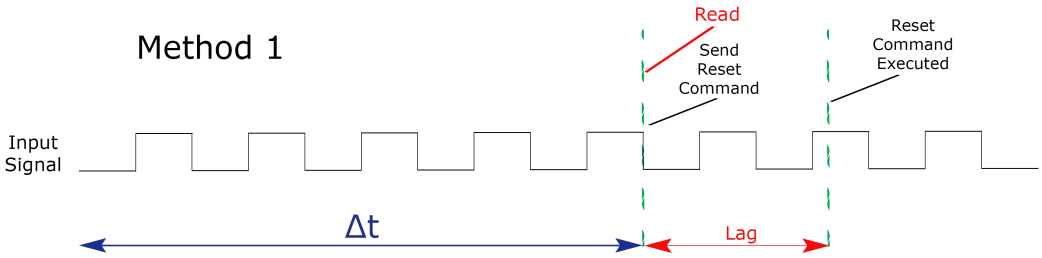

Figure 4.19: Basic principle of how to measure frequency using a counter circuit. To measure the frequency the counter measures the number of pulses for a certain period, then the value of the counter is read and after that the counter is reseted.

In theory the setup should have been able to measure frequencies up to 50 KHz, however there was always an error and a pulsation in the measurement of the frequency of a standard signal. Especially in high frequencies.The reason was then found from the NI's technical manual and was the uncertainty and lag between the commands and their execution by the modules that introduced by the Ethernet interface.

In theory the reset command should immediately follow the read command, and by the term immediately it is meant that the reset command should have been executed before the next pulse. But due to the delay introduced by the Ethernet Interface until the package that contains the command is transmitted and executed, the counter had already counted some more pulses before it was reseted. Then the counted pulses for the next measurement was less than the real number of pulses and the result was an incorrect measurement.

Method 2 To be able to solve this issue an improvement had to be done, to remove the uncertainty introduced by the Ethernet interface.Unfortunately the reset on read function of the module couldn't be used due to the limitations of the hardware. The only way of creating exact measuring intervals and reseting was to use the internal reference signals.

Another counter was used to measure the module's 1 KHz reference signal and the counter was set to be reseted by itself when its value was 999. Then one output of the module was connected internally to this counter and was changing state when the counter was reseting itself. Then a signal with period of 2 *sec* was created with 1 *sec* on-state and 1 *sec* off-state.

Then this output was connected to the gate of the counter that was counting the input signal from the flow or the speed sensor. This counter was set to count only when its gate was in the on-state. During the off-state, which now was sufficient in length, the counter value was read and the counter was reseted as it can be seen in Figure 4.20.

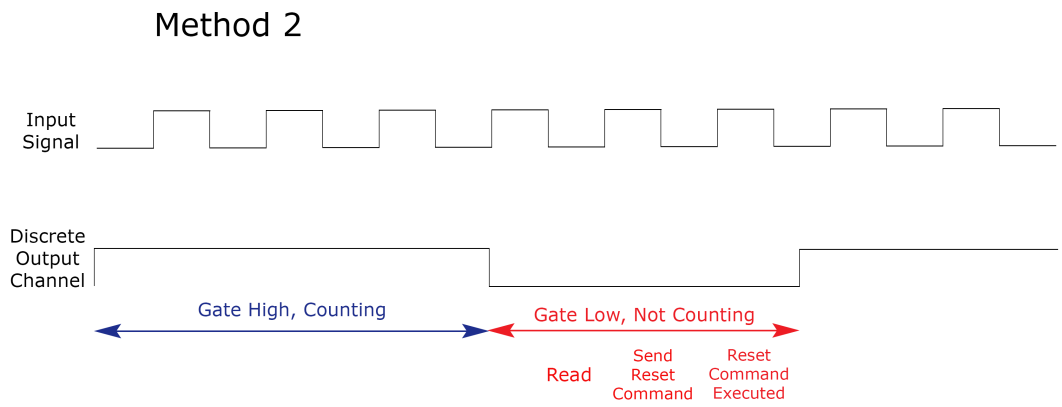

Figure 4.20: Improved method of measuring the frequency using a counter circuit. Another counter circuit is used to create the gate high and gate low signals To measure the frequency the counter measures the number of pulses only during the period that its gate is in high state.During the off-state the value of the counter is read and reseted. The counter is ready for the next measurement.

4.2.7 Frequency to voltage converter

Need for this converter

The speed of the cylinders is measured by using reflective optical sensors. The output of those sensors is a variable frequency signal depending on the speed. Also, the output of the flow-meter is also a variable frequency signal. Those two signals can be monitored and logged by using the second method developed in Section 4.2.6.

However, due to the technique of measuring the pulses that requires a dead time for reading and reseting the counter circuit, it was considered better to use the internal PID controller that the converter is equipped for faster speed control. With the same logic it was decided to use the analog input module for flow control because this would give much faster oil flow control.

To be able to use the converter's PID controller, the feedback signal should be on the analog input of the converter. A converter then had to be constructed, tuned and evaluated. A converter of the same model but differently tuned would be used to feed an analog input in order to use a PID module inside the Lookout software to control the oil flow.

Decision of the Integrated Circuit (IC)

Due to Volvo's internal policy for its suppliers only some available frequency to voltage integrated circuits where evaluated. At the time the evaluation was done the following options were available:

- Texas Instruments (TI) **LM2907**. It a typical voltage to frequency converter IC with 0.3% linearity. It comes with two different packaging option: DIL-8 and DIL-14. The second packaging allows any voltage level to be used as reference to its comparator in contrast with the DIL-8 version where only ground can be used.

- Texas Instruments **LM2917N**. This IC is similar to LM2907 but has a zener diode to regulate the input voltage.
- Texas Instruments **LM231AN**. This IC provides much better linearity of 0.01% but with price almost 6 times higher than the LM2907.
- Analog Devices **AD652BQ**. This IC provides much better linearity of 0.03% and much higher frequency input range up to 2 MHz but with price almost 12 times higher than the LM2907.

The comparison between the different IC to implement the frequency to voltage conversion can be summarized at Table 4.2.

Table 4.2: Comparison between different Voltage to Frequency IC converters.

Integrated Circuit	Frequency Range	Linearity	Volt. Regulation	Price
LM2907	up to 10 KHz	0.3 %	No	13.80 SEK
LM2917	up to 10 KHz	0.3 %	Yes	20 SEK
LM331AN	up to 100 KHz	0.01 %	No	94.40 SEK
AD652DQ	up to 100 KHz	0.002 %	No	298 SEK

At the point of decision the influence of the input voltage regulation was considered negligible and therefore for pricing reasons because the 0.3% linearity was concidered sufficient enough the *Texas Instruments LM2907* was chosen.

Principle of Operation of TI LM2907

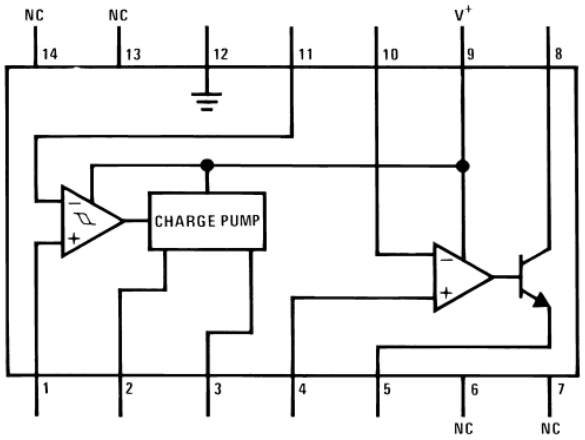

Figure 4.21: Principle of operation of Texas Instruments LM2907 IC.

Before the voltage to frequency conversion circuits are explained a short description about the principle of operation of the IC is required. An overview of LM2907 can be seen in Figure 4.21. The converter consists of 3 stages [42]:

- Input Stage
- Charge Pump
- Output Stage

where the input stage is a differential amplifier which drives a positive feedback flip-flop circuit. The amplifier also has a hysteresis loop for better noise rejection. The ground reference of the amplifier can be adjusted as the DIL-14 version of LM2907 was used.

Following the input stage there is the middle stage that consists of a charge pump. In this stage the frequency is converted to a dc voltage. To do so, a timing capacitor C_1 is used, an output resistor R_1 and a filter capacitor C_2. When the input signals swings around the reference level (reference crossing) the timing capacitor is being charged and discharged between two voltage levels with a current i_c. The voltage difference of those two voltage levels is $V_{cc}/2$. Then in one half of the input frequency the charge in the timing capacitor is $V_{cc}/2 \cdot C_1$ and the average current flowing through the capacitor is

$$\frac{\Delta Q}{T} = i_{c(AVG)} = C_1 \cdot \frac{V_{cc}}{2} \cdot 2f_{in} = V_{cc} \cdot f_{in} \cdot C_1 \tag{4.23}$$

The final stage is the output circuit, whose operation is to mirror this current $i_{c(AVG)}$ to the load resistor R_1 with very high accuracy. The pulses are smoothed by the filter capacitor C_2. The output voltage is then $V_o = i_c \cdot R1$. The filter capacitor C_2 is determined only by the desired output ripple and response time.

The total output equation is

$$V_o = V_{cc} \cdot f_{in} \cdot C_1 \cdot R_1 \cdot K \tag{4.24}$$

where K is the gain constant which is typically 1.

Initial Design

For the initial design of the Frequency to Voltage converter a reference circuit proposed by the manual of LM2907 was used. The schematic of the initial design can be seen in Figure 4.22.

The speed of the cylinder would be maximum of 10000 Rpm then $f_{in(MAX)} = 10000/60 = 166.66\ Hz \approx 170\ Hz$ and the Analog Input of the converter has a range of 0 to 10 V. If $R_1 = 10\ K\Omega$ as the reference design proposes and the power supply voltage is $V_{cc} = 12\ V$ then from equation eq. (4.24)

$$C_1 = \frac{V_o}{V_{cc} \cdot f_{in} \cdot R_1 \cdot K} = \frac{10}{12 \cdot 170 \cdot 10000 \cdot 1} = 0.49\ \mu F \tag{4.25}$$

During the evaluation of the frequency to voltage converter it was discovered that the output was not stable. This was caused by two reasons. The first reason was that the power supply contained ripple and secondly the filter capacitor was too small to filter out the output ripple. Furthermore, the output was much dependent on the input voltage and making the circuit unusable for the adjustable power supply that was used.

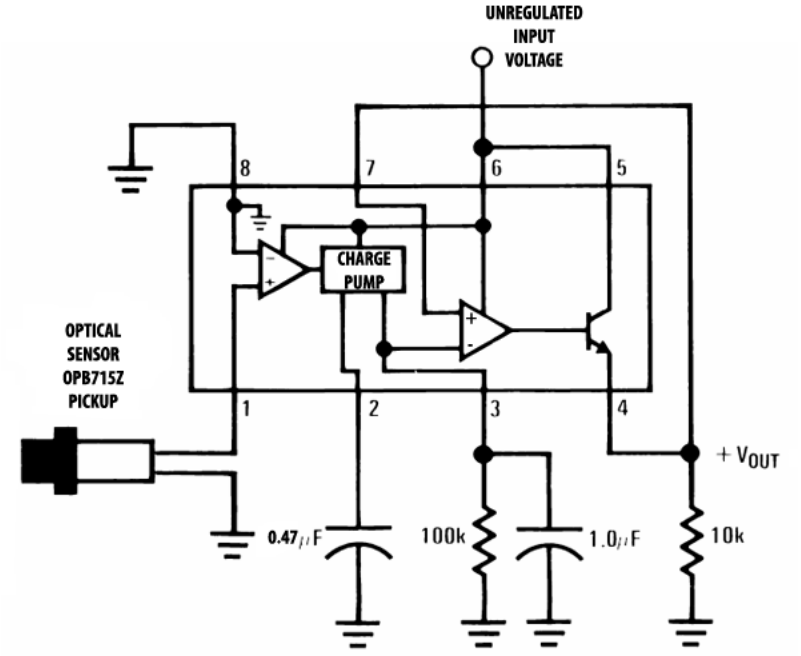

Figure 4.22: Initial design of the frequency to voltage converter as proposed by the technical specification manual of LM2907 IC. This design was not considered sufficient because the output ripple was quite high, especially in low frequencies and the output was strongly dependent on the input voltage and ripple.

Improved design

For the reasons mentioned above an improvement had to be made to eliminate the output ripple and the dependence on the input voltage. At that point it was discovered that the LM2917 would have been a better choice because it uses an internal zener diode to regulate the input voltage.

To solve those problems it was decided to use a linear voltage regulator to eliminate the dependence on the input voltage and to install an output filter to reduce the output ripple as proposed by the LM2907 manual [42].

Linear voltage regulator The linear voltage regulator L7815CV from ST Microelectronics was found in-house and was used. This linear voltage regulator offers a regulated output of $V_o = 15\ V$ for input voltages up to $V_{in(Max)} = 35\ V$. An input capacitor of $C_{in} = 0.33\mu F$ and an output capacitor of $C_{out} = 0.1\mu F$ was also used in the implementation as suggested by its data-sheet [43]. The purpose of the output capacitor is to improve stability and the transient response of the voltage regulator while the input capacitor smooths the input voltage. The latter was considered necessary since the power supply voltage contained ripple. The arrangement can be seen in Figure 4.23.

Output filter In order to reduce the output ripple in low frequencies either a bigger filter C_2 capacitor could be used or a 2 pole Butterworth filter could be used in the output. Because the

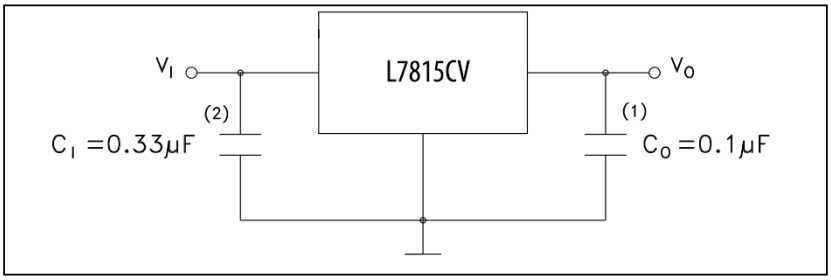

Figure 4.23: Reference circuit for the voltage regulator. The input capacitor (2) smooths the input voltage while the output capacitor (1) improves transient response.

ripple wanted to be eliminated as much as possible the Butterworth filter solution was chosen on the expense of some extra passive components.

Because it was observed that the ripple period was about $f_{ripple} \approx 4\ Hz$, $R = 100\ K\Omega$ and $C = 1\mu F$ were selected for the filter and as a result the pole frequency of the Butterworth filter is

$$f_{pole} = \frac{0.707}{2\pi RC} = \frac{0.707}{2\pi \cdot 100 \cdot 10^3 \cdot 10^{-6}} = 1.1252\ Hz \tag{4.26}$$

and the time response of the output filter is

$$\tau_{responce} = \frac{2.57}{2\pi f_{pole}} = 0.3635\ s \tag{4.27}$$

After those modification the output of the frequency to voltage converter contained ripple of less than $V_{ripple} = 1\ mV\ (p-p)$ and it was independent of the input voltage when $V_{in} > 17\ V$ because of the linear voltage regulator. The schematic of this improved design can be seen in Figure 4.24.

4.3 Experimental setup

To be able to achieve an empirical expression for the heat transfer coefficient, a test setup had to be made. The main focus of this thesis is the improvement of the permanent magnet electric machine by improving the cooling capacity of the rotor. This is done by spraying oil on the inside of the rotor.

To simplify this case with a more general analogy the rotor was replaced with a rotating cylinder where oil was introduced in the far end. The oil flew from one short side to the other cooling the inner surface along the way. The experimental setup can be seen in Figure 4.25. The oil will be flowing in the part between the blue sections. The oil lance is not visible in this figure, but it extends from the red part up to the beginning of the larger cylinder.

The rotating cylinder

The part of the test rig where the oil was flowing during the experiment contains four different types of sections all with a specific purpose. The entire roller drum setup part can be seen in Figure 4.26. All components of this part was manufactured by HB mekaniska which is a local manufacturer in the Gothenburg area.

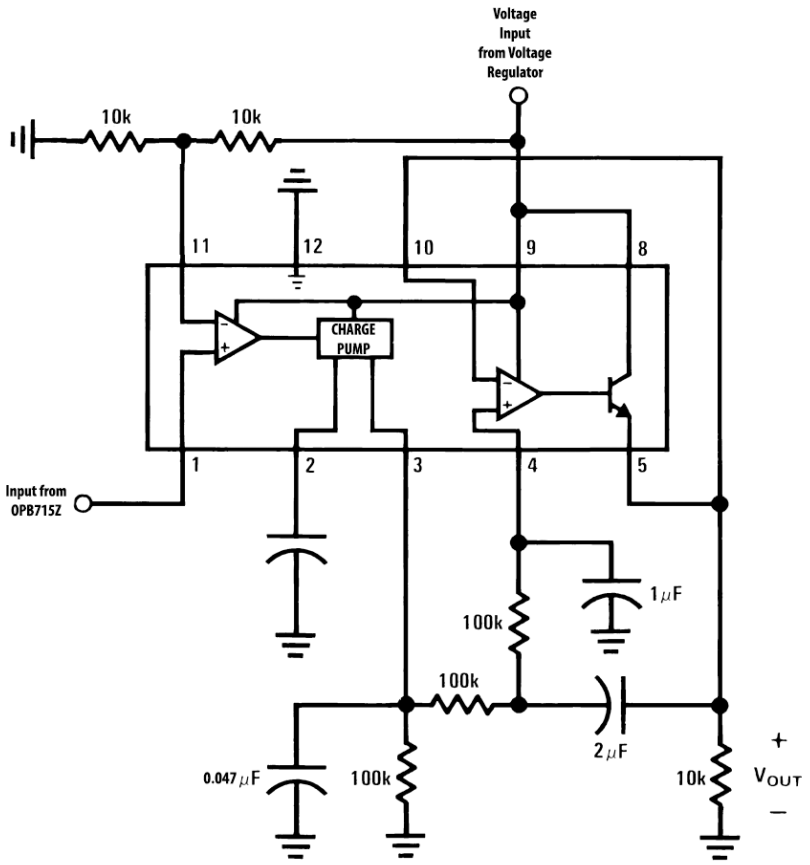

Figure 4.24: Improved design of the frequency to voltage converter. In this design there is a voltage regulator on the input to eliminate the dependence on the input voltage and also a 2 Pole Butterworth Filter is implemented in the output to eliminate the ripple at low frequencies.

Part 1 is the glass part and its lock. Part 2 is the insulation sections which are not identical but have the same function, minimizing the heat losses through the ends of the cylinder. Part 3 is the specific output profile section with the two different profiles . The last part, number 4,contains the surface on which the cooling occurs.

The test section from now will be refereed as "the cylinder", is where the oil was flowing inside and cooling the walls of it.

It was originally meant to be made of steel to have relatively high thermal mass making the impact of heat transmitted to the test setup from the surrounding less significant. However due to economical reason the steel was changed to aluminum with a much lower density and thereby lower thermal mass. This set a higher requirement on the insulation.

The advantages with aluminum apart from the economical reason was the high conductivity which gave a better tolerance for the assumption that the cylinder would have the same temperature through the walls thickness. On the other hand the high thermal conductivity would make it harder to distinguish the behavior of the cooling mechanism when high conductivity in

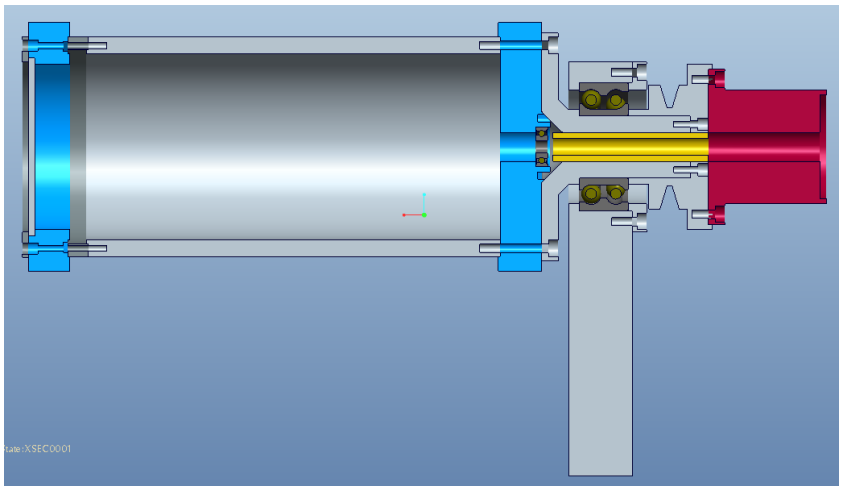

Figure 4.25: Cross Section of the experimental set up.

the material would lead to a uniform temperature throughout the cylinder.

The investigation in Section 3 indicates a rather high heat transfer coefficient of the oil film which makes it possible to determine the behavior of the cooling mechanism even though the thermal conductivity of the material was high.

Cylinder profile section was designed to make sure that there always were oil in the cylinder. In the early stage of the project it was discussed if the high rotational speed would make the oil exit the cylinder to fast. The short time would make it hard for the oil to absorb enough heat from the cylinder wall to be an efficient cooling alternative. Apart from that, another concern was if there would be dry spots in the cylinder wall which would create hot spots.

To ensure that a certain level of oil was kept in the cylinder a section with a different profile, a heel, (Seen from the cross sectional view) was going to be turned. The heel would became a threshold so that the oil level never dropped bellow the level of the heel. This profile however was planned to be placed in the far end located next to the exit as an extension to the cylinder. This would have made it possible to have other types of profiles tested. Later,in the end, it turned out by CFD analysis that there would be no problem with dry-spots and the heel profile was replaced with an ordinary profile. The CFD analysis was done by Kamilla Al Shadidi on Semcon. The other profile that was made and tested was the one that the actual rotor has currently.

The oil is extracted from the cylinder through the channels that can be seen in Figure 4.27.

Another concern with this profile was that the oil would become to viscous. This would lead to the cylinder filling up since the oil would have a hard time evacuating the cylinder. To prevent this from happening the profile in the end provides a free fall over a 90 degree edge. After this the oil was evacuated through holes in the end of the cylinder.

The see-through part was made of a transparent glass disk to provide a good view of the phenomenon taking place inside the cylinder. It was mounted between part 1 and part 2 of the roller drum seen in Figure 4.26.

The securing mechanism can also be seen better in Figure 4.28 where the glass is locked in place with a large washer that is bolted to the part in which the glass is kept.

The insulating sections were located on both far ends, directly connected to the cylinder part,

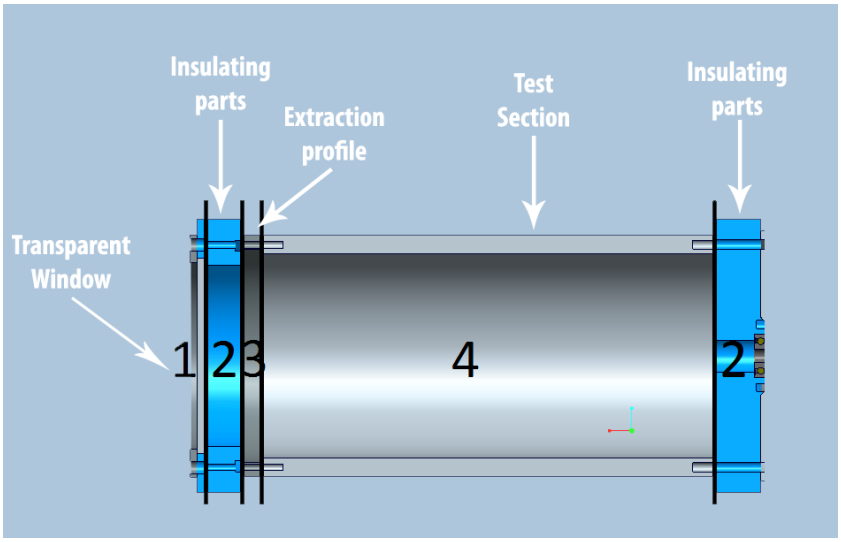

Figure 4.26: Cross Section of the roller drum section and its four parts. From one to four is see through part, insulation, profile and test section.

where the heat transfer to the surrounding occurs.

The material that was used is PEEK or Polyether Ether Ketone which can sustain high temperature and have good thermally insulating properties. The heat transfer coefficient is calculated with the temperature change in the cylinder according to the method described in Section 4.4. It was therefore important to insulate the cylinder from the surrounding as best as possible.

Wiring

To measure temperature locally at different points on the cylinder part, thermocouples had to be wired from the telemetry unit all the way to the cylinder. The wires was mounted outside the cylinder. This introduced some concerns about the forces directed outwards from the center of the cylinder and the only way to induce a centripetal force was by gluing them to the cylinder.

Another concern was that the path that the wires was put could not have any sharp edges. This since the large forces that they would be exposed to from the high rotational speed. A sharp edge of a bend with $< 45°$ would put the wire at risk of tearing.

Also the wire was placed inside the rig as much as possible. This to provide the wires with a solid base for the centripetal force instead of using glue. The section of the path that the wires were put where the oil lance went trough the telemetry system a special part had to be manufactured. The purpose of the part was to make sure that the wires did not come in contact with the rotating oil lance which rotated in a different speed.

Base and bearings

The base was only needed to keep the bearings that would hold the rolling drum construction. It was important that the base was made out of a robust material so that the setup wouldn't start to vibrate.

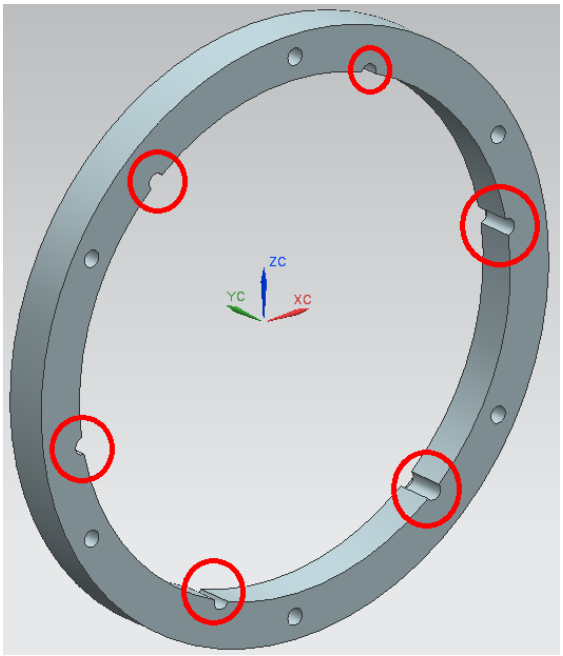

Figure 4.27: Oil channels replicating the channels of the real electrical motor.

The bearing had to sustain the forces from the cylinders weight introduced by gravity. To be able to have clear view at one end of the cylinder it was preferable if the roller drum could only be rested on a bearing on only one side. For this to be possible it was important to find a bearing that could handle the torque generated by the weight of the cylinder. Therefore an angular contact bearing was selected that could withstand forces in the radial and in the axial direction.

Oil lance

The method regarding dimensioning is found in Section 4.1.3. However, there was an upper limit of the lance dimension since it had to go through the telemetry system which had an inner diameter of 14 mm.

Therefore the oil lance had inner diameter of 4 mm and outer of 6 mm. With that O.D. it was sufficient space to place in between the oil lance and the telemetry system a cable holding part and the thermocouple wires as well.

Oil connection

To be able to connect the oil lance and the hose from the oil bath a special connection had to be made.

This connection allowed the hose to be fixed in the axis that the oil lance was rotating around. This by connecting the two by a sealed bearing. The construction can be seen in Figure 4.29.

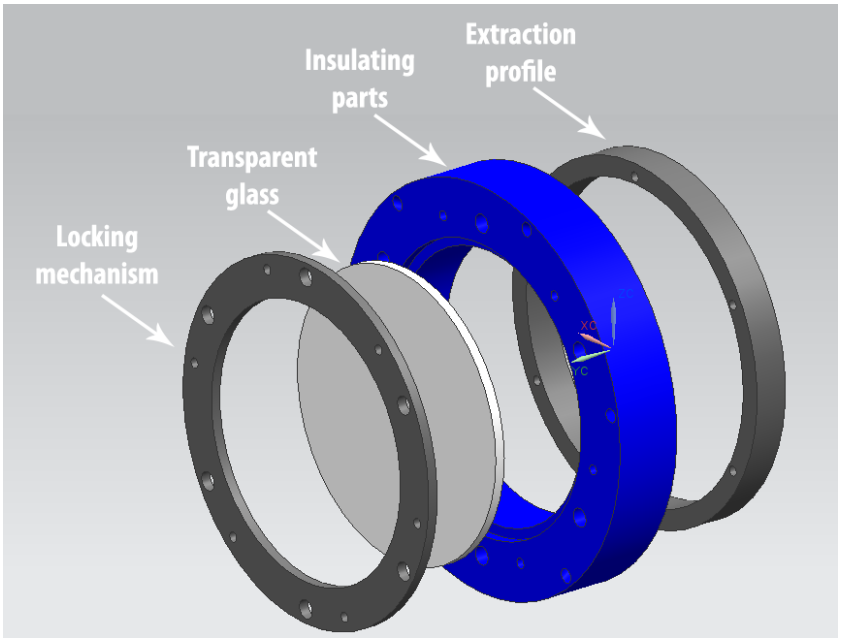

Figure 4.28: Last part of the roller drum. The transparent glass is visible along with its locking mechanism, one insulation material and the metal ring that creates the extraction profile.

The heater

The heater that has been used is the Curved Face Ceramic Radiant Heaters from Omega with the desired power output for the setup. According to the datasheet the heater would give a power output of 1000 Watts. This at max working temperature radiating on objects at a temperature of about $20°C$. [44] The actual heater can be seen in Figure 4.30 bellow.

4.4 Post process data treatment

As stated in 2.2.2 the dimensionless numbers simplifies the calculation of complex phenomenon. An outline of the thesis was to find an empirical relation according to the form of eq. (2.23). The Nusselt eq. (2.25), Prandtl eq. (2.27) and Reynolds eq. (3.8) Number for each specific test situation was determined.

The steady state case

In the steady state test case, equilibrium between heat going to the cylinder and heat removed from the cylinder had to be achieved. During the phase of steady state data would be collected.

The heat transfer coefficient which is a function of the Nusselt number is calculated by its definition from eq. (4.28). The thermal properties of oil, which are important for the calculation, were evaluated for the temperature in each point of the cylinder. These properties were: thermal conductivity, density, specific heat and viscosity. The average value was then used to minimize

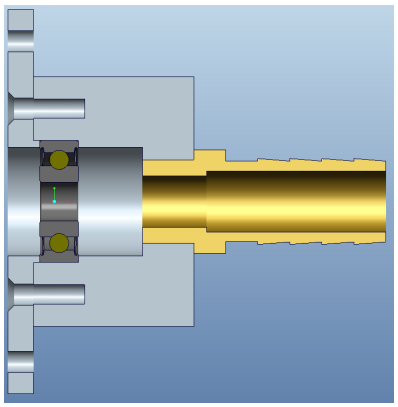

Figure 4.29: The oil connection with its bearing and connecting nozzle for the hose.

Figure 4.30: The heaters used in the test rig. In total two heaters were used that could provide 1000 W of heating power each and they also had a thermocouple to monitor their temperature. They were manufactured by Omega Engineering.

errors due to nonlinear thermal properties.

$$h = \frac{Q}{A\Delta T} \tag{4.28}$$

where Q is the heating energy and A is the area.

Q was to be determined by the temperature difference of the oil in the end of the cylinder compared to its temperature in the beginning. It was thereby assumed that the cylinder is completely adiabatic to its surrounding with exception for the surface in contact with oil. The temperature change in oil would be due to heat flow that could be determined from:

$$Q = \dot{m}c_p\Delta T = \dot{V}\rho c_p\Delta T \tag{4.29}$$

where the mass flow $\dot{m}$ in turn is determined by the volume flow $\dot{V}$ and the density ρ.

The characteristic area is the inner wall of the cylinder where the heat transfer occurs which is $A = 2r\pi L$.

The Reynolds number on the other hand was harder to find from purely experimental data. To achieve this dimensionless number the relative velocity of the fluid compared to the surface over which it flowed had to be determined. The thickness of the fluid was not experimentally determined in this thesis but described analytically according Section 3.1.6.

By calculating the thickness of the oil film an average velocity for the oil could be determined according to :

$$v_o = \frac{\dot{V}}{A_c} \tag{4.30}$$

where A_c is the cross section area of the oil film in a plane perpendicular to the direction of flow (a*xis of cylinder*).

The thickness of the oil film was also used to calculate the Hydraulic diameter according to eq. (3.9) (A*nalogy with long rectangular duct*).

The Prandtl number as displayed in eq. (2.27) is just based on three of the thermal properties of the fluid that are evaluated in the same manor as earlier.

The transient case

In the transient case, the cylinder is heated to a certain temperature, time for temperature to stabilize is given and then heating is removed and cooling is applied simultaneously. The measurement is done in a predetermined time interval with a predetermined sampling rate.

Average situation

In the same manor as the steady state case it was assumed that the thermal properties of the fluid can be represented for the entire interval by using the average of all the individual measuring points. The heat transfer coefficient is also calculated in the same way as the steady state case according to eq. (4.28). Q could in this case be derived from the change in temperature of the cylinder surface. This is the main difference between the transient measurement and the steady state measurement.

Local Treatment

For this post process the heat transfer coefficient could be calculated not as an average but in every measure point there is along the cylinder axis. In this local situation the temperature of the oil was calculated through the heat flux from the previous segment.

Since Nusselt varies with Reynolds and Prandtl exponentially values are evaluated with a logarithmic base to make the dependence linear. The linear correlation is found with linear regression. The code for these three post processes can be found in Appendix B.5.

4.4.1 Results-Discussion

Temperature

The first step was to confirm that all of the thermocouples was working properly. To evaluate this an ordinary temperature plot was created. Strange behavior can be seen in the 7th position in Figure 4.31(a). This could be caused poor contact between thermocouple and the cylinder wall with either air or glue in-between. Also in the 8th position these tendencies appear although not as strongly as in the 7th position.

The same strange behavior of the temperature of the 7th position occurs in the highest speed and volume flow as can be seen in Figure 4.32(a).

The initially lower temperature could be explained with a small air pocket surrounding the thermocouple. This would make the thermocouple insulated. However it initially cools faster than the other positions. A thermocouple out of position could be an explanation for this. If the thermocouple is further out than the others it might be cooled from the air surrounding

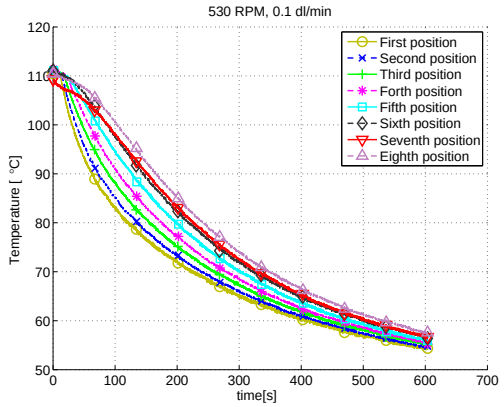

(a) Temperature registered over time for each individual thermocouple.

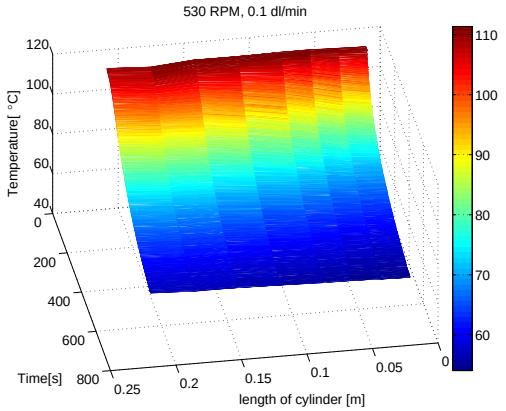

(b) Same as Figure 4.31(a) but mapped in a 3D graph.

Figure 4.31: First set up tested, lowest volume flow and lowest RPM.

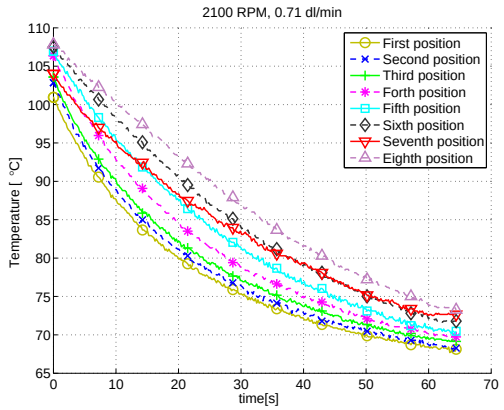

(a) Temperature registered over time for each individual thermocouple.

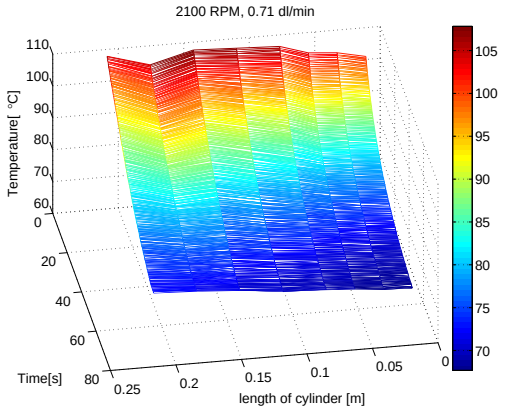

(b) Same as Figure 4.32(a) but mapped in a 3D graph.

Figure 4.32: Highest volume flow and RPM tested. Restriction in speed arose from the oil collection system.

the cylinder. Although this seems unlikely since the cooling capacity of the surrounding air is extremely low compared to the capacity of the oil.

The behavior of the 7th thermocouple is most visible with the highest rotational speed and lowest volume flow, seen in Figure 4.33(a).

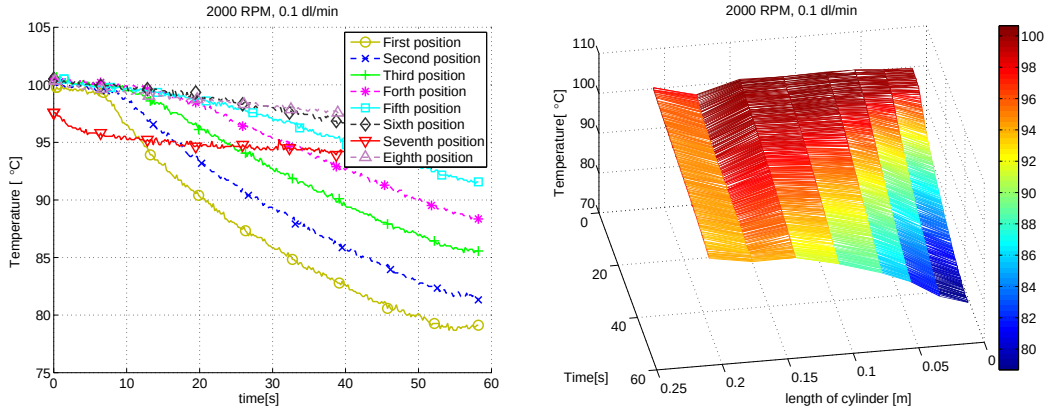

(a) Temperature registered over time for each individual thermocouple.

(b) Same as Figure 4.33(a) but mapped in a 3D graph.

Figure 4.33: Highest RPM and lowest volume flow possible.

Basic cooling comparison

The next step was to compare the different setup with each other. First a comparison between the different rotational speeds were made. How rotational speed influences the cooling can be seen in Figure 4.34(a). The temperature gradient is of larger magnitude with a higher rotational speed. This as expected from the theoretical analysis.

The cause of the larger magnitude is that the oil layer becomes thinner and thereby the heat transfer becomes more efficient. A thinner oil layer permits a greater speed of the oil over the surface due to continuity.

In the second plot, seen in Figure 4.34(b), the rotational speed is kept constant and the volume flow of the oil is altered. As seen in the figure the oil inlet temperature changes with different speed when comparing the 3 presented cases. The reason the oil inlet temperature changes is that there was no recirculation on the plumbing for the oil between reservoir and inlet.

Ideally, when comparing different cases, only one parameter changes at the time. Here both the temperature gradient of the oil inlet and the volume flow of the oil changes between the cases. Even though the temperature difference between cylinder wall and oil is decreasing more rapidly in the higher volume flow case the gradient of the cylinder temperature is still larger. This would indicate a better heat transfer in higher volume flow of the coolant.

When examine the other positions on along the cylinder they exhibits the same behavior. This effect was only visible in higher volume flows.

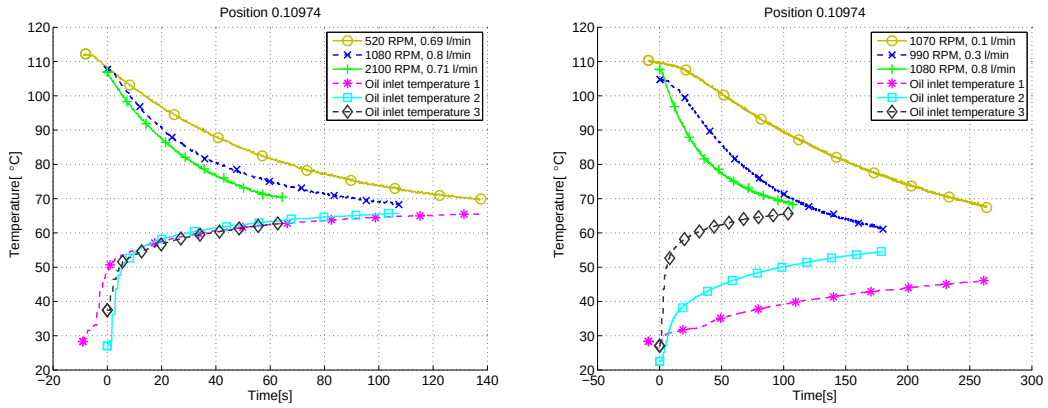

(a) Varying rotational speed. At higher rotational speeds the cooling effect is stronger due to thinner oil film.

(b) Varying volumetric flow. At higher flow rates the thermal mass of the coolant increases. Hence is the cooling effect larger.

Figure 4.34: Temperature variation over time for a specific measuring point.

Heat transfer Coefficient

It can clearly be seen in the plot that higher volume flow of oil, yield a better correlation between theoretic and experimental results. Based on exclusion, this could be caused by inaccuracy of the thickness model for lower volume flow. There is also a quite wide range for the value of the heat transfer coefficient for the same case. Idealy this should be constant during the entire measurement. It is most likely due to the change in inlet temperature of oil. With these test results it would be favourable to re-conduct the test to get new data. With recirculating coolant and all thermocouples secured in their slots more reliability could be ascribed to the data. The behavior of the heat transfer coefficient is irregular. Even though the order of magnitude agrees well for most of the cases with the theoretical analysis. The results are visible in Figures 4.35-4.37.

Two different linear regression analysis were made. Average for the dimensionless numbers spaning the entire test duration was used in the analysis. In the first analysis all of the tests where used. In the second one only the tests with higher volume flow was used. Unfortunately the small selection made results unreliable. The result is presented in Figure 4.39.

The red boxed number is the power coefficient of the Reynolds number. Since the regression is linear it is done on a logarithmic base. A is the Nusselt number, B is the Reynolds number and C is the Prandtl number.

The Nusselt number for these tests agreed the most with the theoretical values. These were for the highest oil flows. The numbers of observations is too small to draw any conclusions.

For comparison the Nusselt number, proportional to the heat transfer coefficient, was generated from the coefficients achieved with regression. It was plotted along with the experimental data for the case of 1000 RPM and 0.3 dl/min and can be seen in Figure 4.40.

This study is only partial so it would be difficult to draw conclusions from it. It is however clearly visible that the experimental values correlate to the theoretical calculations withing less than 1 exponent in order of magnitude. The measured heat transfer coefficient is however lower than the theoretically calculated for the lower volume flow. In these cases the runs are longer

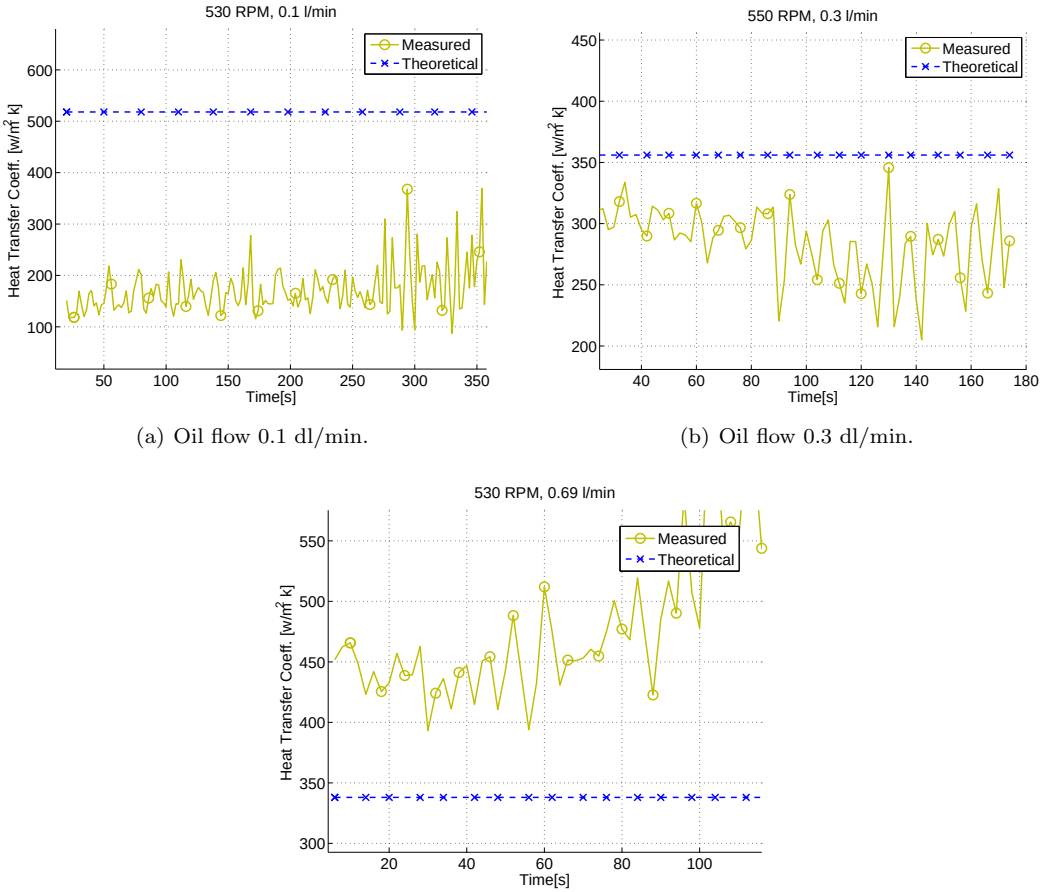

(a) Oil flow 0.1 dl/min.

(b) Oil flow 0.3 dl/min.

(c) Oil flow 0.7 dl/min.

Figure 4.35: Heat transfer coefficient for 500 Rpm and different oil flows.

and the flow has time to stablize before sampling is started. The difference is larger for lower rotation speed of the cylinder. The difference between experimental- and theoretical, in the lower rotational speeds, indicates a restriction in the heat transfer between oil and cylinder wall. This could be caused by an uneven distribution of the oil. With increasing rotation speed they start to converge. In the higher rotational speed and volume flow the measurment sequences are quite short due to various limitations. This could be the cause of the theoretically calculated heat transfer being lower than the experimental one for some specific cases.

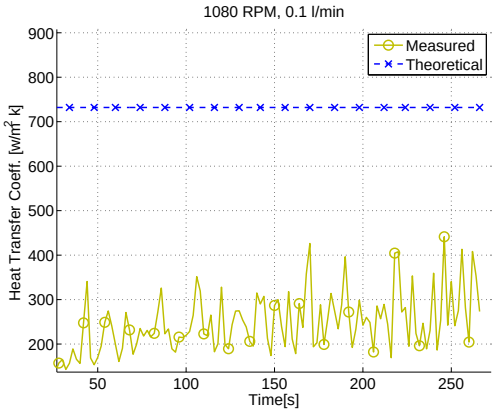

(a) Oil flow 0.1 dl/min.

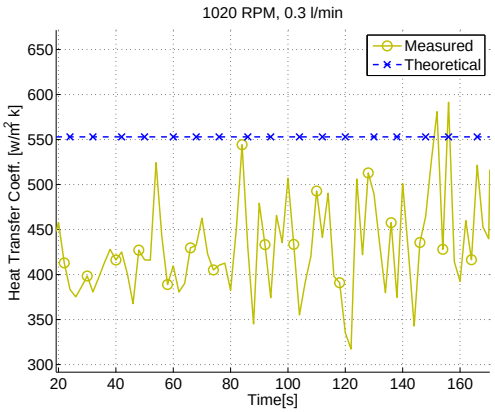

(b) Oil flow 0.3 dl/min.

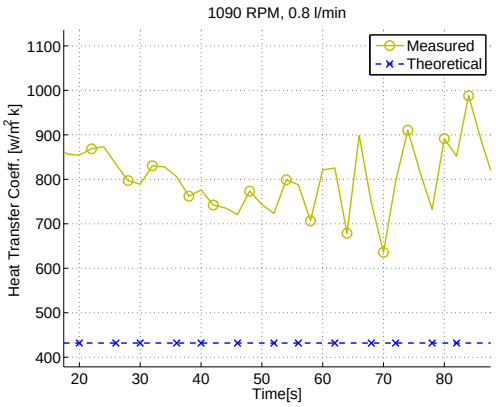

(c) Oil flow 0.8 dl/min.

Figure 4.36: Heat transfer coefficient for 1000 Rpm and different oil flows.

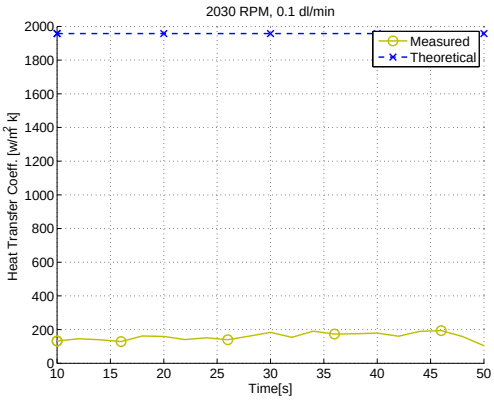

(a) Oil flow 0.1 dl/min.

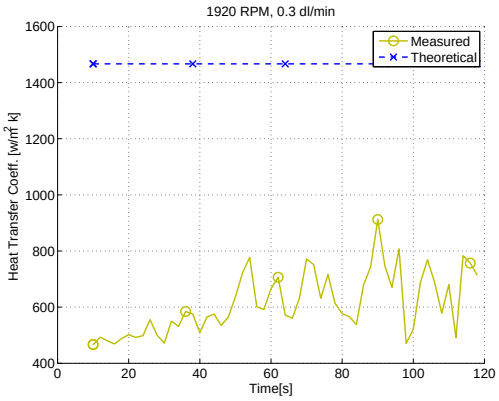

(b) Oil flow 0.3 dl/min.

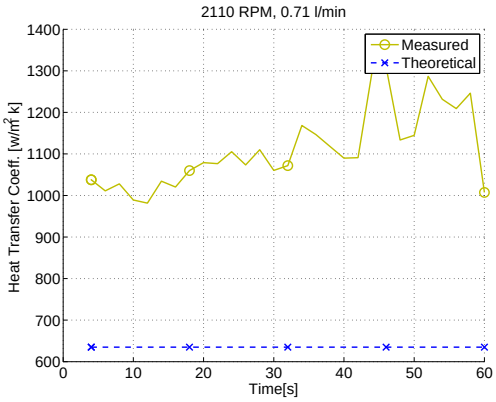

(c) Oil flow 0.7 dl/min.

Figure 4.37: Heat transfer coefficient for 2000 Rpm and different oil flows.

Linear Regression

Regression Statistics	
R	0,9843
R Square	0,96884
Adjusted R Square	0,96439
S	0,42082
Total number of observations	9

A = 1,0428 * B - 0,0438 * C

ANOVA

	d.f.	SS	MS	F	p-level
Regression	2,	38,54593	19,27296	108,83081	0,00001
Residual	7,	1,23964	0,17709		
Total	9,	39,78557			

	Coefficients	Standard Error	LCL	UCL	t Stat	p-level	H0 (2%) rejected?
Intercept	0						
B	1,04284	0,22241	0,37607	1,70961	4,68883	0,00224	Yes
C	-0,04381	0,08423	-0,29631	0,20869	-0,52013	0,61901	No
T (2%)	2,99795						

LCL - Lower value of a reliable interval (LCL)
UCL - Upper value of a reliable interval (UCL)

Residuals

Observation	Predicted Y	Residual	Standard Residuals
1	1,03616	0,28001	0,72019
2	1,77338	0,24575	0,63317
3	2,564	0,06803	0,18167
4	1,19067	0,15303	0,39761
5	1,90883	0,18513	0,47915
6	2,79609	0,1078	0,28271
7	1,55429	-1,01191	-2,56189
8	2,08406	-0,00511	-0,00415
9	2,84864	-0,05404	-0,12845

Figure 4.38: Regression analysis for the total average of each dimensionless number in each test. 9 observations in total.

Linear Regression

Regression Statistics	
R	0,99976
R Square	0,99953
Adjusted R Square	0,99906
S	0,10458
Total number of observations	3

A = 0,7964 * B + 0,0869 * C

ANOVA

	d.f.	SS	MS	F	p-level
Regression	2,	23,159	11,5795	1 058,82544	0,02173
Residual	1,	0,01094	0,01094		
Total	3,	23,16994			

	Coefficients	Standard Error	LCL	UCL	t Stat	p-level	H0 (2%) rejected?
Intercept	0						
B	0,79636	0,45433	-13,66064	15,25336	1,75282	0,33006	No
C	0,08688	0,22795	-7,16648	7,34023	0,38114	0,76818	No
T (2%)	31,82052						

LCL - Lower value of a reliable interval (LCL)
UCL - Upper value of a reliable interval (UCL)

Residuals

Observation	Predicted Y	Residual	Standard Residuals
1	2,65026	-0,01823	-0,24507
2	2,82268	0,08122	1,09975
3	2,8579	-0,06331	-0,85468

Figure 4.39: Regression analysis for the total average of each dimensionless number in the tests with highest oil flow but different rotational speed.

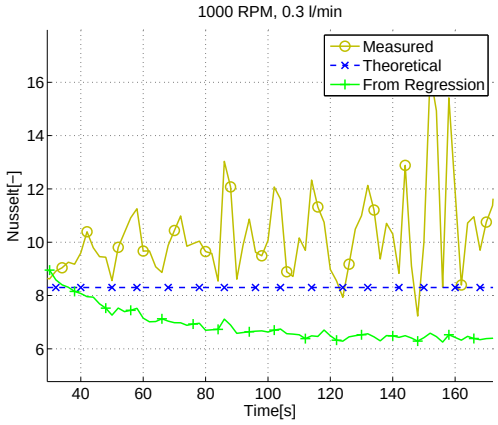

Figure 4.40: Nusselt number presented as for 1000 RPM and flow 0.3 dl/min.

Chapter 5

Permanent magnet temperature

5.1 Temperature Effect in Magnet's Performance

5.1.1 Simulation Topology

Modeling permanent magnet in FEMM software is not straightforward. In the following simulation the permanent magnet is modeled as a ferromagnetic material surrounded by an equivalent surface current [45]. This surface current will create an equivalent field as the permanent magnet coercivity.

Then the B-H demagnetization curve of the permanent magnet seen in Figure 2.7 is shifted to the right by its coercivity H_c and as a result the whole curve moves into the first quadrant starting from (0,0). Now an opposing magnetic field equal to H_c will cause B=0 in the magnet and the magnet is modeled as a normal ferromagnetic material that the software can handle.

To illustrate the temperature effects in a Neodymium Iron Boron magnet a simple magnetic circuit was made in FEMM software. This magnetic circuit can be seen in Figure 5.1. A coil in the left side of the coil is used to create an opposing magnetic field, and the B-H curves for different temperatures seen in Figure 2.7 will be used to illustrate how temperature rise in the magnet can cause demagnetization of them.

Load line of magnetic circuit

The total flux Φ going through the magnetic circuit is:

$$\Phi = B_m A_m = k_1 B_g A_g \tag{5.1}$$

where factor $k_1 \geq 1$ accounts for the leakage of flux outside the gap, ideally one if there is no flux leakage, A_c is the cross-section area of the airgap and magnet respectively and B is the magnetic flux density in the airgap and in the magnet respectively.

Additionally the summation of the MMF drop across the magnet and the airgap is equal to the MMF produced by the coil:

$$H_m l_m + k_2 H_g l_g = NI \tag{5.2}$$

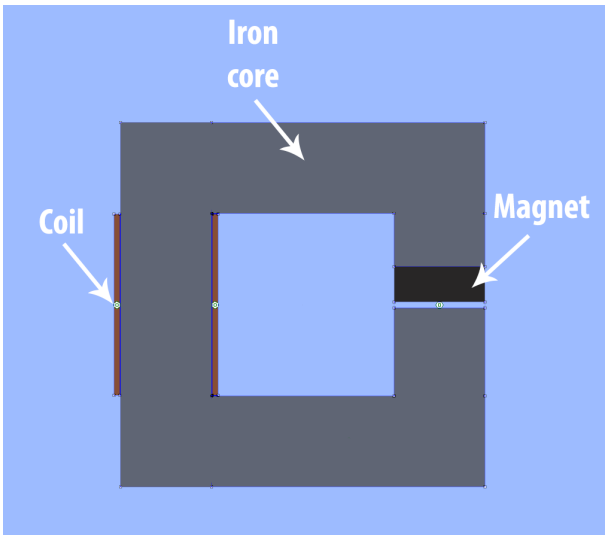

Figure 5.1: Simulation Topology for examining the temperature performance of a permanent magnet in opposing magnetic fields. The gray domain was simulated as pure iron, the black domain is the NdFeB magnet and the light blue is the air domain.

where compensation factor $k_2 \geq 1$ accounts for the finite permeability of the iron core and the loss in the MMF that is introduced in the iron core. H are the magnetic field intensity in the magnet and the air gap respectively, N is the number of turns of the coil and I is the coil current.

The last equation to be used is the relation between magnetic field intensity and density:

$$B_g = \mu_0 H_m \tag{5.3}$$

where μ_0 is the relative permeability of the air.

Finally, the load line of the magnetic circuit in Figure 5.1 can then by calculated by combining eq. (5.1) , eq. (5.2) and eq. (5.3) :

$$B_m = \frac{k1}{k2}\frac{l_m A_g \mu_0}{A_m l_g} H_m + \frac{k1}{k2}\frac{N A_g \mu_0}{A_g l_g} I \tag{5.4}$$

By using the simulation in Section 5.1 different magnet thicknesses were calculated for different magnet temperature in order to produce the same flux density $B_m = 0.717\ T$ in the magnet. Then by using eq. (5.4) the load line for the magnet circuit with the new magnet length was calculated. The results can be seen in Figure 5.2

By observing Figure 5.2 it can be seen that to produce the same magnetic flux $B_m = 0.717\ T$ in the magnet, thicker magnet is needed for higher temperature. The magnet length needed is $l_{m,110°C} = 6.25\ mm$, $l_{m,80°C} = 5.77\ mm$ and $l_{m,50°C} = 5.47\ mm$ respectively.

If a magnetic circuit was designed to operate at a temperature of $50°C$ and suddenly the temperature of the magnet was rised to $110°C$ then the new operating point would be the intersection of the yellow load line and the blue B-H curve. However, this intersection is at the "knee" of the B-H curve and that would lead to partial demagnetization as discussed in Section 2.1.3.

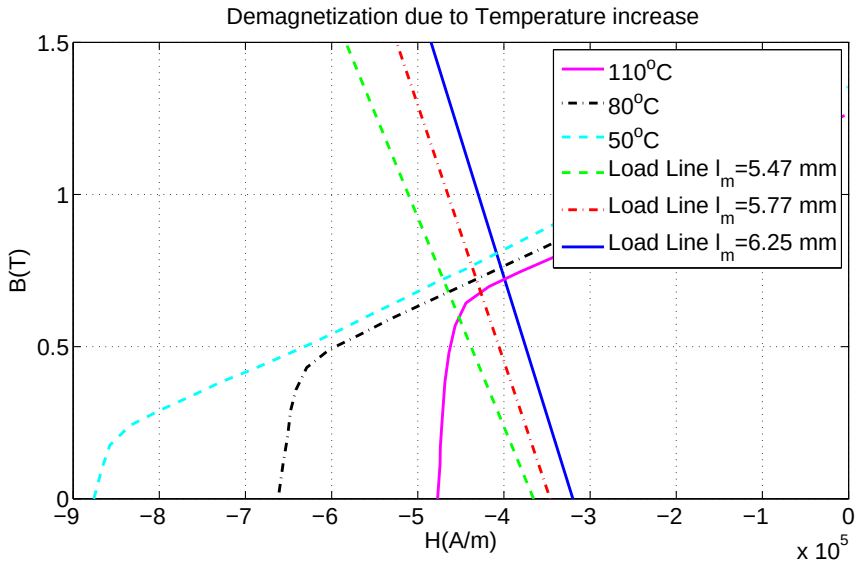

Figure 5.2: Load Lines for different magnet thickness. The magnet thicknesses were calculated to produce the same flux density in the magnet for different magnet temperatures. The intersection with the B-H curves gives the operating point of the magnets.

5.2 Calculation of Permanent Magnet Temperature

5.2.1 Theoretical Calculation of Eddy-Current Loss in Thin Conductor

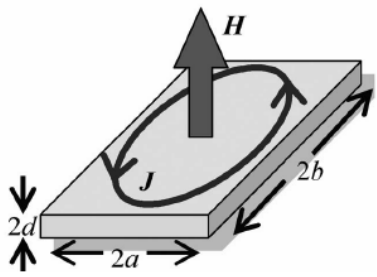

Figure 5.3: Simplified theoretical model for calculating eddy-current losses in a thin conductor. The magnetic field exists in radial direction. 2d is the thickness of the magnet, 2b is the length of the magnet in the axial direction and 2a is the width of the magnet in the tangential dimension.

The analytical expression of eddy current losses in a thin conductor with a uniform field

applied through its surface is proved to be: [19, 46]

$$\begin{aligned} P &= \frac{2d}{\sigma}\int_0^b\int_0^a |J|^2 dxdy \\ &= \frac{2bd}{\sigma\delta}|H|^2\frac{sinh\frac{2a}{\delta}-sin\frac{2a}{\delta}}{cosh\frac{2a}{\delta}+cos\frac{2a}{\delta}} - \frac{128a^4d}{\pi^5}\frac{|\gamma^2H|^2}{\sigma} \\ &\times\sum_{n=0}^{\infty}\frac{(\lambda_n^2-2\beta_{ni}^2)\beta_{nr}\lambda_n^3 sinh2\beta_{nr}b}{(2n+1)^5|\beta_n|^6(cosh2\beta_{nr}b+cos2\beta_{ni}b)} - \frac{128a^4d}{\pi^5}\frac{|\gamma^2H|^2}{\sigma} \\ &\times\sum_{n=0}^{\infty}\frac{(\lambda_n^2-2\beta_{nr}^2)\beta_{ni}\lambda_n^3 sinh2\beta_{ni}b}{(2n+1)^5|\beta_n|^6(cosh2\beta_{nr}b+cos2\beta_{ni}b)} \end{aligned} \tag{5.5}$$

where a, b and d are the half of magnet's width, length and thickness as shown in Figure 5.3, $\delta = \sqrt{\frac{2}{\sigma\omega\mu_r\mu_0}}$ is the skin depth, k is the conductivity of the conductor, n is the number of series solutions and the constants are:

$$\lambda_n = (2n+1)\frac{\pi}{2a} \tag{5.6}$$

$$\gamma = \frac{1+j}{\delta} \tag{5.7}$$

$$\beta_n = \beta_{nr} + j\beta_{ni} = \sqrt{\lambda_n^2+\gamma^2} \tag{5.8}$$

When a magnet is segmented into N segments along its length, the new losses can be found by replacing b in eq. (5.6) with b/N and multiplying the result of eq. (5.6) by N.

The affect of magnet segmentation in eddy current losses for a field of $B = 10\ mT$ for the eq. (5.6) can be seen in Figure 5.4. The length of the magnet is $2a = (25/N_w)\ mm$, $2d = 7\ mm$, $2b = (300/N_l)\ mm$ where N_l is the number of length divisions and N_w is the number of width divisions.

By observing Figure 5.4(a) it can be observed that without width segmentation the eddy-current loss become maximum when the length of the conductor 2b is about twice the skin depth δ which is 4.5mm in this case. The losses with 37 divisions along the length of the magnet are exactly the same as without division and for higher number of devisions the loss of the permanent magnet reduces. For less devisions the losses that are introduced in the permanent magnet are increased.

However, when width segmentation is introduced in the magnets the case is different as can be seen in Figures 5.4(b),5.4(c),5.4(d). When the magnet is segmented in its width then the curve of the losses is only descending and the length division is beneficial. Also, especially in the case of 8 width division in the magnet, the losses are drastically decreased. This indicates the importance of both length and width divisions of the magnets to effectively reduce the eddy current losses in them.

5.2.2 Calculation of PM losses in PM machine

To determine the losses in the PM machine Finite Elements Methods will be used to calculate the magnetic potential A and the magnetic flux density Φ inside the magnets of the PM machine.

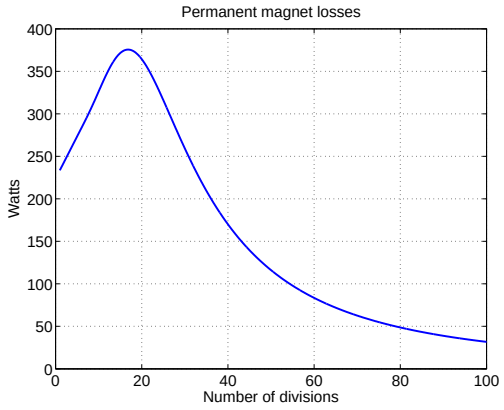

(a) Number of width segmentation $N_w = 1$.

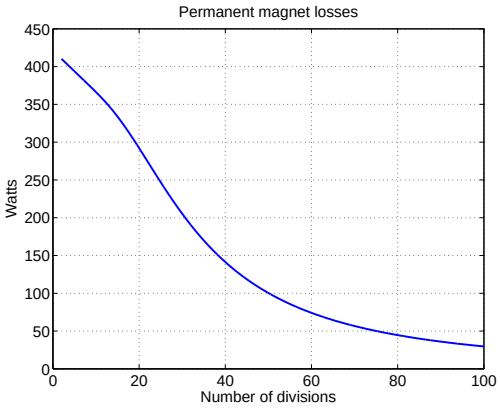

(b) Number of width segmentation $N_w = 2$.

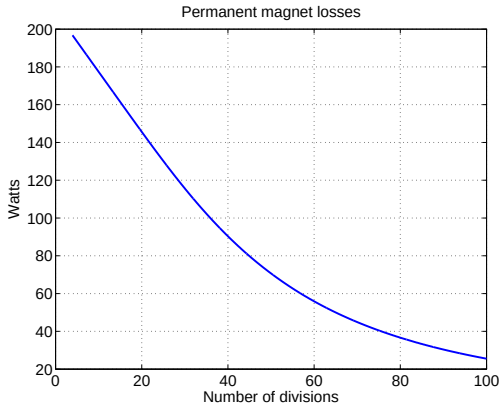

(c) Number of width segmentation $N_w = 4$.

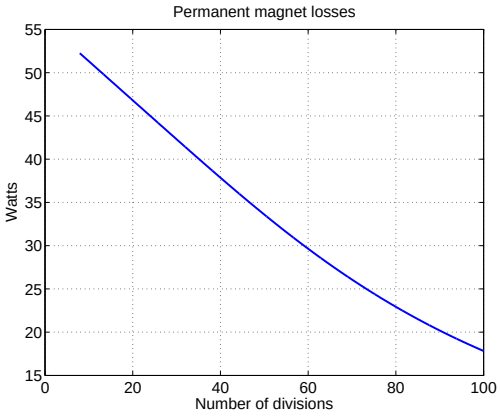

(d) Number of width segmentation $N_w = 8$.

Figure 5.4: Variation of eddy current losses for increasing segmentation *length 2b* of a permanent magnet with total length 2b= 3200 mm, thickness 2d=6 mm and width 2a= 20 mm . The magnetic field has magnitude $|B| = 10\ mT$ and frequency $f = 20\ kHz$. In the different sub-figures different number of width segmentation N_w exist.

Then Maxwell will use eq. (5.5) to calculate the losses in the permanent magnets. Because simulating the whole machine is computationally expensive, the machine was sliced axially into the axial permanent magnet length and only one slice was examined. The results was then multiplied by the number of axial divisions of the magnet to get the total losses in the permanent magnets. The simulation topology can be seen in Figure 5.5.

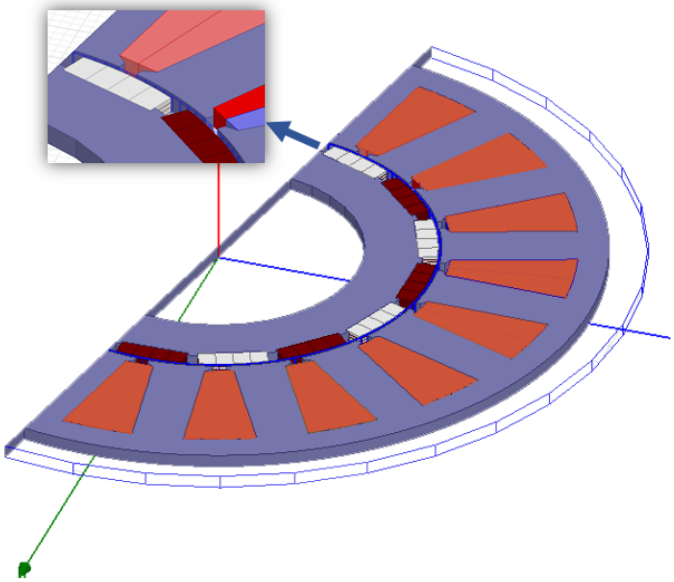

Figure 5.5: Simulation topology for calculation of PM losses in the PM machine. Only 4mm of the stator was simulated in 3D because the simulation is computationally expensive. The magnets in this case are segmented in 4 parts in the tangential direction.

5.2.3 Results

The permanent magnet losses map in the machine for different number of tangential segmentations can be seen in Figure 5.6. As expected from the analytical investigation done in Section 5.2.1 the losses decrease with increased number of segmentation in the permanent magnets.

5.3 Rotor Thermal Model

To be able to determine the temperature of the magnets that seat on to the rotor of the machine, a 2-D thermal model of the rotor was made in FEMM Software. The model can be seen in Figure 5.7. The machine that is examined is an SPM machine with 8 pole pairs and therefore due to symmetries only 1/16 of the entire rotor is modeled.

The stator in this thermal model is modeled by a constant temperature boundary condition of $100°C$ which was considered to be a typical stator operating temperature. In the inner radius of the rotor body, another boundary condition was added. It is a convection heat transfer, in order to examine the cooling effect of the oil spraying technique that is examined in this thesis.

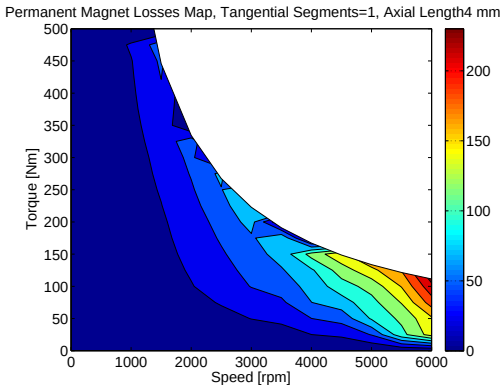

(a) Permanent magnet losses map for no tangential segmentation.

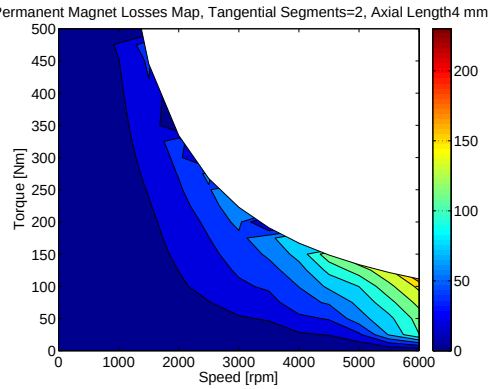

(b) Permanent magnet losses map for 2 tangential segments.

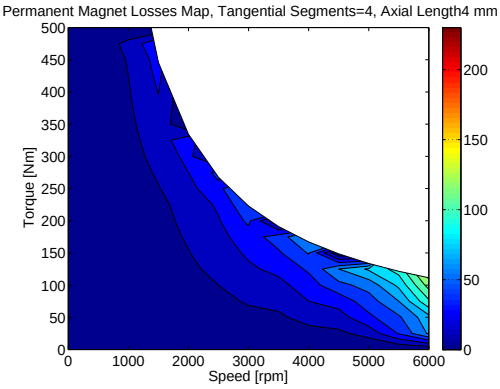

(c) Permanent magnet losses map for 4 tangential segments.

Figure 5.6: Permanent magnet losses for different tangential segmentation. The axial segmentations are 50, forming a length of 4 mm for the magnets.

The power losses that are calculated as described in Section 5.2.2 will be used as input for the thermal model. Concerning the oil convection, the heat transfer coefficient map of the oil spray cooling for different speeds will be used in the model. This map will be determined by the experimental data of this master thesis. The output of this model will be the temperature the permanent magnets. The calculation procedure can be seen in Figure 5.9 .

Figure 5.7: Rotor thermal model in FEMM Software. Due to symmetries in an 8 pole pair machine, only 1/16th of the rotor is modeled.

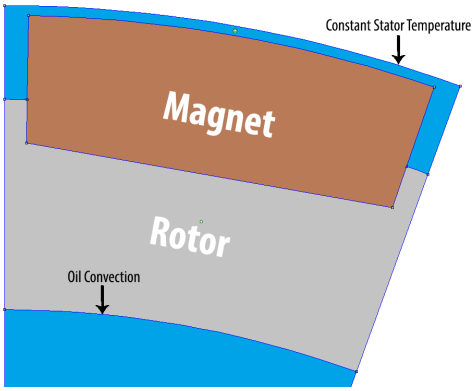

Figure 5.8: Boundaries of the thermal model. The oil convection coefficient will be obtained by the experimental data. The stator is modeled by a constant temperature boundary with a small airgap from the rotor.

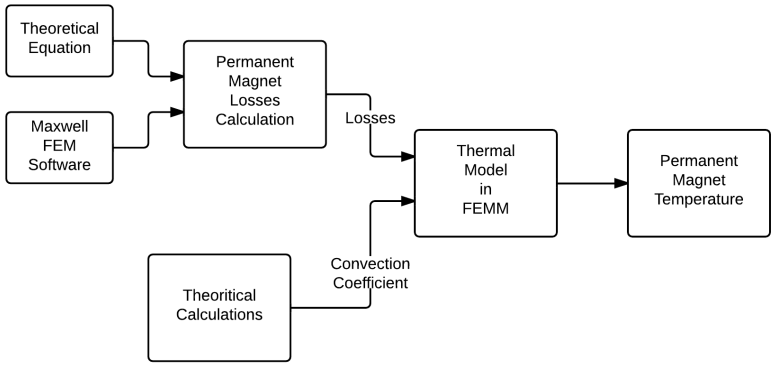

Figure 5.9: Calculation procedure of magnet temperature in the PM machine.

5.3.1 Results

The temperature map of the permanent magnets extracted from the model in Section 5.3 can be seen in Figure 5.10 and in Figure 5.11 for a different number of tangential segmentations of the

permanent magnets. In Figure 5.10 no oil spraying is implemented and in Figure 5.11 oil spray with rate of $0.8[l/min]$ was sprayed inside the rotor.

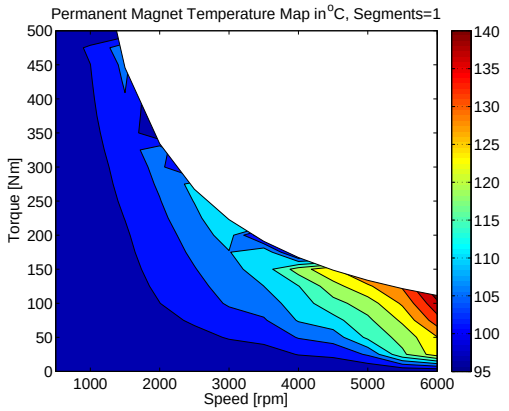

(a) Permanent magnet temperature map for no tangential segmentation.

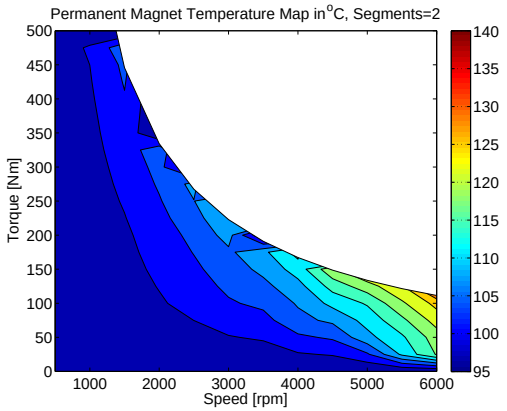

(b) Permanent magnet temperature map for 2 tangential segments.

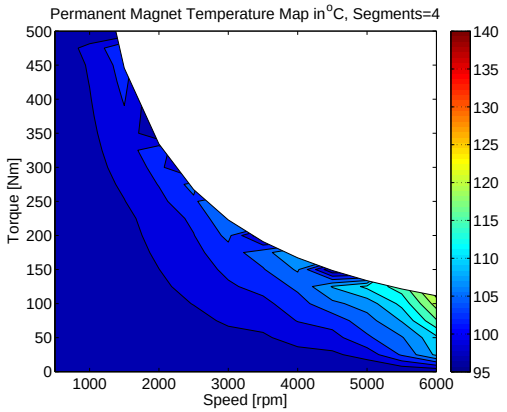

(c) Permanent magnet temperature map for 4 tangential segments.

Figure 5.10: Permanent magnet temperature map with no oil spraying. The axial segmentations are 50, forming a length of 5 mm for the magnets.

5.3.2 Discussion

The results indicate that the oil spraying technique is very efficient. A summary table of Figures 5.11 and 5.10 can be seen in Table 5.1. In case of no oil spraying 4 segments are needed to maintain the temperature of the magnets below $125°C$ which is necessary for the magnets protection. When oil spraying is used the drop in the temperature is significant. Even in case of no tangential segmentation and double axial segments, the temperature of the magnet was kept bellow 90 $°C$.

The heat transfer coefficient is so high and therefore the temperature difference between the case of 4 tangential segments and no segmentation is only $3°C$. That suggests that the heat

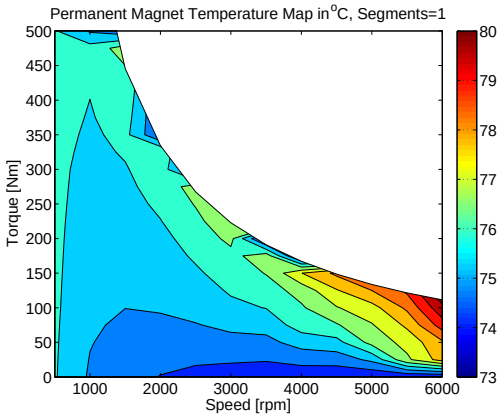

(a) Permanent magnet temperature map for no tangential segmentation.

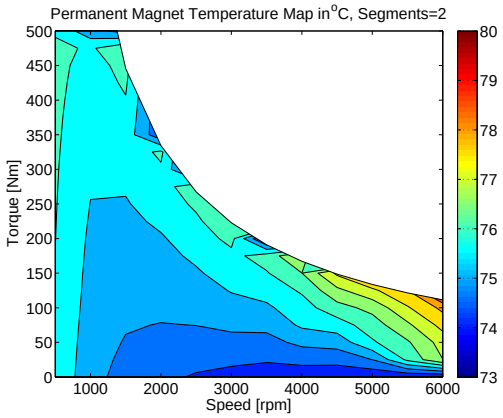

(b) Permanent magnet temperature map for 2 tangential segments.

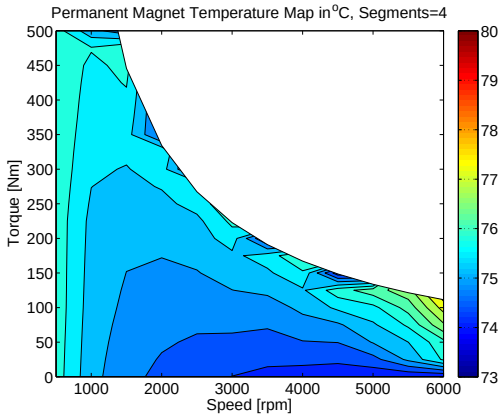

(c) Permanent magnet temperature map for 4 tangential segments.

Figure 5.11: Permanent magnet temperature map for oil spraying at 0.8 l/min. The axial segmentations are 50, forming a length of 4 mm for the magnets.

transfer is so efficient that basically the temperature of the magnets depends very much on the oil temperature that is sprayed. If the oil that was sprayed was at 60 degrees, a temperature just above 70 degrees is expected in the magnets.

Table 5.1: Summary table of the losses and the temperature with and without oil spraying for different tangential semgentation and different axial segmentation

Number of Tangential segments	Axial Segmentation Length [mm]	Maximum Losses [W]	Maximum Temp. Air Cooled [$°C$]	Maximum Temp. Oil Cooled 0.8 l/min [$°C$]
4	4	143	124	77
2	4	204	135	79
1	4	254	145	80
1	8	582	202	89

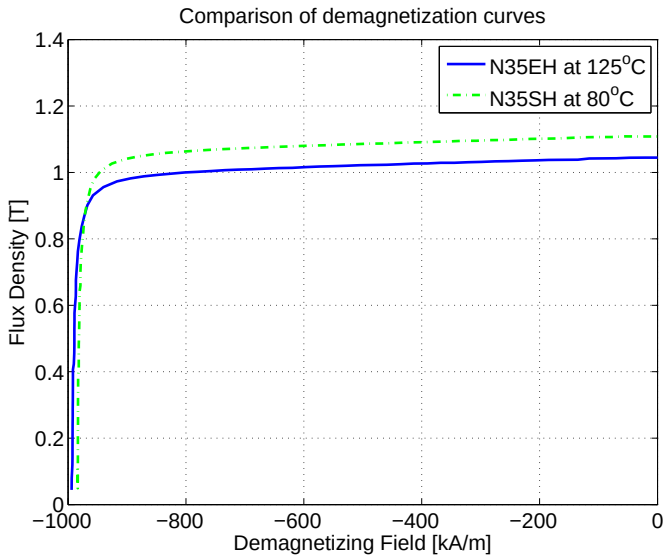

Figure 5.12: Demagnetization Curves for different temperatures

Currently in the machine, the N35EH [47] magnet is used. The B-H curve of this magnet for 125$°C$ can be seen in Figure 5.12. When the oil spraying is used, the magnet that could be used is the N35ESH [48] which has the same energy product but is two temperature classes lower magnet. Its B-H characteristic for 80$°C$is also visible in Figure 5.12, and it can be observed that its characteristic is very close to the N35EH at a temperature of 125$°C$. That in combination with 4 times lower segmentation in the magnets would result in significant cost reduction in the motor.

On the other hand, if performance is the case, magnets with higher energy product could be used. For the EH class the maximum BH product available for magnet is 38, but for the temperature class SH it is 45. The maximum torque of a motor is directly proportional to the

flux produced by the magnets. By keeping the working temperature of the magnets in lower levers higher power density can be achieved. That means smaller motors for the same torque or higher torque for the same size of machine.

Chapter 6

Conclusion and future work

6.1 Conclusions

6.1.1 Heat Transfer

Almost all of the test results is within the *same power of magnitude* as the theoretical calculations. The number of tests though, is to small to establish a relation with high accuracy but it can be used as a hint of the cooling methods capability.

For higher volume flow of oil there was a better correlation between theoretic and experimental results. This could be caused by inaccuracy of the thickness model for lower volume flow. Also it was observed during the measurements that the oil was dripping for 0.1 and 0.3 l/min and was spraying during 0.8 l/min. That is also a potential cause for the poor correlation between the theoretical and the experimental data for lower oil flows.

Two different linear regression analysis were made. The average dimensionless numbers, spanning the entire test duration, was used in the analysis. In the first analysis all of the tests where used. In the second one only the tests with higher volume flow was used. Unfortunately the small selection made results unreliable. The result is presented in Figure 4.39.

6.1.2 PMSM Design

The number of segments in the PMSM was decreased by 4 times. With oil cooling it is not necessary to segment the magnets in the axial direction. Thus, segmentation is only needed in one direction reducing the labor cost because of the time consuming cutting process. Having only segments in the axial direction could decrease the price of the magnets by 27%.

With oil spraying the temperature class of the magnet was reduced from EH to SH which is 29% cheaper according to Arnold magnetics. Also the $(BH)_{max}$ for the SH class is 45 while for the EH class is 38. That means that magnets with higher magnetic flux can be used in the machine. That would increase the power density of the machine which is especially important in automotive applications. Also using lower temperature grade magnets will lead to a significant cost reduction. The reason for this is the smaller percentage of Dysprosium used on those magnets. Dysprosium's price is about 5 times higher than the price of Neodymium.

The losses of the magnets increased from 143 W to 254 W which corresponds to only 0.1%

of the rated power of the machine. As a result, the overall efficiency of the machine has not changed.

6.1.3 Issues

There are some practical issues regarding the project and that is the reason for the few number of tests that were conducted. The initial plan was to conduct more tests. The performance at higher speeds, with other coolants and steady state tests where initially programmed but never conducted. The main issue was that the oil collection part, was not working as expected, arising security issues.

Possible solutions for improved designs were found but due to time limitations could not be done during this master thesis. For this experiment to be more successful a few alterations of the test rig are suggested:

- *Oil collection.* The part with highest priority of reconstruction is the oil collection system. The original design did not perform as expected and many "last minute" solutions that were implemented didn't worked in a satisfactory level. To correct this mistake another plastic part had to be manufactured. The time it would require was unreasonable for this thesis.

- *Rotating Connection.* Another issue with the set up was the rotating oil connection system seen in Figure 4.29. Initially the oil lance was designed to rotate with the cylinder. A misconception of the bearings sealing function lead to an unstoppable leaking where the lance had to be replaced with a non rotating one.

- *Not constant oil inlet temperature.* Also the delivery system of oil did not provide oil with constant temperature. A possible solution would be to circulate the oil from the tank to a point close to the oil connection continuously. That would avoid the transient ramping of the oil temperature when the experiment started because the oil in the pipe was cooler than the oil in the reservoir. The resulting temperature change in the coolant inlet during the run made it harder to analyze the results.

- *Thickness measurement.* It would have been valuable to measure the oil film thickness instead of approximating it from theory. The strong dependence of the heat transfer coefficient to the oil thickness was realized in the later stages of the master thesis. In order to include a thickness sensor another telemetry system version would have been required that could handle those kind of data. Unfortunately due to time and budget constrains the idea of measuring it had to be put aside.

6.2 Future work

It would have been preferable to conduct a steady state experiment for the heat transfer coefficient. This could be used to confirm the results of the transient test and the theoretical model. The effect of the rotating oil lance can also be studied, because it will change the relative speed of the oil and the inner rotor wall. Different profiles could be used for the wall and oil extraction, and different oils can be tested to examine the effect of their thermal properties.

The heat transfer model could be improved by including conduction inside the cylinder. If the conduction inside the cylinder is high the results can change considerably. An estimation of the heat lost to the surrounding would also be useful. This would require more thermal sensors in the test setup. Also heat transfer through the plastic insulation part could be useful to investigate.

Another fact that would be very interesting to examine is whether the oil spraying could work with passive control or active control. Also a completely re-designed electric machine with the oil spraying implemented would be interesting to examine, in order to set the new power density limits.

Bibliography

[1] Ishak Dahaman, Z. Q. Zhu, and David Howe. "Eddy-Current Loss in the Rotor Magnets of Permanent-Magnet Brushless Machines Having a Fractional Number of Slots Per Pole". In: *IEEE TRANSACTIONS ON MAGNETICS* 41 (2005), pp. 2462 –2469.

[2] A. E. Fitzgerald, C. Kingsley, and S. Umans. *Electric Machinery*. McGraw- Hill, 2003. ISBN: 0073660094.

[3] Stephen Chapman. *Electric machinery fundamentals*. Maidenhead: McGraw-Hill Education, 2003. ISBN: 0071151559.

[4] Austin Hughes. *Electric motors and drives fundamentals, types and applications*. Oxford: Newnes, 2013. ISBN: 9780080983325.

[5] Gieras and F. Jacek. *Permanent magnet motor technology design and applications*. Boca Raton: CRC Press, 2010. ISBN: 1420064401.

[6] VACUUMSCHMELZE GmbH & Co. KG. *Rare-Earth Permanent Magnets VACODYM-VACOMAX*. PD002. Grüner Weg 37 D-63450 Hanau, 2012. URL: http://www.vacuumschmelze.com/fileadmin/Medienbiliothek_2010/Downloads/DM/Vdym_Vmax_en.pdf.

[7] J. Cros and P. Viarouge. "Synthesis of high performance PM motors with concentrated windings". In: *Energy Conversion, IEEE Transactions on* 17.2 (June 2002), pp. 248–253. ISSN: 0885-8969. DOI: 10.1109/TEC.2002.1009476.

[8] F. Magnussen and C. Sadarangani. "Winding factors and Joule losses of permanent magnet machines with concentrated windings". In: *Electric Machines and Drives Conference, 2003. IEMDC'03. IEEE International*. Vol. 1. June 2003, 333–339 vol.1. DOI: 10.1109/IEMDC.2003.1211284.

[9] N. Bianchi et al. "Design considerations for fractional-slot winding configurations of synchronous machines". In: *Industry Applications, IEEE Transactions on* 42.4 (July 2006), pp. 997–1006. ISSN: 0093-9994. DOI: 10.1109/TIA.2006.876070.

[10] A.M. EL-Refaie and T.M. Jahns. "Optimal flux weakening in surface PM machines using fractional-slot concentrated windings". In: *Industry Applications, IEEE Transactions on* 41.3 (May 2005), pp. 790–800. ISSN: 0093-9994. DOI: 10.1109/TIA.2005.847312.

[11] P. Salminen et al. "Concentrated Wound 45 kW, 420 rpm Permanent Magnet Machine with Embedded Magnets". In: *Power Electronics, Machines and Drives, 2006. The 3rd IET International Conference on*. Apr. 2006, pp. 494–498.

[12] Nady Boules. “Impact of slot harmonics on losses of high-speed permanet magnet machines with a magnet retaining ring”. In: *Electric Machines & Power Systems* 6.6 (1981), pp. 527–539. DOI: 10.1080/03616968108960089. eprint: http://www.tandfonline.com/doi/pdf/10.1080/03616968108960089. URL: http://www.tandfonline.com/doi/abs/10.1080/03616968108960089.

[13] P. J. Hor, Z.Q. Zhu, and D. Howe. “Eddy current loss in a moving-coil tubular permanent magnet motor”. In: *Magnetics, IEEE Transactions on* 35.5 (July 1999), pp. 3601–3603. ISSN: 0018-9464. DOI: 10.1109/20.800603.

[14] K. Atallah et al. “Rotor loss in permanent-magnet brushless AC machines”. In: *Industry Applications, IEEE Transactions on* 36.6 (Nov. 2000), pp. 1612–1618. ISSN: 0093-9994. DOI: 10.1109/28.887213.

[15] Fang Deng and T.W. Nehl. “Analytical modeling of eddy-current losses caused by pulse-width-modulation switching in permanent-magnet brushless direct-current motors”. In: *Magnetics, IEEE Transactions on* 34.5 (July 1998), pp. 3728–3736. ISSN: 0018-9464. DOI: 10.1109/20.718535.

[16] Fang Deng. “Commutation-caused eddy-current losses in permanent-magnet brushless DC motors”. In: *Magnetics, IEEE Transactions on* 33.5 (July 1997), pp. 4310–4318. ISSN: 0018-9464. DOI: 10.1109/20.620440.

[17] K. Yamazaki and Y. Fukushima. “Effect of Eddy-Current Loss Reduction by Magnet Segmentation in Synchronous Motors With Concentrated Windings”. In: *Industry Applications, IEEE Transactions on* 47.2 (Mar. 2011), pp. 779–788. ISSN: 0093-9994. DOI: 10.1109/TIA.2010.2103915.

[18] K. Yamazaki et al. “Effect of Eddy Current Loss Reduction by Segmentation of Magnets in Synchronous Motors: Difference Between Interior and Surface Types”. In: *Magnetics, IEEE Transactions on* 45.10 (Oct. 2009), pp. 4756–4759. ISSN: 0018-9464. DOI: 10.1109/TMAG.2009.2024159.

[19] K. Yamazaki and A. Abe. “Loss Investigation of Interior Permanent-Magnet Motors Considering Carrier Harmonics and Magnet Eddy Currents”. In: *Industry Applications, IEEE Transactions on* 45.2 (Mar. 2009), pp. 659–665. ISSN: 0093-9994. DOI: 10.1109/TIA.2009.2013550.

[20] N. Takahashi et al. “Analysis of Eddy Current Losses of Segmented NdFeB Sintered Magnets Considering Contact Resistance”. In: *Magnetics, IEEE Transactions on* 45.3 (Mar. 2009), pp. 1234–1237. ISSN: 0018-9464.

[21] N. Takahashi et al. “Factors affecting eddy current losses of segmented Nd-Fe-B sintered magnets without insulation in large PM motors”. In: *Electric Machines and Drives Conference, 2009. IEMDC ’09. IEEE International*. May 2009, pp. 24–29.

[22] Frank P. Incropera et al. *Principles of Heat and Mass Transfer*. John Wiley & Sons, 2013. ISBN: 9780470646151.

[23] *Wikipedia image of radiation*. Apr. 2014. URL: http://en.wikipedia.org/wiki/File:Hot_metalwork.jpg/.

[24] Federico Ghirelli. “Analysis and design of in-rotor oil cooling of an electrical engine”. Report of. Apr. 2014.

[25] F.M. White. *Fluid Mechanics*. McGraw-Hill international editions. McGraw-Hill, 2003. ISBN: 9780072402179. URL: http://books.google.com.au/books?id=1DYtptq3OC4C.

[26] Frank P. Incropera. *Fundamentals of Heat and Mass Transfer*. John Wiley & Sons, 2006. ISBN: 0470088400.

[27] Valery Rudnev et al. *Handbook of Induction Heating*. Ed. by Ioan Marinescu. Marcel Dekker, 2003. ISBN: 0824708482.

[28] D.A. Howey, P.R.N. Childs, and A.S. Holmes. "Air-Gap Convection in Rotating Electrical Machines". In: *Industrial Electronics, IEEE Transactions on* 59.3 (Mar. 2012), pp. 1367–1375. ISSN: 0278-0046. DOI: 10.1109/TIE.2010.2100337.

[29] K. M. Becker and Joseph Kaye. "Measurements of Diabatic Flow in an Annulus With an Inner Rotating Cylinder". In: *Journal of Heat Transfer* 84.2 (1962), pp. 97–104. DOI: http://dx.doi.org/10.1115/1.3684335.

[30] Sheng-Chung Tzeng. "Heat transfer in a small gap between co-axial rotating cylinders". In: *International Communications in Heat and Mass Transfer*. Ed. by Elsevier Ltd. Vol. 33. Elsevier Ltd, Mar. 2006.

[31] *ThermoPor msds - CHRODA Eco Limited*. 1.3. CHRODA Eco Limited. CHRODA Eco Ltd The Croft 97 Bretforton Road Badsey, Evesham WR11 7XQ. URL: http://www.chroda-eco.co.uk/documents/ThermoPor%20Safety%20Datasheet%20v1.3.pdf.

[32] *Thermal Insulating Plaster/Render - Product information and Method Statement*. 1.0. CHRODA Eco Limited. The Croft 97 Bretforton Road Badsey, Evesham WR11 7XQ. URL: http://www.chroda-eco.co.uk/documents/ThermoPor_Product_Info_&_Method_Statement_V1.0.pdf.

[33] *Thermopor Product Datasheet*. 3.0. CHRODA Eco Limited. The Croft 97 Bretforton Road Badsey, Evesham WR11 7XQ. URL: http://www.chroda-eco.co.uk/documents/ThermoPor_Product_Datasheet_v3.0.pdf.

[34] Inc. Compliance Consulting Group (CCG) EH&S Services for BNZ Materials. *Material Safety Data Sheet BNZ 40-103*. 2nd ed. BNZ Materials, Inc. 6901 S. Pierce St, Suite 260 Littleton, CO 80128 U.S.A., June 2012. URL: http://www.bnzmaterials.com/wp-content/uploads/2013/02/BNZ-40-103-460-Cement-MSDS.pdf.

[35] Pittsburgh Corning Corporation. *Foamglas product manual - Pittsburgh Conrning*. Pittsburgh Corning Corporation. Albertkade, 1 B-3980 Tessenderlo Belgium, July 2009. URL: http://www.industry.foamglas.com/__/frontend/handler/document.php?id=294&type=42.

[36] *Foamglas Material Safety Data Sheet - Pittsburgh Conrning*. 1st ed. Pittsburgh Corning Corporation. Feb. 2009. URL: http://www.glasscellisofab.com/sheets/cellular/msds/Fittings.pdf.

[37] *Thermisol - Product information*. Thermisol AB. Braxenvagen 8, 761 41 Norrtalje. URL: http://www.thermisol.se/assets/files/sverige/Villagrunder/TH_produktoversikt08_web[1].pdf.

[38] Magnus Wallin. *Thermisol - SAFETY SHEET EPS*. Thermisol AB. Braxenvagen 8, 761 41 Norrtalje, Jan. 2012. URL: http://www.thermisol.se/assets/files/sverige/EPS/SDS%20Thermisol%20Cellplast%202012-01-12.pdf.

[39] *Insulfrax S blanket - MSDS*. Unifrax. 600 Riverwal Parkwat, Siote 120 Tonawanda, NY 14150, Apr. 2013. URL: http://www.unifrax.com/MSDSAPPR.nsf/byMSDS/M0189.

[40] *Series UP3/4 Gear Pumps for Water & Engine Oil*. Clark Solutions. 10 Brent Drive Hudson, MA 01749. URL: http://www.clarksol.com/html/UP3-4_Pump.cfm%20.

[41] Yunus A. Çengel and John M. Cimbala. *Fluid Mechanics Fundamentals and Applications*. McGraw-Hill, 2010. ISBN: 9780071284219.

[42] Texas Instruments. *LM2907/LM2917 Frequency to Voltage Converter*. March 2013. Mar. 2013. URL: www.ti.com/lit/ds/symlink/lm2907-n.pdf.

[43] STMicroelectronics. *Positive voltage regulator ICs*. March 2014. Apr. 2014. URL: http://www.st.com/web/en/resource/technical/document/datasheet/CD00000444.pdf.

[44] *Radiant Process Heat (NEW)*. URL: http://www.omega.com/Heaters/pdf/CRB_Series.pdf.

[45] David Meeker. *Finite Element Method Magnetics*. Pittsburgh Corning Corporation. Feb. 2009. URL: http://www.femm.info/Archives/doc/manual.pdf.

[46] K. Yamazaki and Y. Fukushima. "Effect of eddy-current loss reduction by magnet segmentation in synchronous motors with concentrated windings". In: *Electrical Machines and Systems, 2009. ICEMS 2009. International Conference on*. Nov. 2009, pp. 1–6. DOI: 10.1109/ICEMS.2009.5382795.

[47] *N35EH NeFeB Magnet Specification Sheet*. Arnold Magnetic Technologies Corp. URL: http://www.arnoldmagnetics.com/WorkArea/linkit.aspx?LinkIdentifier=id&ItemID=5015.

[48] *N35SH NeFeB Magnet Specification Sheet*. Arnold Magnetic Technologies Corp. URL: http://www.arnoldmagnetics.com/WorkArea/linkit.aspx?LinkIdentifier=id&ItemID=5019.

[49] Giuseppe Grosso. *Solid state physics*. Waltham, Massachusetts: Elsevier, 2014. ISBN: 978-0-12-385030-0.

[50] Wm. F. Roeser. "Thermoelectric Thermometry". In: *Journal of Applied Physics* 11.6 (1940), pp. 388–407. DOI: http://dx.doi.org/10.1063/1.1712788. URL: http://scitation.aip.org/content/aip/journal/jap/11/6/10.1063/1.1712788.

[51] Thomas Kerlin. *Practical thermocouple thermometry*. Research Triangle Park, NC: Instrument Society of America, 1999. ISBN: 9781615835768.

[52] J. R. Davis. *Metals handbook*. Materials Park, Oh: ASM International, 1998. ISBN: 9780871706546.

Part I

Appendix

Appendix A

Thermocouples

A.1 Thermoelectric Phenomena

"Thermoelectric Effect" or *"Peltier–Seebeck effect"* is the development of an EMF across a material due to the temperature difference into different parts of it and the opposite. This effect can be used to generate electricity, to measure temperature or even to control temperature. The later is possible due to the fact that the direction of the temperature difference is control by the polarity of the applied voltage. Three effects compose the Thermoelectric effect: Seebeck-, Peltier- and Thomson Effect.

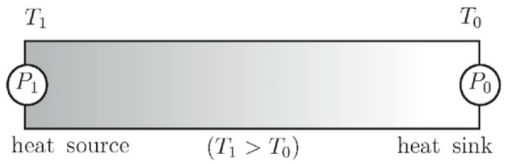

Figure A.1: Schematic representation of a bar of homogeneous material, whose ends are kept at different temperatures.[49]

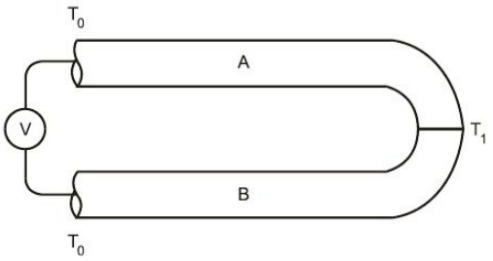

Figure A.2: Basic Thermocouple Circuit.[50]

The bar in Figure A.1 has its two ends in different temperatures. The two basic transport equations for this bar are [49]:

$$\mathbf{J} = e^2 K_0 \left[\mathbf{E} + \frac{1}{e} \nabla \mu - S(T) \nabla T \right] \tag{A.1}$$

with

$$S(T) = -\frac{1}{eT} \frac{K_1}{K_0} \tag{A.2}$$

where $\mathbf{J}$ is the Current Density,
E is the Electric field intensity,
S is the Seebeck coefficient $[\mu V/^\circ C]$,

μ is the chemical potential,
e is the elementary charge,
K_n are the Kinetic Coefficients.

From eq. (A.1) it can be seen that the current density $\mathbf{J}$ consists of three parts. The first term, $e^2K_0\mathbf{E}$ is the standard drift term $\sigma_0\mathbf{E}$, where σ_0 is the conductivity of the metal. The second term, $e^2K_0\left(\frac{1}{e}\nabla\mu\right)$, is due to the inhomogeneity of the chemical potential. The third term, $-e^2K_0\left(S(T)\nabla T\right)$, is due to the presence of temperature gradient. [49]

A.2 Seebeck Effect

The bar in Figure A.1 is subjected to a temperature gradient. In an open circuit condition $\mathbf{J} = 0$ in the bar and from eq. (A.1) an electric field:

$$\mathbf{E} = -\frac{1}{e}\nabla\mu + S(T)\nabla T \tag{A.3}$$

has to set in, in order to prevent any net carrier flux.
Then the potential difference between the two end points $P_0$and P_1 at the bar in Figure A.1 can be calculated:

$$\phi_1 - \phi_0 = -\int_{P_0}^{P_1} \mathbf{E}\cdot d\mathbf{l} = \frac{1}{e}(\mu_1 - \mu_0) - \int_{T_0}^{T_1} S(T)dT \tag{A.4}$$

and as a result the difference in the electrochemical potentials at the ends of the bar is related to the line integral of the Seebeck Coefficient.

A.3 Thermocouple loop

As seen in Section A.2 a conductor that experiences a temperature gradient produces a voltage:

$$V = S(T_2 - T_1) \tag{A.5}$$

where S is the Seebeck coefficient.

A basic thermocouple circuit can be seen in Figure A.2. If we try to measure the voltage V, and we start summing up the potentials in conductors A and B we will end up in:

$$V = \underbrace{S_A(T_1 - T_0)}_{\text{Contribution from conductor A}} + \underbrace{S_B(T_1 - T_0)}_{\text{Contribution from conductor B}} \tag{A.6}$$

which can be written

$$V = S_A(T_1 - T_0) - S_B(T_1 - T_0) = (S_A - S_B)(T_1 - T_0) = S_{AB} \tag{A.7}$$

where S_{AB}= $S_A - S_B$ which is called *relative Seebeck coefficient* and it is of practical interest in thermocouple thermometry. In Figure A.3 the relative Seebeck coefficient for common types of thermocouples, which consist of metal combinations, can be seen.

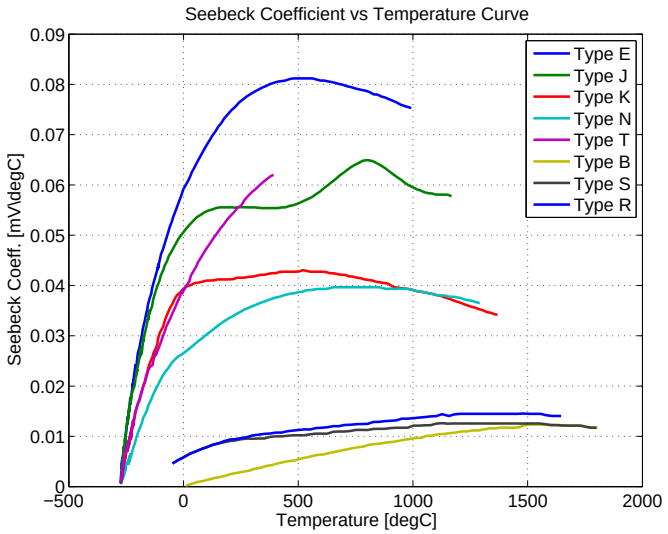

Figure A.3: Seebeck Coefficients for common thermocouple types. [51]

A.4 Required Characteristics

As seen previously although EMF is produced from junctions of any two dissimilar metals, which are at different temperatures, only a few combinations of metals are being used in practice. This is because the thermocouples need to have certain characteristics [50]:

1. Produced EMF from the junction should increase continuously over the temperature range in which the thermocouple is intended to use.
2. The produced EMF is measurable with an acceptable accuracy.
3. The thermoelectric characteristics of the thermocouple are not changing considerably during calibration and usage by internal changes or contamination of the materials used.
4. The thermocouple is resistant to actions that destroy the wire such as oxidation, corrosion etc.
5. The materials used are reproducible, readily available in a uniform quality.
6. The melting point of the materials used is higher than the highest measured temperature.

A.5 Common Types of Thermocouples

The most common type of metal combinations that meet the requirements discussed before are:

- **Type J** (Iron – Constantan) thermocouples are used widely due to their versatility and low cost. It can withstand temperatures from $-40°C$ to $760°C$ which is narrower than Type K thermocouple, but has a higher sensitivity of 50 $\mu V/°C$.

Table A.1: Base composition, melting point and electrical resistivity of seven standard thermocouples. [52]

Type	Thermo-elements	Base Composition	Melting Point $°C$	Resistivity $n\Omega \cdot m$	Recommended Service	Maximum Temperature	
						$°C$	$°F$
J	JP	Fe	1450	100	Oxidizing or reducing	760	1400
	JN	44Ni-55Cu	1210	500			
K	KP	90Ni-9Cr	1350	700	Oxidizing	1260	2300
	KN	94Ni-Al, Mn, Fe, Si, Co	1400	320			
N	NP	84Ni-14Cr-1.4Si	1410	930	Oxidizing	1260	2300
	NN	95Ni-4.4Si-0.15Mg	1400	370			
T	TP	OFHC Cu	1083	17	Oxidizing or reducing	370	700
	TN	44Ni-55Cu	1210	500			
E	EP	90Ni-9Cr	1350	700	Oxidizing	870	1600
	EN	44Ni-55Cu	1210	500			
R	RP	87Pt-13Rh	1860	196	Oxidizing or inert	1480	2700
	RN	Pt	1769	104			
S	SP	90Pt-10Rh	1850	189	Oxidizing or inert	1480	2700
	SN	Pt	1769	104			
B	BP	70Pt-30Rh	1927	190	Oxidizing, vacuum or inert	1700	3100
	BN	94Pt-6Rh	1826	175			

- **Type K** (Chromel – Alumel) thermocouples, are the most widely used and general-purpose thermocouples. Type K thermocouples can be used at temperatures from $-200°C$ up to $1260°C$ in oxidizing atmospheres and have a sensitivity of 41 $\mu V/°C$. They should only be used in oxidizing atmospheres and not reducing atmospheres because of the oxidization of chromium.

- **Type N** (Nicrosil – Nisil) thermocouples was developed for higher oxidation resistance and EMF stability compared to type K thermocouples at high temperatures. They are used in the laboratory and in several industrial applications especially in high temperatures. They are suitable for temperatures between $-270°C$ to $1260°C$ and they have sensitivity of 39 $\mu V/°C$ which is slightly lower than Type K and J.

- **Type T** (Copper – Constantan) thermocouples are used extensively for low temperature measurements. Type T couples can be used in either oxidizing or reducing atmospheres. Their temperature range is from $-200°C$ to $370°C$ with the limiting factor for the high temperature to be the poor oxidization resistance of the copper. They have sensitivity of 43 $\mu V/°C$.

- **Type E** (Chromel – Constantan) thermocouples have recommended operating temperature range between $-200°C$ to $870°C$. They have high sensitivity of 68 $\mu V/°C$ which makes them well suitable for low temperatures use.

Type B, R, and S thermocouples use *Platinum* or a *Platinum/Rhodium* alloy for each conductor. This makes them between the most expensive thermocouples and the most stable ones.

Table A.2: Tolerances for new thermocouples. [51]

Thermocouple Type	**Temperature Range °C**	**Tolerance (Reference Junction at 0°C)**	
		Standard Tolerance	**Special Tolerance**
		°C or percentage of °C (whichever is greater)	**°C or percentage of °C (whichever is greater)**
T	0 to 300	±1 or ±0.75%	±0.5 or ±0.75%
J	0 to 700	±2.2 or ±0.75%	±1.1 or ±0.75%
E	0 to 900	±1.7 or ±0.6%	±1 or ±0.75%
K or **N**	0 to 1250	±2.2 or ±0.75%	±1.1 or ±0.75%
R or **S**	0 to 1450	±1.5 or ±0.25%	±0.6 or ±0.1%
B	670 to 1700	±0.5%	0.25%
T	-200 to 0	±1 or ±1.5%	–
E	-200 to 0	±1.7 or ±1%	–
K	-200 to 0	±2.2 or ±2%	–

On the other hand they have lower sensitivity approximately 10 $\mu V/°C$ and therefore are usually used only for high temperature measurements

- **Type S** (Pt/Rh 90%/10% – Pt, by weight) thermocouple is very stable at high temperatures and has very high chemical resistance in oxidizing atmospheres. Both the materials are ductile and therefore this thermocouple can be constructed in very thin wires make it suitable for special applications. Type S couple is widely used in for calibration of base-metal thermocouples and other temperature-sensing instruments in industrial applications. It can be used in temperatures up to 1480°C.
- **Type R** thermocouple (Pt/Rh 87%/13% – Pt, by weight) has characteristics and end-use applications very similar to those of the type S couple.
- **Type B** (Pt/Rh 70%/30% – Pt/Rh 94%/6%, by weight) thermocouples have operating temperature range between 870°C and 1700°C Because both of its legs are platinum-rhodium alloys, the type B couple is less sensitive to pickup of trace impurities from insulators or from the operating environment.

Base composition, melting point and other characteristics for those common type thermocouples are summarized in Table A.1 while the temperature range and the tolerances for new thermocouples can be seen in Table A.2.

Appendix B

Matlab Code

B.1 Induction Heating

```
clear all
close all
clc

%%%%%%%%%%%%%%%%%%%%%%%%Defining Problem Dimensions and Variables %%%%%%%%%%%%%%%%%%%

%%%%%%%%%%%%%%%%%%%%Everything should be in mellimeters!!!!!!!!!! [mm]%%%%%%%%%%%%%%%


or_c=5;                 %%%%%%Outer Radius of the small cylinder
ir_c=2.5;               %%%%%%Inner Radius of the small cylinder
IR_c=45;                %%%%%%Inner Radius of the big Cylinder
L_c=200;                %%%%%%Length of the Big Cylinder
l_c=350;                %%%%%%Length of the Small Cylinder
w_c=7.5;                %%%%%%Width of the Big Cylinder
w_s=5;                  %%%%%%Width of the outlet shield [mm]
or_sh=35;               %%%%%%Outer Radius of the shaft
ir_sh=29;               %%%%%%Inner Radius of the shaft
l_sh=50;                %%%%%%Shaft length
w_sh=7.5;               %%%%%%Shaft wall thinckness
dist_c_w=2;             %%%%%%Distance between the Cylinder and the Wires
w_w=1.25;               %%%%%%Width of the Wire
h_w=1.25;               %%%%%%Height of the Wire
wires=100;              %%%%%%Number of Wires
groups=4;               %%%%%%Groups of Conductors (Must be even!!)
I=10;                       %%%%%%Current through the Wires [A]
or_tel=22.5;            %%%%%%Outer Radius of small cylinder telemetry system
OR_tel=37.5;            %%%%%%Outer Radius of big cylinder telemetry system
ir_tel=7;               %%%%%%Inner Radius of telemetry system for oil lance
w_tel=8;                %%%%%%Thickness of telemetry system
W_tel=49;               %%%%%%Thickness of the telemetry system (2)
%%%%Cylinder Mesh Options
c_v_segm=50;            %%%%%%Number of Vertical Segments
v_min=0.01;             %%%%%%Minimum Distance between V. Lines
```

```
v_step=5;               %%%%%%Number of Vertical Lines

%%2Materirials Cylinder
al_depth=6.5;              %%%Alluminum Depth in case of 2 layer cylinder
%%%%%%%%%%%%%%%%%%%%−Defining Problem%%%%%%%%%%%%%%%%%%%%%%%%%%%%%%%%%%%%%%%%%%%%−

delta=0.31;

Induction;
Induction_post;
% heattranfer;
% heattranfer_2layers;
path='C:\Users\Odyssefs\Google Drive\Thesis_Volvo_file\Written_documents\...
 ...Final_Report\mfiles\';
copyfile('main_induction.m',path,'f')
copyfile('Induction.m',path,'f')
copyfile('Induction_post.m',path,'f')
copyfile('heattranfer.m',path,'f')
copyfile('heattranfer_2layers.m',path,'f')
copyfile('heattranfer_post.m',path,'f')




%Inductive Heating of Cylinder
% %%%%%%%%%%%%%%%%%%%%%%%%%%%%%%%%%%%%%%%%%%%%%%%%%%%%%%−

% The package must be initialized with the openfemm command.
% This command starts up a FEMM process and connects to it
addpath('C:\femm42\mfiles');
openfemm;




 newdocument(0)     %Creating New Document

%%%%%%%%%%%%%%%%%%%%%%%%%%%%%%−setcompatibilitymode(0)  %%%%%%−Setting the ...
 ...Compatibility mode for FEMM 4.2 as against FEMM 4.1

% showconsole()
% clearconsole()
% hidepointprops()



mi_probdef(50000,'millimeters','axi',1E−08, 10 ,20);    %%%%%%Defining the Problem
mi_saveas('Cylinder.fem');              %%%%%%Saving the Problem
mi_setfocus('Cylinder.fem') ;           %%%%%%Focussing on the Problem
hideconsole();
mi_close();

opendocument('Cylinder.fem');                   %%%%%%Opening the saved file
mi_setfocus('Cylinder.fem');                %%%%%%Setting the focus on the problem

%%%%−Defining Electrical Circuit (1)%%%%%%%%%%−
```

```
mi_addcircprop('I1', I, 1);

%%%%—Defining Electrical Circuit (2)%%%%%%%%%%—
mi_addcircprop('I2', —I, 1);



%%%%%%%%%%%%%%%%%%—Drawing The Geometry%%%%%%%%%%%%%%%%%%%%%%%%%%%%%%%%%%%%%%%%%%%%%%%%—


%%%%—Drawing Air Domain (1)%%%%%%%%%%%%%%%%%%%%%
mi_seteditmode('nodes');
mi_addnode(0,—2*L_c);
mi_addnode(0,3*L_c);
mi_addnode(8*(IR_c+w_c+dist_c_w+w_w),—2*L_c);
mi_addnode(8*(IR_c+w_c+dist_c_w+w_w),3*L_c);

mi_seteditmode('segments');
mi_addsegment(0,—2*L_c,0,3*L_c);
mi_addsegment(0,3*L_c,8*(IR_c+w_c+dist_c_w+w_w),3*L_c);
mi_addsegment(0,—2*L_c,8*(IR_c+w_c+dist_c_w+w_w),—2*L_c);
mi_addsegment(8*(IR_c+w_c+dist_c_w+w_w),—2*L_c,8*(IR_c+w_c+dist_c_w+w_w),3*L_c);

mi_seteditmode('blocks');
mi_addblocklabel(6*IR_c/2,L_c/2);


%%%%—Drawing Air Domain (2)%%%%%%%%%%%%%%%%%%%%%
mi_seteditmode('nodes');
%%%%—mi_addnode(0.75*IR_c,—0.3*L_c);
%%%%—mi_addnode(0.75*IR_c,2*L_c)
mi_addnode(0,—0.3*L_c);
mi_addnode(0,2*L_c);
mi_addnode(2*(IR_c+w_c+dist_c_w+w_w),—0.3*L_c);
mi_addnode(2*(IR_c+w_c+dist_c_w+w_w),2*L_c);

mi_seteditmode('segments');
mi_addsegment(0,—0.3*L_c,0,2*L_c);
mi_addsegment(0,2*L_c,2*(IR_c+w_c+dist_c_w+w_w),2*L_c);
mi_addsegment(0,—0.3*L_c,2*(IR_c+w_c+dist_c_w+w_w),—0.3*L_c);
mi_addsegment(2*(IR_c+w_c+dist_c_w+w_w),—0.3*L_c,2*(IR_c+w_c+dist_c_w+w_w),2*L_c);

mi_seteditmode('blocks');
mi_addblocklabel(0.8*IR_c,L_c/2);

%%%%—Drawing Cylinder (1) %%%%%%%%%%%%%%%%%%%%%
mi_seteditmode('nodes');
mi_drawrectangle(IR_c,0,IR_c+w_c,L_c)

h_step=L_c/c_v_segm;

%%Examine Heat Distribution
for i=1:c_v_segm
    mi_seteditmode('nodes');
    mi_drawline(IR_c,i*h_step,IR_c+w_c,i*h_step)
    mi_seteditmode('blocks');
```

```
    mi_addblocklabel(IR_c+w_c/2,(i-0.5)*h_step);
end
%%Examine skin effect
% mi_seteditmode('blocks');
% mi_addblocklabel(IR_c+w_c/2,L_c/2);
% for j=-1.6:1.6/v_step:0
%     mi_seteditmode('nodes');
%     mi_drawline(IR_c+w_c-2*delta*10^(j),L_c,IR_c+w_c-2*delta*10^(j),0);
%     mi_seteditmode('blocks');
%     mi_addblocklabel(IR_c+w_c-2*delta*10^(j)+0.0025,L_c/2);
% end

%%%%-Drawing Cylinder (2) %%%%%%%%%%%%%%%%%%%%%%
mi_seteditmode('nodes');
mi_addnode(ir_c,0);
mi_addnode(ir_c,l_c);
mi_addnode(or_c,0);
mi_addnode(or_c,l_c);

mi_seteditmode('segments');
mi_addsegment(or_c,0,or_c,l_c);
mi_addsegment(ir_c,0,or_c,0);
mi_addsegment(or_c,l_c,ir_c,l_c);
mi_addsegment(ir_c,l_c,ir_c,0);

mi_seteditmode('blocks');
mi_addblocklabel((ir_c+or_c)/2,l_c/2);

%%%%-Drawing Shaft%%%%%%%%%%%%%%%%%%%%%%%%%%%%%%%
mi_seteditmode('nodes');
mi_addnode(ir_sh,L_c-w_sh);
mi_addnode(ir_sh,L_c);
mi_addnode(or_sh,L_c-w_sh);
mi_addnode(or_sh,L_c);
mi_addnode(ir_sh,L_c+l_sh);
mi_addnode(or_sh,L_c+l_sh);
mi_addnode(IR_c,L_c-w_sh);

mi_seteditmode('segments');
mi_addsegment(ir_sh,L_c-w_sh,IR_c,L_c-w_sh);
mi_addsegment(IR_c,L_c,or_sh,L_c);
mi_addsegment(or_sh,L_c,or_sh,L_c+l_sh);
mi_addsegment(ir_sh,L_c+l_sh,or_sh,L_c+l_sh);
mi_addsegment(ir_sh,L_c+l_sh,ir_sh,L_c-w_sh);

mi_seteditmode('blocks');
mi_addblocklabel((ir_sh+or_sh)/2,L_c+l_sh/2);

%%%%-Drawing Outlet Shield%%%%%%%%%%%%%%%%%%%%%%%%%%%%
mi_seteditmode('nodes');
mi_addnode(or_c,0);
mi_addnode(or_c,w_s);
mi_addnode(IR_c,0);
mi_addnode(IR_c,w_s);

mi_seteditmode('segments');
```

```
mi_addsegment(or_c,0,or_c,w_s);
mi_addsegment(or_c,w_s,IR_c,w_s);
mi_addsegment(IR_c,w_s,IR_c,0);
mi_addsegment(IR_c,0,or_c,0);

mi_seteditmode('blocks');
mi_addblocklabel(IR_c/2,w_s/2);
%%%%—Drawing Telemetry%%%%%%%%%%%%%%%%%%%%%%%%%%%%%%%%
mi_seteditmode('nodes');
mi_addnode(ir_tel,L_c+l_sh);
mi_addnode(OR_tel,L_c+l_sh);
mi_addnode(OR_tel,L_c+l_sh+w_tel);
mi_addnode(or_tel,L_c+l_sh+w_tel);
mi_addnode(or_tel,L_c+l_sh+w_tel+W_tel);
mi_addnode(ir_tel,L_c+l_sh+w_tel+W_tel);

mi_seteditmode('segments');
mi_addsegment(ir_tel,L_c+l_sh,OR_tel,L_c+l_sh);
mi_addsegment(OR_tel,L_c+l_sh,OR_tel,L_c+l_sh+w_tel);
mi_addsegment(OR_tel,L_c+l_sh+w_tel,or_tel,L_c+l_sh+w_tel);
mi_addsegment(or_tel,L_c+l_sh+w_tel,or_tel,L_c+l_sh+w_tel+W_tel);
mi_addsegment(or_tel,L_c+l_sh+w_tel+W_tel,ir_tel,L_c+l_sh+w_tel+W_tel);
mi_addsegment(ir_tel,L_c+l_sh+w_tel+W_tel,ir_tel,L_c+l_sh);

mi_seteditmode('blocks');
mi_addblocklabel((or_tel)/2,L_c+l_sh+(w_tel+W_tel)/2);

%%%%—Drawing Wires%%%%%%%%%%%%%%%%%%%%%%%%%

segm=L_c/(2*wires);

for i=1:wires

    mi_seteditmode('nodes');
    mi_addnode(IR_c+w_c+dist_c_w,(2*i—1)*segm—h_w/2);
    mi_addnode(IR_c+w_c+dist_c_w+w_w,(2*i—1)*segm—h_w/2);
    mi_addnode(IR_c+w_c+dist_c_w,(2*i—1)*segm+h_w/2);
    mi_addnode(IR_c+w_c+dist_c_w+w_w,(2*i—1)*segm+h_w/2);
    mi_seteditmode('segments');
    mi_addsegment(IR_c+w_c+dist_c_w,(2*i—1)*segm—h_w/2,IR_c+w_c+dist_c_w+w_w,(2*i—1)...
     ...*segm—h_w/2);
    mi_addsegment(IR_c+w_c+dist_c_w,(2*i—1)*segm+h_w/2,IR_c+w_c+dist_c_w+w_w,(2*i—1)...
     ...*segm+h_w/2);
    mi_addsegment(IR_c+w_c+dist_c_w,(2*i—1)*segm—h_w/2,IR_c+w_c+dist_c_w,(2*i—1)*...
     ...segm+h_w/2);
    mi_addsegment(IR_c+w_c+dist_c_w+w_w,(2*i—1)*segm—h_w/2,IR_c+w_c+dist_c_w+w_w,(2*...
     ...i—1)*segm+h_w/2);
    mi_seteditmode('blocks');
    mi_addblocklabel(IR_c+w_c+dist_c_w+w_w/2,(2*i—1)*segm);
end;

mi_clearselected();

%%%%%%%%%%%%%%%%%%%%%%%%%%%%%%%%%%%%%%%%%%%%%%%%%%%%Defining Materials%%%%%%%%%%%%%%%%%%%

mi_getmaterial('Air');
```

```
mi_getmaterial('1010 Steel');
mi_getmaterial('16 AWG');
mi_getmaterial('Aluminum, 1100');

%%%%—Air Domain (1) Material%%%%%%—
mi_seteditmode('blocks');
mi_clearselected();
mi_selectlabel(6*IR_c/2,L_c/2);
mi_setblockprop('Air',0,10,0,0,0,0);

%%%%—Air Domain (2) Material%%%%%%—
mi_seteditmode('blocks');
mi_clearselected();
mi_selectlabel(0.8*IR_c,L_c/2);
mi_setblockprop('Air',0,3,0,0,0,0);

%%%%—Cylinder (1) Material%%%%%%%%

mi_seteditmode('blocks');
mi_clearselected();
mi_selectlabel(IR_c+w_c/2,L_c/2);
%%Enable for temp distr
for i=1:c_v_segm
    mi_seteditmode('blocks');
    mi_selectlabel(IR_c+w_c/2,(i—0.5)*h_step);
    mi_setblockprop('1010 Steel',0,0.5,0,0,0,0);
end
%%Enable for skin effect
%mi_setblockprop('1010 Steel',0,0.5,0,0,0,0);
% for j=—1.6:1.6/v_step:0
%     mi_clearselected();
%     mi_selectlabel(IR_c+w_c—2*delta*10^(j)+0.0025,L_c/2);
%     mi_setblockprop('1010 Steel',1,0,0,0,0,0);
% end


%%%%—Cylinder (2) Material%%%%%%%%
mi_seteditmode('blocks');
mi_clearselected();
mi_selectlabel((ir_c+or_c)/2,l_c/2);
mi_setblockprop('1010 Steel',0,1,0,0,0,0);

%%%%—Outlet Shield Material%%%%%%—
mi_seteditmode('blocks');
mi_clearselected();
mi_selectlabel(IR_c/2,w_s/2);
mi_setblockprop('Air',0,2,0,0,0,0);



%%%%—Wires Material%%%%%%%%%%%%
for j=0:2:(groups—1)

    for i=j*wires/groups+1:(j+1)*wires/groups
        mi_seteditmode('blocks');
        mi_clearselected();
```

```
        mi_selectlabel(IR_c+w_c+dist_c_w+w_w/2,(2*i-1)*segm);
        mi_setblockprop('16 AWG',1,0,'I1',0,0,0);
        mi_clearselected();
    end;

    for i=(((j+1)*wires/groups)+1):((j+2)*wires/groups)
        mi_seteditmode('blocks');
        mi_clearselected();
        mi_selectlabel(IR_c+w_c+dist_c_w+w_w/2,(2*i-1)*segm);
        mi_setblockprop('16 AWG',1,0,'I2',0,0,0);
        mi_clearselected();
    end;
    mi_clearselected();
end;
mi_clearselected();

%%%%-Shaft Material%%%%%%%%
mi_seteditmode('blocks');
mi_clearselected();
mi_selectlabel((ir_sh+or_sh)/2,L_c+l_sh/2);
mi_setblockprop('1010 Steel',0,2,0,0,0,0);


%%%%-Telemetry Material%%%%%%%%
mi_seteditmode('blocks');
mi_clearselected();
mi_selectlabel((or_tel)/2,L_c+l_sh+(w_tel+W_tel)/2);
mi_setblockprop('Aluminum, 1100',0,2,0,0,0,0);


mi_clearselected();
%%%%%%%%%%%%%%%%%%%%%%%%%%%%%%%%%%%%%%%%%%Creating Mesh%%%%%%%%%%%%%-
mi_createmesh();
mi_showmesh();

%%%%%%%%%%%%%%%%%%%%%%%%%%%%%%%%%%%%%%-Running Analysis%%%%%%%%%%%%
mi_analyze();



%%%%%%POST PROCESSING%%%%%%%%%%
 mi_clearselected();

%%%%%%%%%%%%%%%%%%%%%%%%%%%%%%%%%%%%Loading Solution %%%%%%%%%%%%
 mi_loadsolution();

%%%%%%%%%%%%%%%%%%%%%%%%%%%%%%%%%%%Extracting Data Points%%%%%%
% mo_seteditmode('contour');
% mo_selectpoint(IR_c+w_c,0);
% mo_selectpoint(IR_c+w_c,L_c);
% mo_makeplot(8,1000,'Surface Current Density.txt',1);
%%Extract Heat Distribution
heat=zeros(1,c_v_segm);
for i=1:c_v_segm
    mo_seteditmode('blocks');
    mo_selectblock(IR_c+w_c/2,(i-0.5)*h_step);
```

```
    heat(i)=abs(mo_blockintegral(6));
    mo_clearblock();
end
plot(heat);
xlabel('Segment Number');
ylabel('Power [W]');
title('Heat Generation in each Segment');

%                          Print the plots
filename=strcat('C:\Users\Odyssefs\Google Drive\Thesis_Volvo_file\Written_documents\...
 ...Final_Report\MatlabFigurer\solenoid_power.eps');
print('-depsc',filename)



%Inductive Heating of Cylinder
% ------------------------------------------------------------------------

% The package must be initialized with the openfemm command.
% This command starts up a FEMM process and connects to it
addpath('C:\femm42\mfiles');
openfemm;



 newdocument(2)     %Creating New Document

%------------------------------setcompatibilitymode(0)  ------Setting the ...
 ...Compatibility mode for FEMM 4.2 as against FEMM 4.1

% showconsole()
% clearconsole()
% hidepointprops()

%--------------------Defining Problem----------------------------------------------------------

hi_probdef('millimeters','axi',1E-08, 10 ,20);  %------Defining the Problem
hi_saveas('Cylinder.feh');              %------Saving the Problem
hi_setfocus('Cylinder.feh') ;           %------Focussing on the Problem
hideconsole();
hi_close();

opendocument('Cylinder.feh');                   %------Opening the saved file
hi_setfocus('Cylinder.feh');                %------Setting the focus on the problem

%--------------------Drawing The Geometry------------------------------------------------------

%%%%-Drawing Cylinder (1) ----------------------
hi_seteditmode('nodes');
hi_drawrectangle(IR_c,0,IR_c+w_c,L_c)


%%Examine Heat Distribution

h_step=L_c/c_v_segm;
```

```
for i=1:c_v_segm
    hi_seteditmode('nodes');
    hi_drawline(IR_c,i*h_step,IR_c+w_c,i*h_step)
    hi_seteditmode('blocks');
    hi_addblocklabel(IR_c+w_c/2,(i-0.5)*h_step);
end


%%%%%%%%%%%%%%%%%%%%%%%%%%%%%%%%%%%%%%%%%%Defining Materials%%%%%%%%%%%%%%%%%%
hi_getmaterial('347 Stainless Steel');


%%%%-Cylinder (1) Material%%%%%%%%

hi_seteditmode('blocks');
hi_clearselected();
hi_selectlabel(IR_c+w_c/2,L_c/2);

for i=1:c_v_segm
    hi_seteditmode('blocks');
    hi_selectlabel(IR_c+w_c/2,(i-0.5)*h_step);
    hi_setblockprop('347 Stainless Steel',0,0.5,0);
end
%%Create Convection Boundary
hi_addboundprop('Convection',2,0,0,353.15,650,0);

%%Create Heat Sources
for i=1:c_v_segm
    source_name=strcat('heat_segm_',num2str(i));
    hi_addconductorprop(source_name,0,heat(i),0);
    hi_selectsegment(IR_c+w_c,(i-0.5)*h_step);
    hi_setsegmentprop('<None>',0,1,0,0,source_name);
    hi_clearselected();
    hi_selectsegment(IR_c,(i-0.5)*h_step);
    hi_setsegmentprop('Convection',0,1,0,0,'<None>');
    hi_clearselected();
end

hi_clearselected();
%%%%%%%%%%%%%%%%%%%%%%%%%%%%%%%%%%%%%%%%%%%%Creating Mesh%%%%%%%%%%%%%%-
hi_createmesh();
hi_showmesh();

%%%%%%%%%%%%%%%%%%%%%%%%%%%%%%%%%%%%%%%%-Running Analysis%%%%%%%%%%%%
hi_analyze();




%%%%%%POST PROCESSING%%%%%%%%%%
hi_clearselected();

%%%%%%%%%%%%%%%%%%%%%%%%%%%%%%%%%%%%%%Loading Solution %%%%%%%%%%%%
hi_loadsolution();

%%%%%%%%%%%%%%%%%%%%%%%%%%%%%%%%%%%%%Extracting Data Points%%%%%%
```

```
% mo_seteditmode('contour');
% mo_selectpoint(IR_c+w_c,0);
% mo_selectpoint(IR_c+w_c,L_c);
% mo_makeplot(8,1000,'Surface Current Density.txt',1);
%%Extract Heat Distribution
temperature=zeros(1000,1);
for i=1:1000
temperature(i),Fx,Fy,Gx,kx,ky=ho_getpointvalues(IR_c,i*L_c/1000);
end
plot(temperature,i/5)
```

B.2 Convective Cooling

```
%% Auther of script: Johan Froeb
% Convectiv heat transfer coefficient calculation of oil flowing in between
% two parallel plates

%% %%%%%%%%%%%%%%%%%%%%-------- Assumptions ---------%%%%%%%%%%%%%%%%%%%%%%%%%%
%%%%%%%%%%%%%%%%%%%%%%%%%%%%%%%%%%%%%%%%%%%%%%%%%%%%%%%%%%%%%%%%%%%%%%%%%%%%%%%
%
% * Thin oil film approximated with infinite square duct
% * Steady state and adiabatic outer surfaces
% * Constant oil properties given by the mean value of the
%   avrage temperature of the oil and the surface temperature.
% * Incompressible flow
% * Negliable radiation effects.


%% %%%%%%%%%%%%%%%%-------- collecting parameters --------%%%%%%%%%%%%%%%%%%%%%%
%%%%%%%%%%%%%%%%%%%%%%%%%%%%%%%%%%%%%%%%%%%%%%%%%%%%%%%%%%%%%%%%%%%%%%%%%%%%%%%
parameters;

%% %%%%%%%%%%%%%%%%%%%%----------- Solution ------------%%%%%%%%%%%%%%%%%%%%%%%%%
%%%%%%%%%%%%%%%%%%%%%%%%%%%%%%%%%%%%%%%%%%%%%%%%%%%%%%%%%%%%%%%%%%%%%%%%%%%%%%%

for m=1:10
    for    p=1:10;
        %Heat transfer part
        while abs((Ti + To)/2 - Ta(p,m)) >= 0.00000001;

            Ta(p,m)   = (Ti + To) / 2;            % - [oC]
            Te   = (Ta(p,m) + Ts)/2;              % - [oC]
            [Cp,rho,my,k] = O_prop_heat( Te );
            To   = Ti + Q / (Cp * rho * Vf(p));   % - [oC]
            Re   = fRe(cf(p),Dh(m),my,rho);
            Pr   = fPr(Cp,my,k);

            if Re < 2300
                Ll = 0.05.*Re.*Dh(m);             % - [m]
                Lh = Ll*Pr;                % - [m]
```

```
            if l < Lh     % Only entery region conditions

                aNu = aNuf(Dh(m),l,Re,Pr);

            else          %Partly entrance conditions partly fully developed
                aNu1 = aNuf(Dh(m),l,Re,Pr);
                aNu = 8.24*Lh ./ l + aNu1 * (1 -(Lh/l));
            end

        elseif Re > 10000               % In this case everything can be ...
         ...approximated to fully
            % developed flow since turbulence occurs in around 10*Dh(m) since Dh...
             ...(m) << l
            f = (0.790 .* log(Re) - 1.64).^-2;
            aNu = aNutf( f,Re,Pr );

        else              % Flow changes between laminar and turbulent randomly ...
         ...still assumed to be fully developed
            f = (0.790 .* log(Re) - 1.64).^-2;
            aNu = aNuf(Dh(m),l,Re,Pr) + (exp((2617-Re)/207)+ aNutf( f,Re,Pr)^-0...
             ....95)^-0.95;

        end
        ah  = aNu.*k./Dh(m);                % - [w/m2 k]
        Ts  = q./ah + (Ti + To)./2;         % - [oC]

        % Shear stress at surface of oil
        Tau = fTau( cf(p),rho,my,l );
        Taur = fTau( cr(p),rho,my,l,d(m) );
    end
    ahm(p,m) = ah;
    Tsm(p,m) = Ts;
    Rem(p,m) = Re;
    Prm(p,m) = Pr;
    Cpm(p,m) = Cp;
    Taum(p,m) = Tau;
    Taurm(p,m) = Taur;

end

end

%% %%%%%%%%%%------------------ Ploting -----------------%%%%%%%%%%%%%%%%%%%%%
%%%%%%%%%%%%%%%%%%%%%%%%%%%%%%%%%%%%%%%%%%%%%%%%%%%%%%%%%%%%%%%%%%%%%%%%%%%

albin = figure;
set(albin, 'Position', [300 300 700 600])
mesh(rot,Vf*60*1000,ahm);
xlabel('Rotational speed [rpm]','FontSize',12);
ylabel('Volume flow [l / min]','FontSize',12);
zlabel('heat transfer coefficient [w / m^2 K]','FontSize',12);
title('Heat transfer coefficient for different fluid volume flows and rotational ...
 ...speed','FontSize',13,'FontWeight','bold');
view(135,45);
print('-depsc','Z:\Written_documents\Latex_Teplate_Main_Report\MatlabFigurer\...
 ...h_inf_plate.eps');
```

```
bertil = figure;
set(bertil, 'Position', [300 300 700 600])
mesh(rot,Vf*60*1000,Rem);
xlabel('Rotational speed [rpm]','FontSize',12);
ylabel('Volume flow [l / min]','FontSize',12);
zlabel('Reynolds Number [-]','FontSize',12);
title('Reynolds Number for different fluid volume flows and film thickness','...
 ...FontSize',13,'FontWeight','bold');
view(135,45);
print('-depsc','Z:\Written_documents\Latex_Teplate_Main_Report\MatlabFigurer\...
 ...Reynolds_inf_plate.eps');

caesar = figure;
set(caesar, 'Position', [300 300 700 600])
mesh(rot,Vf*60*1000,Prm);
xlabel('Rotational speed [rpm]','FontSize',12);
ylabel('Volume flow [l / min]','FontSize',12);
zlabel('Prandtl Number [-]','FontSize',12);
title('Prandtl Number for different fluid volume flows and film thickness','FontSize...
 ...',13,'FontWeight','bold');
view(135,45);
print('-depsc','Z:\Written_documents\Latex_Teplate_Main_Report\MatlabFigurer\...
 ...Prandtl_inf_plate.eps');

david = figure;
set(david, 'Position', [300 300 750 600])
mesh(rot,Vf*60*1000,Tsm);
xlabel('Rotational speed [rpm]','FontSize',12);
ylabel('Volume flow [l / min]','FontSize',12);
zlabel('Avrage temperature of surface [oC]','FontSize',12);
title('Avrage surface temperature for different fluid volume flows and film ...
 ...thickness','FontSize',13,'FontWeight','bold');
view(135,45);
print('-depsc','Z:\Written_documents\Latex_Teplate_Main_Report\MatlabFigurer\...
 ...average_temperature_inf_plate.eps');

erik = figure;
set(erik, 'Position', [300 300 950 600])
mesh(Dh/2*1000,Vf*60*1000,Taum);
xlabel('fluid layer thickness [mm]','FontSize',12);
ylabel('Volume flow [l / min]','FontSize',12);
zlabel('Stress of fluid top layer [N / m2]','FontSize',12);
title('Avrage shear stress of fluid layer in contact with air for different fluid ...
 ...volume flows and film thickness','FontSize',13,'FontWeight','bold');
view(135,45);

fredrik = figure;
set(fredrik, 'Position', [300 300 950 600])
mesh(Dh/2*1000,cr,Taum);
xlabel('fluid layer thickness [mm]','FontSize',12);
ylabel('Ratational speed of cylinder [rpm]','FontSize',12);
zlabel('Stress of fluid top layer [N / m2]','FontSize',12);
title('Avrage shear stress of fluid layer in contact with air for different ...
 ...rotational speeds and film thickness','FontSize',13,'FontWeight','bold');
view(135,45);
```

```
print('-depsc','Z:\Written_documents\Latex_Teplate_Main_Report\MatlabFigurer\...
 ...average_shear_inf_plate.eps')

copyfile('aNuf.m','Z:\Written_documents\Latex_Teplate_Main_Report\mfiles')
copyfile('aNutf.m','Z:\Written_documents\Latex_Teplate_Main_Report\mfiles')
copyfile('fPr.m','Z:\Written_documents\Latex_Teplate_Main_Report\mfiles')
copyfile('fRe.m','Z:\Written_documents\Latex_Teplate_Main_Report\mfiles')
copyfile('fTau.m','Z:\Written_documents\Latex_Teplate_Main_Report\mfiles')
copyfile('main_inf_sq.m','Z:\Written_documents\Latex_Teplate_Main_Report\mfiles')
copyfile('O_prop_heat.m','Z:\Written_documents\Latex_Teplate_Main_Report\mfiles')
copyfile('parameters.m','Z:\Written_documents\Latex_Teplate_Main_Report\mfiles')



%%% Initiziating
% Clearing history and old paramters
clear
close
clc
%% Geometrical properties (l,d,A)
% Input of parameters for the base geometry. The cylinder is converted into
% a flat plate

% Lenght and inner diameter of cylinder
l  = 0.245;           % - [m]
D  = 0.091;             % - [m]

% Interior surface area
As = pi*D*l;            % - [m^2]
%% Heat flux generated by eddy currents (Q,q)
% It is assumed that all of the heat is evenly distributed over the flat
% plate and the specific heat is calculated

% Total heat flux

Q = 120;             % - [w]

% Specific heat flux
q  = Q/As;              % - [w/m^2]
clear('As')

%% Temperature of oil (Tx)
% Setting inlet temperature and creating some temperature parameters that
% will be needed in the calculations later
%
%Ti corresponding to Inlet temperature of oil, Te corresponding to
%evaluation temperature of oil, To outlet temperature of oil, Tm value of
%inlet and outlet of oil, Ts surface temperature of cylinder.

Ti  = 70;                   % - [C]
Te  = 0;                    % - [C]
To  = 75;                   % - [C]
Ts  = 80;                   % - [C]
Ta  = zeros(10,10);         % - [C]
%% Flow properties of the oil (c, V, dh)
% Setting a flow for the calculation and evaluation of speed of oil in
% oil film
```

```
Vf = zeros(1,10);
d=zeros(1,10);
d = D-[0.002 0.0014 9.8052e-4 6.9374e-4 4.9084e-4 4.009e-4 3.4726e-4 3.1065e-4 2...
 ....8962e-4 2.5371e-4];    % -
rot = [250 500 1000 2000 4000 6000 8000 10000 12000 15000];
cr=zeros(1,10);
for j=1:10
Vf(j) = j*1e-6;          % - [m^3/s]
cr(j) = 12000/10*j;      % - [m]
end
Dh = (D - d);            % - [m]
A  = pi/4*(D.^2-d.^2);   % - [m^2]
cf = Vf./A;              % - [m/s]
clear('A')

%% Zero matrices for script speed
ahm = zeros(10,10);
Rem = zeros(10,10);
Prm = zeros(10,10);
Cpm = zeros(10,10);
Tsm = zeros(10,10);
Taum = zeros(10,10);
Taumr = zeros(10,10);
```

```
function [ cp,rho,mu,k ] = O_prop_heat( Te )
%O_prop Evaluates the properties of the oil
%   Calculates specific heat, density, kinematic viscosity
%   and thermal conductivity of the oil for the input temperature

cp  = 8.56347497578923E-10*Te^6 - 5.60679777499191E-07*Te^5 + 1.46041698395822E-04*...
 ...Te^4 - 1.92163363495118E-02*Te^3 + 1.33413696987957E+00*Te^2 - 4.20275266498549E...
 ...+01*Te + 2.65171116405800E+03;           %cp  -   [w/kg,k]
rho = 861+0.65*(Te-20);               %rho -   [kg/m^3]
nu = 1.42990531930781E-16*Te^6 - 1.07775218991638E-13*Te^5 + 3.28913896710315E-11*Te...
 ...^4 - 5.21839373386197E-09*Te^3 + 4.58574164157495E-07*Te^2 - 2.17102813727036E...
 ...-05*Te + 4.59663172327839E-04;
mu  = nu*rho;        %mu  -   [m^2/s]
k   = -0.00000000000001355424*Te^6 + 0.00000000000851457904*Te^5 - 0...
 ....00000000207107699164*Te^4 + 0.00000024356008224605*Te^3 - 0...
 ....00001410866527912790*Te^2 + 0.00047475111017918000*Te + 0.13946681765144700000;...
 ...        %k   -   [w/m,k]
end
```

```
function [ Pr ] = fPr( Cp,mu,k )
%fPr Calculates Prandtl Number
%   Prandtl number is evaluated based on the parameters which are given as
%   input arguments.

Pr=Cp.*mu./k;
end
```

```
function [ Re ] = fRe( cf,Dh,my,rho )
```

```
%fRe Calculates Reynolds Number
%   Reynolds number is evaluated based on the parameters which are given as
%   input arguments.

Re=rho.*cf.*Dh./my;
end



function [ aNu ] = aNuf(Dh,l,Re,Pr)
%aNuf Average Nusselt Number two parallel plates.
%   Calculates the nusselt number with the given inputs Re, the reynolds
%   number and Pr the prandtl number.

%   The relation is empirical for two parallel plates
%   with a constant heat flux

aNu = 8.24 + (0.03.*(Dh ./ l).*Re.*Pr) / (1+0.016.*((Dh / l).*Re.*Pr).^(2/3));

end



function [ aNu ] = aNutf( f,Re,Pr )
%aNutf Average Nusselt Number two parallel plates.
%   Calculates the nusselt number with the given inputs Re, the reynolds
%   number and Pr the prandtl number.

%   The relation is empirical for two parallel plates
%   with a constant heat flux turbulent flow

aNu = (f/8).*(Re - 1000).*Pr/(1 + 12.7.*(f/8).^0.5.*(Pr.^(2./3)-1));

end



function [ Tau ] = fTau( c,rho,my,l,d )
%fTau Returns the shear stress of the fluid surface against air
%   Approximation of shear stress of fluid surface against air. The oil
%   surface is assumed to behave like a solid wall. All properties are
%   assumed to be constant along the wall
if nargin == 4

    Tau=2*0.332 / 3*c*sqrt(rho*my*c*l);

% for rotational velocity. Assumning that, indepentent of rotational speed,
% the surface and boundary layer is stable after one revolution
elseif nargin == 5

    Tau=2*0.332 / 3*c/60*d*pi*sqrt(rho*my*c/60*d*pi*d*pi);

end
```

B.3 Resistance heating over airgap

```
%% Auther of script: Johan Froeb
% Convectiv heat transfer coefficient calculation between steel cylinders
% in air-gap of various size


%% %%%%%%%%%%%%%%-------- Table of parameters --------%%%%%%%%%%%%%%%%%%%%%%%
%%%%%%%%%%%%%%%%%%%%%%%%%%%%%%%%%%%%%%%%%%%%%%%%%%%%%%%%%%%%%%%%%%%%%%%%%%%%
% D: Diameter
% Re: Reynolds number
% g: gap
% nu: kinematic viscosity
% l: Thickness
% Ta: Taylor Number
% L: Length of cylinder
% Q: Heat
% k: Thermal conductivity
% h: Convective heat transfer coefficient
% R: Thermal resistance equivalent
% F: Geometrical factor
% Nu: Nusselt Number
% S: Superconstant


%-%-%-SUBSCRIPT-%-%-%
% ic: inner cylinder
% a: air
% oc: outer cylinder
% h: Hydralic
% ss: Stainless Steel
% Cr: Critical
% g: gap
% o: Tangential
% tot: Total

%% Geometrical dimensions
D_ic = 105e-3;                                  % - [m]
l_ic = 7.5e-3;                                  % - [m]
a = D_ic / 2;                                   % - [m]
g_a = 0.5e-3;                                   % - [m]
d_oc = D_ic + 2*g_a;                            % - [m]
l_oc = 3e-3;                                    % - [m]
b = d_oc / 2;                                   % - [m]
D_h_g = 2*g_a;                                  % - [m]
D_h = pi / 4 * (d_oc^2 - D_ic^2);               % - [m]
L = 200e-3;                                     % - [m]
RPS=zeros(1,100);
p=zeros(1,100);
q=zeros(1,100);
h=zeros(1,100);
dT=zeros(1,100);
dT_g=zeros(1,100);
```

```
for i=1:100
    RPS(i) = i*150/60;                          % - [s^-1]
end

Q = 400;                                    % - [W]
T_a = 100+273.15;
nu_a = (9.5e-11*T_a^2 + 3.873e-8*T_a -  4.2775e-6);
k_a = -0.00000002*T_a^2 + 0.0000886 * T_a + 0.0015;
k_ss = 16.6;

%% %%%%%%%%%%%%%%%%%%%%---------- Solution ----------%%%%%%%%%%%%%%%%%%%%%%%%
%%%%%%%%%%%%%%%%%%%%%%%%%%%%%%%%%%%%%%%%%%%%%%%%%%%%%%%%%%%%%%%%%%%%%%%%%%%

for i=1:100
    % Taylor number
    Ta_m_cr = 41.19;
    Ta_m = (2*pi*RPS(i)* (D_ic + g_a)^0.5 * g_a^1.5) / nu_a;

    %Geometrical parameters
    S = 0.0571 * (1-0.652 * (b - a) / a) + 0.00056 * (1-0.652*(b-a)/a)^-1;
    F_g = pi^2/Ta_m_cr/sqrt(S) * (1-(b-a)/2/(a/2 + b/2))^-1;

    if Ta_m^2/F_g^2 <= 1700
        Nu = 2* ((b-a)/a)/log(1+(b-a)/a);
    elseif Ta_m^2/F_g^2 > 10^7
        disp('Out of bounds')

    else
        if Ta_m <= Ta_m_cr

            Nu = 0.128 * (Ta_m^2/F_g^2)^0.367;
        else
            Nu = 0.409 * (Ta_m^2/F_g^2)^0.241;

        end

    end
    h(i) = Nu*k_a/(2*(b-a));                    % - [w/m2 k]
    p(i) = Ta_m;
    q(i) = Nu;



    %Sum of thermal resistance

    R_oc = log((b+l_oc) / b) / (2 * pi * L * k_ss);
    R_ic = log((a+l_ic) / a) / (2 * pi * L * k_ss);
    R_g = 1 / (h(i) * 2 * pi * (a+l_ic) * L);

    R_tot = R_oc + R_ic + R_g;

    dT_g(i) = Q * R_g;
    dT(i) = Q * R_tot;
end
```

```
figure(1); plot(RPS*60,dT_g,RPS*60,dT)
title('Temperature over gap','FontSize',14,'FontWeight','bold')
xlabel('Rotatinal speed [RPM]    ','FontSize',13)
ylabel('Temperature [oC]    ','FontSize',13)
g=legend('Without cylinder wall considered','With cylinder wall considered');
set(g,'position',[0.5 0.60 .25 .13]);
print('-depsc','Z:\Written_documents\Latex_Teplate_Main_Report\MatlabFigurer\...
 ...heating_over_airgap.eps')

figure(2); plot(RPS*60,dT)
title('Temperature over entire insulating lenght','FontSize',14,'FontWeight','bold')
xlabel('Rotatinal speed [RPM]      ','FontSize',13)
ylabel('Temperature [oC]       ','FontSize',13)
print('-depsc','Z:\Written_documents\Latex_Teplate_Main_Report\MatlabFigurer\...
 ...heating_over_airgap_and_cylinder.eps')

figure(3); plot(RPS*60,h)
title('Convevtive heat transfer coefficient in air gap','FontSize',14,'FontWeight','...
 ...bold')
xlabel('Rotatinal speed [RPM]    ','FontSize',13)
ylabel('Heat transfer coefficient [w/m  ^2 K]    ','FontSize',13)

figure(4); plot(RPS*60,p)
title('Taylor number to characterize the flow')
xlabel('Rotatinal speed [RPM]')
ylabel('Taylor number [-]')

figure(5); plot(RPS*60,q)
xlabel('Rotatinal speed [RPM]')
ylabel('Nusselt number [-]')
title('Nusselt Number to calculate the heat transfer coefficient')


copyfile('air_gap.m','Z:\Written_documents\Latex_Teplate_Main_Report\mfiles')
```

B.4 Pump performance

```
%%
[disc,txt] = xlsread('pump_curv.txt');
% Tube characteristics
d = [4e-3; 10e-3];                  % Diameter of pipe - [m]
e = [0.002 ; 0.002];                % Surface roughtness - [mm]
T_o = 70 + 273.15;                  % Temperature of oil - [K]
g = 9.81;                           % gravitational constant
in=80;
n = 100;                             % Number of different flows - [-]
i_l = 1.25e-6;                      % Increment lenght - [m3/s]


Vf_o = zeros(1,n);                  % creating zeros for faster calculation
Vf_op1 = zeros(1,in);
dP_p1 = zeros(1,in);
hL = zeros(1,n);
```

```
f = zeros(1,n);
dP_p=zeros(round(length(txt)),2);
Vf_op=zeros(round(length(txt)),2);

A = d.^2 ./4 .*pi;                  % Area of duct / pipe - [m2]
Dh = d.*pi;                         % Wet perimiter - [m]
L = [0.35 ; 2];                     % Length of pipe - [m]
Kl = [0.8 ; 0.5];                   % Minor losses factor - [-]

[nu,rho] = O_prop_pump(T_o);                % Kinematic viscosity

for i = 1:n
    Vf_o(i) = i * i_l;               % Volumeflow - [m3/s]
    [vL, mL, out3] = pipeloss(Vf_o(i),L,A,Dh,e,Kl,nu); % - function
    hL(i) = sum(vL) + sum(mL);
    f(i) = sum(out3);
end
dP = rho * g * hL;

for i=1:round(length(txt))
    Vf_op(i,1)=str2double(cell2mat(txt(i,2)));
    Vf_op(i,2)=Vf_op(i,1)*0.06309;
    dP_p(i,1)=str2double(cell2mat(txt(i,1)));
    dP_p(i,2)=dP_p(i,1)*6.894757;
end

p = polyfit(Vf_op(:,2),dP_p(:,2),2);

n=Vf_op(1,2)/in;

for m=1:in
    Vf_op1(m)=n*m;
    dP_p1(m)=p(1)*Vf_op1(m)^2+p(2)*Vf_op1(m)+p(3);
end

dP_px = [dP_p1  dP_p(:,2)'];
Vf_opx = [Vf_op1  Vf_op(:,2)'];

[xout,yout] = intersections(Vf_op1,dP_p1,Vf_o*1000,dP/1000,1);

figure(1); plot(Vf_o*1000*600,dP/1000,Vf_op1*600,dP_p1,Vf_op(:,2)*600,dP_p(:,2),xout...
 ...*600,yout,'o')
xlabel('volume flow [dl/min]');
ylabel('Pressure drop [kPa]');
legend('System curve','Pump curve fitted','pump curve manufactureer')
title('Pump and system curves with Pressure drop as a funktion of volume flow in SI-...
 ...units')
print('-depsc','Z:\Written_documents\Latex_Teplate_Main_Report\MatlabFigurer\...
 ...pump_sys_curv.eps')

%
figure(2)
plot(dP_p(:,1),Vf_op(:,1),dP_p1/6.894757,Vf_op1/0.06309)
ylabel('volume flow [Gpm]');
xlabel('System curve [Psi]');
legend('Original from manufacturer','Polyfit from matlab')
```

```
title('Pump curve')
print('-depsc','Z:\Written_documents\Latex_Teplate_Main_Report\MatlabFigurer\...
 ...poly_manu.eps')

figure(3)
plot(dP_p(:,1),Vf_op(:,1))
ylabel('volume flow [Gpm]');
xlabel('System curve [Psi]');
title('Pump curve (Original from manufacturer)')
print('-depsc','Z:\Written_documents\Latex_Teplate_Main_Report\MatlabFigurer\...
 ...pump_sheet.eps')

% Saving the documents into report m.folder

copyfile('Pipelosses_comp.m','Z:\Written_documents\Latex_Teplate_Main_Report\mfiles'...
 ...)
copyfile('moody.m','Z:\Written_documents\Latex_Teplate_Main_Report\mfiles')
copyfile('O_prop_pump.m','Z:\Written_documents\Latex_Teplate_Main_Report\mfiles')
copyfile('intersections.m','Z:\Written_documents\Latex_Teplate_Main_Report\mfiles')
copyfile('pipeloss.m','Z:\Written_documents\Latex_Teplate_Main_Report\mfiles')


function [ out1,out2,out3,out4] = O_prop_pump( Te )
%O_prop Evaluates the properties of the oil
%   Calculates specific heat, density, kinematic viscosity and thermal conductivity ...
 ...of the oil for the input temperature

cp  = 1820.306276 + 3.668076738*Te - 2.73673*10^-6 *Te.^2 ;           %cp  -   [w/kg...
 ...,k]
rho = 864.328071 - 0.624086175*Te - 0.000114349*Te.^2;                %rho -   [kg/m...
 ...^3]
mu  = exp(-1.612780981 - 0.051250279*Te + 0.000155818*Te.^2) ;        %mu   -   [m...
 ...^2/s]
k   = 0.137105815 - 7.75251*10^-5 *Te + 3.78396*10^-8 *Te.^2 ;        %k   -   [w/m,...
 ...k]
nu = mu / rho;

if nargout == 1
    out1=nu;
elseif nargout == 2
    out1 = nu;    out2 = rho;
elseif nargout == 4
    out1 = cp;    out2 = rho;
    out3 = mu;    out4 = k;
else
    error('only 1, 2 or 4 output arguments are allowed');

end


function [out1,out2,out3] = pipeloss(Q,L,A,Dh,e,Kl,nu)
%%
%  Q volumeflow, L Length for each section of the pipe,
%  A cross-section area, Dh Hydralic diameter, e pipe roughness, Kl minor
%  losses and nu kinematic viscousity
```

```
g = 9.81;

if isempty(L)
    hv = 0;  f = [];
else
    c = Q./A;
    f = zeros(size(L));
    for k=1:length(f)
        f(k) = moody(e(k)/Dh(k),c(k)*Dh(k)/nu);
    end
    hv = f.*(L./Dh).*(c.^2)/(2*g);
end

if isempty(Kl)
    hm = 0;                          %  no minor lossess
else
    hm = Kl.* mean(c)^2 / (2*g);     %  minor lossess
end

if nargout==1
    out1 = sum(hv) + sum(hm);    %  return hL = total head loss
elseif nargout==2
    out1 = hv;  out2 = hm;       %  return vectors of viscous and minor losses
elseif nargout==3
    out1 = hv;  out2 = hm;       %  return vectors of viscous and minor losses
    out3 = f;                    %  and friction factors
else
    error('Only 1, 2 or 3 output arguments are allowed');
end



function f = moody(ed,Re,Var)
%% moody
%
if Re<0
    error(sprintf('Reynolds number = %f cannot be negative',Re));
elseif Re<2000
    f = 64/Re;  return      %  laminar flow
else
    f = sqrt(1/(-1.8*log10((6.9/Re)+(ed/3.7)^1.11))); %Turbulent flow

end
if ed>0.05
  warning(sprintf('epsilon/diameter ratio = %f is not on Moody chart',ed));
end

findf = inline('1.0/sqrt(f) + 2.0*log10( ed/3.7 + 2.51/( Re*sqrt(f)) )','f','ed','Re...
 ...');
fi = 1/(1.8*log10(6.9/Re + (ed/3.7)^1.11))^2;   %  initial guess at f
dfTol = 5e-6;
f = fzero(findf,fi,optimset('TolX',dfTol,'Display','off'),ed,Re);
end
```

B.5 Post process of experimental data

```
function [ cp,rho,my,k ] = O_prop( Te )
%O_prop Evaluates the properties of the oil
%   Calculates specific heat, density, kinematic viscosity and thermal conductivity ...
 ...of the oil for the input temperature

cp  = 1820.306276 + 3.668076738*Te - 2.73673*10^-6 *Te.^2 ;          %cp  -   [w/kg...
 ...,k]
rho = 864.328071 - 0.624086175*Te - 0.000114349*Te.^2;               %rho -   [kg/m...
 ...^3]
my  = exp(-1.612780981 - 0.051250279*Te + 0.000155818*Te.^2) ;       %\mu  -   [m...
 ...^2/s]
k   = 0.137105815 - 7.75251*10^-5 *Te + 3.78396*10^-8 *Te.^2 ;       %k   -   [w/m,...
 ...k]
end



%% Acquire data

%Assumes that there is a thermocouple in the far end of the cylinder
%Assumes that oil initial temperature is 75 degress C
%Temperature is numbered from inlet to outlet, T1 being closest to the
%inlet
clear all;close all;clc
% Enter file name

Filename = 'Data\untouched\500_03_new.csv';

% Retrieving data

[TIME, T1, T2, T3, T4, T5, T6, T7, T8, OMEGA, VOLFLOW, T_in, Disc, V_FEED_FLOW] = ...
 ...csvimport(Filename, 'columns', [1:14],'rows',[120:900], 'noHeader', true, '...
 ...delimiter', ',');

%Removing the heading of the vector
rem_tot=120;
rem = 1:rem_tot/2;
TIME(rem) = [];
T1(rem) = [];
T2(rem) = [];
T3(rem) = [];
T4(rem) = [];
T5(rem) = [];
T6(rem) = [];
T7(rem) = [];
T8(rem) = [];
OMEGA(rem) = [];
VOLFLOW(rem) = [];
T_in(rem) = [];
V_FEED_FLOW(rem) = [];

%Manipulating the temepratures for Kelvin, converting to numbers and
%filtering the data
```

```
OMEGA = str2double(OMEGA);
VOLFLOW = str2double(VOLFLOW);
V_FEED_FLOW = smooth(str2double(V_FEED_FLOW),100) * 22 * 0.5 * 6 * 1E-3 * 1E-3 / 60;
T1 = smooth(str2double(T1),20)+273.15;
T2 = smooth(str2double(T2),20)+273.15;
T3 = smooth(str2double(T3),20)+273.15;
T4 = smooth(str2double(T4),20)+273.15;
T5 = smooth(str2double(T5),20)+273.15;
T6 = smooth(str2double(T6),20)+273.15;
T7 = smooth(str2double(T7),20)+273.15;
T8 = smooth(str2double(T8),20)+273.15;
T_in = smooth(str2double(T_in),20)+273.15;


%Decreasing the number of data points
dt = 0.2; % Actual timestep
adt = 5; % desired timestep
short = adt / dt; % Scale factor
n=length(T1);

TIMEn=zeros(n/short,1);
T1n=zeros(n/short,1);
T2n=zeros(n/short,1);
T3n=zeros(n/short,1);
T4n=zeros(n/short,1);
T5n=zeros(n/short,1);
T6n=zeros(n/short,1);
T7n=zeros(n/short,1);
T8n=zeros(n/short,1);
T_inn=zeros(n/short,1);
OMEGAn=zeros(n/short,1);
VOLFLOWn=zeros(n/short,1);
V_FEED_FLOWn=zeros(n/short,1);

%Fragment of further filtering [UNUSED]
%mean(   :i*short)

% Filtering the data
for i=1:floor(n/short)
    T1n(i) = T1(1+short*(i-1));
    T2n(i) = T2(1+short*(i-1));
    T3n(i) = T3(1+short*(i-1));
    T4n(i) = T4(1+short*(i-1));
    T5n(i) = T5(1+short*(i-1));
    T6n(i) = T6(1+short*(i-1));
    T7n(i) = T7(1+short*(i-1));
    T8n(i) = T8(1+short*(i-1));
    T_inn(i) = T_in(1+short*(i-1));
    OMEGAn(i) = OMEGA(1+short*(i-1));
    VOLFLOWn(i) = VOLFLOW(1+short*(i-1));
    V_FEED_FLOWn(i)= V_FEED_FLOW(1+short*(i-1));
end
clear V_FEED _FLOWVOLFLOW OMEGA T_in T_out T7 T6 T5 T4 T3 T2 T1
T_s = [T1n T2n T3n T4n T5n T6n T8n];

[n,mp] = size(T_s); % Number of samples x numbers of measuring points
```

```
% Properties of aluminum
k_Al    =   9.708333333E-6*T_s.^3 - 1.2937500000001E-2*T_s.^2 + 5.604166666667190*T_s...
 ... - 616.000000000082;
cp_Al  = 5.458333333E-6*T_s.^3 - 6.812500000006E-3*T_s.^2 + 3.249166666669800*T_s + ...
 ...365.999999999537;
rho_Al(1:n,1:mp) = 2770;

% Oil flow [THIS PART CAN BE REPLACED WITH SAMPLED DATA]
% ##########################################################DOUBLECHECK
% VOLTAGE

Q=V_FEED_FLOWn;

%dt = 1; % This is the timestep for the sampeling
t = linspace(adt,n*adt,n); % Corresponding times to the sampled data
R = 53e-3;
r = 45.5e-3;
L_max = 210e-3;
%-------------------------------------------------------------------------
%MIGHT CHANGE DUE TO UNEVEN DISTRIBUTION
%L_p is the actual point of the themocouple while L_l is the length
%surrounding the thermocouple for energy balance calculation
L_dead = 0.0005 + 0.001;
inc = (L_max-L_dead)/19;
L_p = [inc*(2-1+0.0005) inc*(4-1+0.0005) inc*(6-1+0.0005) inc*(8-1+0.0005) inc...
 ...*(11-1+0.0005) inc*(14-1+0.0005) inc*(20-1+0.0005)];

L_l = zeros(1,mp);
L_l(1,1) = L_p(1) + (L_p(2)-L_p(1))/2;
for bgga = 1:mp-2
    L_l(1+bgga) = (L_p(bgga+1)-L_p(bgga))/2 + (L_p(bgga+2)-L_p(bgga+1))/2;
end
L_l(1,mp)=L_max-L_p(mp)+(L_p(mp)-L_p(mp-1))/2;
%% Temperature of Oil and heat transfer coefficient
%T_i____T_1____T_2____T_3____T_4____T_5____T_6___T_o
dEdt = zeros(n,mp);
dEdt_tot = zeros(n,1);
T_o = zeros(n,mp+2);
T_o(:,1)= T_inn; % Oil inlet temperature
for ts=2:n
    % Calculating heat transfer in each measurement point
    dEdt(ts,:) = (cp_Al(ts-1,:) + cp_Al(ts,:))/2 .* (R^2-r^2) .* pi .* L_l .* (...
     ...rho_Al(ts-1,:)+rho_Al(ts,:))/2 .* (T_s(ts-1,:)-T_s(ts,:)) ./ (t(ts) - t(ts...
     ...-1));


        dEdt_tot(ts) =sum(dEdt(ts,:),2); % Sum upp all the heat



[ cp_O,rho_O,~,~ ] = O_props( T_inn(ts)-273.15);
T_o(ts,mp+2) = T_inn(ts) + dEdt_tot(ts)/Q(ts)/cp_O/rho_O; % Oil outlet temperature
for it=(1:10)
    T_o(ts,mp+2) = T_inn(ts) + dEdt_tot(ts)./Q(ts)/cp_O/rho_O; % Oil outlet ...
     ...temperature
```

```
    T_oe(ts) = (T_o(ts,1) + T_o(ts,mp+2))/2;
    [ cp_O,rho_O,~,~ ] = O_props( T_oe(ts)-273.15 );
end
for q=2:mp+1
    % Calculate temperature by assuming that its distribution looks
    % like the heat transfer distribution
    T_o(ts,q) = T_o(ts,q-1) + (T_o(ts,mp+2)-T_o(ts,1)) * dEdt(ts,q-1) / dEdt_tot(ts)...
     ...;

end
end

rem = 1:floor(rem_tot/short/2);
n=n-floor(rem_tot/short/2);
T_o(rem,:) = [];
dEdt(rem,:) = [];
dEdt_tot(rem) = [];
cp_Al(rem,:) = [];
rho_Al(rem,:) = [];
k_Al(rem,:) = [];
OMEGAn(rem,:) = [];
Q(rem,:) = [];
T_s(rem,:) = [];
%Heat transfer is proportional to the temperature differance since all the
%other parameters are quite constant. Thereby we get that

%% Properties of Oil - DONE!!!
T_oe = T_o - 273.15;
[ cp_O,rho_O,mu_O,k_O ] = O_props( T_oe );

%% THICKNESS MODEL
% Enter mp as well
p = 20000; % number of element the length of the cylinder will be devided in
rps = mean(OMEGAn)/60; % rotational speed of cylinder in RPS [Data can be insterted ...
 ...here as well]

% Mean thermal properties over entire length.
mu_a = mean(mu_O,2);
rho_a = mean(rho_O,2);
ed = 0.002; % ---------- NEEDS ADJUSTMENT AFTER CYLINDER ROUGHNESS---------

[ Th_O , v ] = thickness(Q,p,L_p,L_max,r,rps,ed,rho_a,mu_a,mp,n);

% thick = thickness(V,T_a,rpm,p,n,mu_a,rho_a);
clear ('mu_a','rho_a');
%%

d_h = 2 * real(Th_O);

dEdt_tot_O = Q .* (cp_O(:,mp+2).*rho_O(:,mp+2).*T_o(:,mp+2) - cp_O(:,1).*rho_O(:,1)....
 ...*T_o(:,1)); %Heat absorbed by the oil

l=zeros(n,mp);
for jj = 1:n
    l(jj,:)=L_l(1,:);
end
```

```
h_O = fh(dEdt,T_o(:,2:mp+1),T_s,l*2*r*pi);

Nu = fNu(h_O,d_h,k_O(:,2:mp+1));

Re = fRe(v,d_h,mu_O(:,2:mp+1),rho_O(:,2:mp+1));

Pr = fPr(cp_O(:,2:mp+1),mu_O(:,2:mp+1),k_O(:,2:mp+1));

Bi = fBi(h_O,k_Al(:,2:mp+1),R-r);

if Bi < 0.1

else
    disp('Warning: high biot number. Assumption of uniform temperature in aluminium ...
     ...might be false')
end

%-------------------------------------------------------------------------

h_O_tot = fh(dEdt_tot_O,(T_o(:,mp+2)+T_o(:,1))/2,(T_s(:,1)+T_s(:,mp))/2,L_max*2*r*pi...
 ...);

figure;plot(h_O_tot);

Nu_tot = fNu(h_O_tot,mean(d_h,2),mean(k_O(:,2:mp+1),2));

plot(Nu_tot);

Re_tot = fRe(mean(v,2),mean(d_h,2),mean(mu_O(:,2:mp+1),2),mean(rho_O(:,2:mp+1),2));

Pr_tot = fPr(mean(cp_O(:,2:mp+1),2),mean(mu_O(:,2:mp+1),2),mean(k_O(:,2:mp+1),2));

Bi_tot = fBi(h_O_tot,mean(k_Al(:,1:mp),2),R-r);

if Bi_tot < 0.1

else
    disp('Warning: high biot number. Assumption of uniform temperature in aluminium ...
     ...might be false')
end

%% Regression analysis

Puting them on vector form and removing the first value
Re_v=zeros((n-1)*mp,1);
Pr_v=zeros((n-1)*mp,1);
Nu_v=zeros((n-1)*mp,1);
for kk=1:mp
    Re_v(1+(n-1)*(kk-1):(n-1)*kk,1)=Re(2:n,kk);
    Pr_v(1+(n-1)*(kk-1):(n-1)*kk,1)=Pr(2:n,kk);
    Nu_v(1+(n-1)*(kk-1):(n-1)*kk,1)=Nu(2:n,kk);
end

Regression analysis
[beta,Sigma,E,CovB,logL] = mvregress([log(Re_v) log(Pr_v)],log(Nu_v));
```

```
[beta_tot,Sigma_tot,E_tot,CovB_tot,logL_tot] = mvregress([log(Re_tot(3:n)) log(...
 ...Pr_tot(3:n))],log(Nu_tot(3:n)));

%% Saving m.files for report
copyfile('fNu.m','Z:\Written_documents\Latex_Teplate_Main_Report\mfiles')
copyfile('post_process_transient.m','Z:\Written_documents\Latex_Teplate_Main_Report\...
 ...mfiles')
copyfile('post_process_SS.m','Z:\Written_documents\Latex_Teplate_Main_Report\mfiles'...
 ...)
copyfile('thickness.m','Z:\Written_documents\Latex_Teplate_Main_Report\mfiles')
copyfile('fPr.m','Z:\Written_documents\Latex_Teplate_Main_Report\mfiles')
copyfile('fh.m','Z:\Written_documents\Latex_Teplate_Main_Report\mfiles')
copyfile('fBi.m','Z:\Written_documents\Latex_Teplate_Main_Report\mfiles')



%% Acquire data

%Assumes that there is a thermocouple in the far end of the cylinder
%Assumes that oil initial temperature is 75 degress C
%Temperature is numbered from inlet to outlet, T1 being closest to the
%inlet
clear all; close all;clc

%Assumption : All power transfered to the heater reaches the cylinder and
%that we have an adiabatic surrounding

%--Surface Temperatures T_i----T_1----T_2----T_3----T_4----T_5----T_6---T_o
% and corresponding properties of Aluminum


T_s = [273.15+150  273.15+160  273.15+165  273.15+170  273.15+175  273.15+180  273...
 ....15+182;
    273.15+150  273.15+160  273.15+165  273.15+170  273.15+175  273.15+180  273.15...
     ...+182;
    273.15+150  273.15+160  273.15+165  273.15+170  273.15+175  273.15+180  273.15...
     ...+182;];

P = [2000 ;2000 ;2000];

[n,mp] = size(T_s); % Number of samples x numbers of measuring points
k_Al   =   0.000009708333333*T_s.^3 - 0.012937500000001*T_s.^2 + 5.604166666667190*...
 ...T_s - 616.000000000082000;
cp_Al  = 0.000005458333333*T_s.^3 - 0.006812500000006*T_s.^2 + 3.249166666669800*T_s...
 ... + 365.999999999537000;
rho_Al(1:n,1:mp) = 2770;

% Oil flow
for bgga = 1:n
    Q(bgga,1) = 2E-4 / 60; % dl^3/min * 60^-1 s/min * 1000^-1 dl^3/m^3
end
clear bgga;
%Q = [1 ; 2 ; ];

dt = 1; % This is the timestep for the sampeling speed
R = 53e-3;
```

```
r = 45.5e-3;
L_max = 245e-3;
%--------------------------------------------------------------------------
%MIGHT CHANGE DUE TO UNEVEN DISTRIBUTION
%L_p is the actual point of the themocouple while L_l is the length
%surrounding the thermocouple for energy balance calculation

L_p = zeros(1,mp);
for bgga = 1:mp
    L_p(bgga) = L_max/mp*bgga;
end

L_l = zeros(1,mp);
L_l(1,1) = L_p(1) + (L_p(2)-L_p(1))/2;
for bgga = 1:mp-2
    L_l(1+bgga) = (L_p(bgga+1)-L_p(bgga))/2 + (L_p(bgga+2)-L_p(bgga+1))/2;
end
L_l(1,mp)=L_max-L_p(mp)+(L_p(mp)-L_p(mp-1))/2;
%% Temperature of Oil and heat transfer coefficient
%T_i----T_1----T_2----T_3----T_4----T_5----T_6---T_o
T_o = zeros(n,2);
T_o(:,1) = 273.15 + 75;
T_o(:,2) = 273.15 + 75 + 7;

%Heat transfer is proportional to the temperature differance since all the
%other parameters are quite constant. Thereby we get that

%% Properties of Oil - DONE!!!
T_oe = T_o - 273.15;
[ cp_O,rho_O,mu_O,k_O ] = O_props( T_oe );

%% THICKNESS MODEL
% Enter mp as well
p = 20000; % number of element the length of the cylinder will be devided in
rps = 10000/60; % rotational speed of cylinder in RPS
mu_a = mean(mu_O,2);
rho_a = mean(rho_O,2);
ed = 0.002; % ---------- NEEDS ADJUSTMENT AFTER CYLINDER ROUGHNESS---------

[ Th_O , v ] = thickness(Q,p,L_p,L_max,r,rps,ed,rho_a,mu_a,mp,n);

% thick = thickness(V,T_a,rpm,p,n,mu_a,rho_a);
clear ('mu_a','rho_a');
%%

d_h = 2 * real(Th_O);

dEdt_tot_O = Q .* (cp_O(:,2).*rho_O(:,2).*T_o(:,2) - cp_O(:,1).*rho_O(:,1).*T_o(:,1)...
 ...);

l=zeros(n,mp);
for jj = 1:n
    l(jj,:)=L_l(1,:);
end
%--------------------------------------------------------------------------
```

```
h_O_tot = fh(dEdt_tot_O,(T_o(:,2)+T_o(:,1))/2,(T_s(:,1)+T_s(:,mp))/2,l(1,mp)*2*r*pi)...
 ...;

Nu_tot = fNu(h_O_tot,mean(d_h,2),mean(k_O(:,1:2),2));

Re_tot = fRe(mean(v,2),mean(d_h,2),mean(mu_O,2),mean(rho_O,2));

Pr_tot = fPr(mean(cp_O,2),mean(mu_O,2),mean(k_O,2));

Bi_tot = fBi(h_O_tot,mean(k_O,2),R-r);

if Bi_tot < 0.1

else
    disp('Warning: Low biot number. Assumption of uniform temperature in aluminium ...
     ...might be false')
end

%% Regression analysis
[beta_tot,Sigma_tot,E,CovB_tot,logL_tot] = mvregress([log(Re_tot) log(Pr_tot)],log(...
 ...Nu_tot));



%% Oil thickness calculation one dimentional
function [ Th_O, speed ] = thickness(Q,p,L,L_max,r,rps,ed,rho_a,mu_a,mp,n)
%Assumed that the temperature of the oil for each timestep is within an
%interval where the properties does not vary much.
%Also assumed that the thickness of the oil film differs to little to be
%noticed over the entire lenght. -CALCULATION NOT DESIGNED THAT WAY ANYMORE

y = zeros(n,p);
dh_cdx = zeros(n,p);
Fr = zeros(n,p);
V = zeros(n,p);
Th_O = zeros(n,mp);
speed = zeros(n,mp);
S = zeros(n,p);
f = zeros(n,p);
Re = zeros(n,p);

v = rps*2*r*pi;
g = -v^2/r;
h_c = real((Q.^2/(r*2*pi).^2/g).^(1/3));
y(:,p)= h_c;

%Calculating the oil thickness over the entire cylinder.

for m=1:p-1

V(:,p-m+1) = Q ./(r^2-(r-y(:,p-m+1)).^2) ./ pi;
D_h = 4 *(r.^2-(r-y(:,p-m+1)).^2) * pi / (2*pi*r);
Re(:,p-m+1) = fRe(V(:,p-m+1),D_h,mu_a,rho_a);

Fr(:,p-m+1) = V(:,p-m+1) ./ (g * h_c / 2).^0.5;
```

```
f(:,p-m+1) = moody(ed,Re(:,p-m+1));
S(:,p-m+1) = f(:,p-m+1) .* V(:,p-m+1).^2 ./ y(:,p-m+1) / 2 / g;
dh_cdx(:,p-m+1) = -S(:,p-m+1) ./ (1 - Fr(:,p-m+1).^2);
y(:,p-m)=y(:,p-m+1) + dh_cdx(:,p-m+1) * (L_max / p);

end

% Extract the points of interest
for pp=1:mp
Th_O(:,pp) = real(y(:,round((L(pp)./L_max.*p))));
speed(:,pp) = real(V(:,round((L(pp)./L(mp).*p))));
end

end


function [ h ] = fh(q,T_f,T_s,A)
%fPr Calculates Prandtl Number
%   Prandtl number is evaluated based on the parameters which are given as
%   input arguments.

h = q./(T_s-T_f)./A;
end


function [ Bi ] = fBi( h,k,thickness )
%UNTITLED Summary of this function goes here
%   Detailed explanation goes here

Bi=h.*thickness./k;

end
```

B.6 Rotor Thermal Model

```
%file main.m
close all
clear all
clc

%Cooling Performance
Oil_Temp=70;                                                %Oil Temperature oC
flow=4;                                                         %0.8 l/min oil ...
 ...flow=3, No oil flow=4
%Options
segments_map=[1,2,4];%Number of tangnential magnet segments
for k=1:length(segments_map)
    segments=segments_map(k);
    filename=strcat('losses_map_',num2str(segments),'.mat');
    load(filename);
    load heat_transf.mat
    % load operating_points.mat
```

```
    temp_map=zeros(length(losses_map(:,1)),length(losses_map(1,:)));
    for i=1:length(losses_map(:,1))
        for j=1:length(losses_map(1,:))
                Power=losses_map(i,j);
                h_oil=h_map(j,flow);
                temp_map(i,j)=FEMM( Power,h_oil,Oil_Temp)-273.14;
        end
    end
    %%%%%%%%%%%%%%%%%%%%%%%%Post Processing%%%%%%%%%%%%%%%%%%%%%%%%%%%%%%%%%%%%
    %%Plotting
    figure;
    contourf(speed_map(:,2:end),torque_map(:,2:end),temp_map(:,2:end),10)%,'ShowText...
     ...','on');
    hold on
    Max_Torque=70000./(2.*pi.*speed(2:end)./60);
    fill([speed(2:end),6000],[Max_Torque,500],'w')
    colorbar('location','eastoutside')
    filename=strcat('temperature_map_',num2str(segments),'.mat');
    save(filename,'temp_map','speed_map','torque_map','speed','Max_Torque');
    xlabel('Speed [rpm]');
    ylabel('Torque [Nm]');
    title_string=strcat('Permanent Magnet Temperature Map in ^oC, Segments=',num2str...
     ...(segments));
    title(title_string);


    %%Print the plots
    filename=strcat('C:\Users\Odyssefs\Desktop\Master Thesis\...
     ...Latex_Teplate_Main_Report\MatlabFigurer\Temperature_map_',num2str(segments),...
     ...'_',num2str(flow),'.eps');
    print('-depsc',filename)
end

%% Saving m.files for report
copyfile('main.m','C:\Users\Odyssefs\Desktop\Master Thesis\Latex_Teplate_Main_Report...
 ...\mfiles\Thermal')
copyfile('FEMM.m','C:\Users\Odyssefs\Desktop\Master Thesis\Latex_Teplate_Main_Report...
 ...\mfiles\Thermal')
copyfile('geometry.m','C:\Users\Odyssefs\Desktop\Master Thesis\...
 ...Latex_Teplate_Main_Report\mfiles\Thermal')
copyfile('heat_tran_coef_map.m','C:\Users\Odyssefs\Desktop\Master Thesis\...
 ...Latex_Teplate_Main_Report\mfiles\Thermal')
copyfile('Losses_Map.m','C:\Users\Odyssefs\Desktop\Master Thesis\...
 ...Latex_Teplate_Main_Report\mfiles\Thermal')
copyfile('Operating_Points.m','C:\Users\Odyssefs\Desktop\Master Thesis\...
 ...Latex_Teplate_Main_Report\mfiles\Thermal')



%file FEMM.m
function [T_magn] = FEMM( Power,h_oil,Oil_Temp)
%FEMM Calculates the temperature of the magnet in the rotor, by calling
%FEMM and running the simulation.
%   Detailed explanation goes here
%
%Reading Geometry Variables
geometry;
```

```
%Deviding the losses for the specific segment
Power=Power/(16*2.79872e-5);                                    %convert losses to watts...
 .../m3, 16 is pole pares, the starnge number is volume.

%Initializing FEMM
addpath('C:\femm42\mfiles');
openfemm;
newdocument(2)      %Creating New Document

%%%%%%%%%%%%%%%%%%%%%%%%Defining Problem%%%%%%%%%%%%%%%%%%%%%%%%%%%%%%%%%%%%
hi_probdef('millimeters','planar',1E-08,rotor_length,20);
prob_name='rotor_thermal.feh';
hi_saveas(prob_name);               %%%%%%Saving the Problem
hi_setfocus(prob_name)  ;           %%%%%%Focussing on the Problem
hideconsole();
hi_close();

opendocument(prob_name);             %%%%%%Opening the saved file
hi_setfocus(prob_name);             %%%%%%Setting the focus on the problem


% %Geometry
%%%%%%%%%%%%%%%%%%%%%%Drawing Geometry%%%%%%%%%%%%%%%%%%%%%%%%%%%%%%%%%%%%%%
%Drawing Steel Rotor
hi_addnode(sind(symetry_angle)*rotor_inner_r,cosd(symetry_angle)*rotor_inner_r);
hi_addnode(sind(symetry_angle)*rotor_outer_r,cosd(symetry_angle)*rotor_outer_r);
hi_addnode(0,rotor_inner_r);
hi_addnode(0,rotor_outer_r);
 hi_addarc(sind(symetry_angle)*rotor_inner_r,cosd(symetry_angle)*rotor_inner_r,0,...
  ...rotor_inner_r,symetry_angle,1);
 hi_addarc(sind(symetry_angle)*rotor_outer_r,cosd(symetry_angle)*rotor_outer_r,0,...
  ...rotor_outer_r,symetry_angle,1);
 hi_addsegment(0,rotor_inner_r,0,rotor_outer_r);
  hi_addsegment(sind(symetry_angle)*rotor_inner_r,cosd(symetry_angle)*rotor_inner_r,...
   ...sind(symetry_angle)*rotor_outer_r,cosd(symetry_angle)*rotor_outer_r);
%Add Block Labels
 hi_seteditmode('blocks');
hi_addblocklabel(sind(symetry_angle/2)*(rotor_inner_r+(rotor_outer_r-rotor_inner_r)...
 .../2),cosd(symetry_angle/2)*(rotor_inner_r+(rotor_outer_r-rotor_inner_r)/2));


  %Drawing Magnets

hi_addnode(sind((symetry_angle-magn_angle)/2)*magn_outer_r,cosd((symetry_angle-...
 ...magn_angle)/2)*magn_outer_r);
hi_addnode(sind((symetry_angle-magn_angle)/2)*magn_inner_r,cosd((symetry_angle-...
 ...magn_angle)/2)*magn_inner_r);
hi_addnode(sind(symetry_angle-(symetry_angle-magn_angle)/2)*magn_outer_r,cosd(...
 ...symetry_angle-(symetry_angle-magn_angle)/2)*magn_outer_r);
hi_addnode(sind(symetry_angle-(symetry_angle-magn_angle)/2)*magn_inner_r,cosd(...
 ...symetry_angle-(symetry_angle-magn_angle)/2)*magn_inner_r);
hi_addarc(sind(symetry_angle-(symetry_angle-magn_angle)/2)*magn_outer_r,cosd(...
 ...symetry_angle-(symetry_angle-magn_angle)/2)*magn_outer_r,sind((symetry_angle-...
 ...magn_angle)/2)*magn_outer_r,cosd((symetry_angle-magn_angle)/2)*magn_outer_r,...
 ...magn_angle,1);
```

```
hi_addsegment(sind((symetry_angle-magn_angle)/2)*magn_outer_r,cosd((symetry_angle-...
 ...magn_angle)/2)*magn_outer_r,sind((symetry_angle-magn_angle)/2)*magn_inner_r,cosd...
 ...((symetry_angle-magn_angle)/2)*magn_inner_r);
hi_addsegment(sind(symetry_angle-(symetry_angle-magn_angle)/2)*magn_outer_r,cosd(...
 ...symetry_angle-(symetry_angle-magn_angle)/2)*magn_outer_r,sind(symetry_angle-(...
 ...symetry_angle-magn_angle)/2)*magn_inner_r,cosd(symetry_angle-(symetry_angle-...
 ...magn_angle)/2)*magn_inner_r);
hi_addsegment(sind((symetry_angle-magn_angle)/2)*magn_inner_r,cosd((symetry_angle-...
 ...magn_angle)/2)*magn_inner_r,sind(symetry_angle-(symetry_angle-magn_angle)/2)*...
 ...magn_inner_r,cosd(symetry_angle-(symetry_angle-magn_angle)/2)*magn_inner_r);

% %Add Block Labels
 hi_seteditmode('blocks');
hi_addblocklabel(sind(symetry_angle/2)*(rotor_outer_r-1),cosd(symetry_angle/2)*(...
 ...rotor_outer_r-1));
 hi_addblocklabel(sind(symetry_angle/2)*(rotor_outer_r+1),cosd(symetry_angle/2)*(...
  ...rotor_outer_r+1));

%Draw Air Domain

hi_addnode(0,0);
hi_addnode(0,stator_r);
hi_addnode(sind(symetry_angle)*stator_r,cosd(symetry_angle)*stator_r);
hi_addsegment(0,0,0,rotor_inner_r);
hi_addsegment(0,0,sind(symetry_angle)*rotor_inner_r,cosd(symetry_angle)*...
 ...rotor_inner_r);
hi_addsegment(0,stator_r,0,rotor_outer_r);
hi_addsegment(sind(symetry_angle)*stator_r,cosd(symetry_angle)*stator_r,sind(...
 ...symetry_angle)*rotor_outer_r,cosd(symetry_angle)*rotor_outer_r);
hi_addarc(sind(symetry_angle)*stator_r,cosd(symetry_angle)*stator_r,0,stator_r,...
 ...symetry_angle,1);
%add block labels
hi_seteditmode('blocks');
 hi_addblocklabel(sind(symetry_angle/2)*(rotor_inner_r/2),cosd(symetry_angle/2)*(...
  ...rotor_inner_r/2));
 hi_addblocklabel(sind(symetry_angle/2)*(magn_outer_r+(stator_r-magn_outer_r)/2),...
  ...cosd(symetry_angle/2)*(magn_outer_r+(stator_r-magn_outer_r)/2));


%%%%%%%%%%%%%%%%%%Defining Materials%%%%%%%%%%%%%%%%%%%%%%%%%%%%%%%%%%%%%%%%
%Add Materials from Model Library
hi_addmaterial('N35EH',magn_thermal_cond,magn_thermal_cond,Power,0);
hi_addmaterial('M270-35A',steel_thermal_cond,steel_thermal_cond,0,0);
hi_getmaterial('Air');



% %Assigning Materials to geometry
%Steel Domain
hi_seteditmode('blocks');
hi_clearselected();
hi_selectlabel(sind(symetry_angle/2)*(rotor_inner_r+(rotor_outer_r-rotor_inner_r)/2)...
 ...,cosd(symetry_angle/2)*(rotor_inner_r+(rotor_outer_r-rotor_inner_r)/2));
hi_setblockprop('M270-35A',1,1,0);

%Magnet Domain
```

```
hi_seteditmode('blocks');
hi_clearselected();
hi_selectlabel(sind(symetry_angle/2)*(rotor_outer_r-1),cosd(symetry_angle/2)*(...
 ...rotor_outer_r-1));
hi_selectlabel(sind(symetry_angle/2)*(rotor_outer_r+1),cosd(symetry_angle/2)*(...
 ...rotor_outer_r+1));
hi_setblockprop('N35EH',1,1,0);

%Air Domain
hi_seteditmode('blocks');
hi_clearselected();
hi_selectlabel(sind(symetry_angle/2)*(rotor_inner_r/2),cosd(symetry_angle/2)*(...
 ...rotor_inner_r/2));
hi_setblockprop('Air',1,1,0);
hi_clearselected();
hi_selectlabel(sind(symetry_angle/2)*(magn_outer_r+(stator_r-magn_outer_r)/2),cosd(...
 ...symetry_angle/2)*(magn_outer_r+(stator_r-magn_outer_r)/2));
hi_setblockprop('Air',0,0.2,0);



hi_clearselected();


%%%%%%%%%%%%%%%%%%%%%%%%%%%%%Define Boundary Conditions
%Defining Boundaries
hi_addboundprop('Oil_Convection',2,0,0,Oil_Temp+273.14,h_oil,0);
hi_addboundprop('Stator',0,stator_T+273.14,0,0,0);
%Assigning Boundaries
%Oil Spray
hi_clearselected();
 hi_seteditmode('arcsegments');
 hi_selectarcsegment(0,rotor_inner_r);
 hi_setarcsegmentprop(1,'Oil_Convection',0,0,'<None>');

 %Stator Temp
 hi_clearselected();
  hi_seteditmode('arcsegments');
 hi_selectarcsegment(0,stator_r);
 hi_setarcsegmentprop(1,'Stator',0,0,'<None>');

  hi_clearselected();



%Create Mesh and Solve
%Zoom
hi_zoomnatural();
%mesh
hi_createmesh();
%Runing Solver
hi_analyze();


% % Getting Solution
hi_loadsolution();
```

```
temp=ho_getpointvalues(sind(symetry_angle/2)*(magn_outer_r-1),cosd(symetry_angle/2)...
 ...*(magn_outer_r-1));
T_magn=temp(1);
end


%file geometry.m
%%%%%%%%%%%%%%%%%%%%%%%%Defining Parameters%%%%%%%%%%%%%%%%%%%%%%%%%%%%%%%%%%
%Dimensions
%Everything is in [mm]!!!
stator_r=68;                                                    %Stator radius
rotor_inner_r=52.5;                                            %Rotor Inner ...
 ...Diameter
rotor_outer_r=(61+2.22);                                         %Rotor Outer ...
 ...Diameter
magn_outer_r=(67.5);                                           %Magnet ...
 ...Thickness
magn_inner_r=61;                                          %Magnet Deepness inside ...
 ...the steel rotor
magn_width=21.1;                                               %Magnet Width
magn_angle=magn_width*360/(2*pi*magn_outer_r);
rotor_length=200;
symetry_angle=20;                                              %Symetry Angle in ...
 ...Degrees
%Thermal Conductivities in [Watts/(mC)]
magn_thermal_cond=6;
steel_thermal_cond=10;
%Stator Temperature
stator_T=100;                                                   %Stator ...
 ...Temperature


%file heat_transf_coef_map.m
%here we create the heat tranfer coefficient map
Speed=500:500:6000;
Flow=[0.1,0.3,0.8];
h_map=zeros(length(Speed),length(Flow));

h_map=[0,150,150,10;
                268,679,578,10;
                294, 957,815,10;
                0,0,996,10;
                0,0,1148,10;
                0,0,1281,10;
                0,0,1401,10;
                0,0,1512,10;
                0,0,1614,10;
                0,0,1711,10;
                0,0,1802,10;
                0,0,1888,10;
                0,0,1971,10];

save('heat_transf.mat','h_map');
```

```
%file Losses_Map.m
%in this file the losses map is created by loading the opeating points and
%the data from the csv files that comes out of the simulation
clear all
clc
close all
%set number or segments you want the map 1,2,4
segments=1;

%load opeating points
load operating_points;
n=length(operating_points);
%n=29;
%Load the losses for every operating point
magn_losses=zeros(n,2);
for i=1:n
    Speed=operating_points(i,1);
    Current=operating_points(i,2);
    Angle=operating_points(i,3);
    filename=strcat('data_',num2str(segments),'segm','\p_loss_',num2str(Speed),'_',...
     ...num2str(Current),'_',num2str(Angle),'deg_data_table.csv');
   loss=csvimport(filename, 'columns',[2],'noHeader' , true, 'delimiter', ',');
    torque=csvimport(filename, 'columns', [3],'noHeader', true, 'delimiter', ',');
    magn_losses(i,1)=round(str2double(torque(2)));
    magn_losses(i,2)=round(str2double(loss(2)));
end

loss_map=[operating_points(1:n,1), magn_losses(:,1),magn_losses(:,2)];

for i=1:length(loss_map(:,2))
loss_map(i,2)=round2(loss_map(i,2),25);
end
save('losses_map.mat','magn_losses');

torque=0:25:500;
speed=0:500:6000;
[speed_map,torque_map]=meshgrid(speed,torque);
losses_map=zeros(length(torque),length(speed));
for i=1:length(losses_map(1,:))
    for j=1:length(losses_map(:,1))
        index=find(and(loss_map(:,1)==speed_map(j,i),loss_map(:,2)==torque_map(j,i))...
         ...);
        if not(isempty(index))
            for k=1:length(index)
            losses_map(j,i)=loss_map(index(k),3);
            end
         end
    end
end

% Trying to smooth the data
for i=2:length(losses_map(1,:))
    for j=2:length(losses_map(:,1))-1
        if and( losses_map(j,i)==0,speed_map(j,i)*2*pi/60*torque_map(j,i)<=70000)
            cor_index=find(losses_map((j):end,i)~=0);
            for k=1:1:min(cor_index)-1
```

```
            losses_map(k+j-1,i)=losses_map(j-1,i)+(k)*(losses_map(j+min(cor_index)...
             ...-1,i)-losses_map(j-1,i))/(min(cor_index));
            end
% %             losses_map(j,i)=(losses_map(j-1,i)+losses_map(j+1,i))/2;
        end
    end
end

contourf(speed_map,torque_map,losses_map,10)%,'ShowText','on');
hold on
Max_Torque=70000./(2.*pi.*speed(2:end)./60);
%plot(speed,Torque)
fill([speed(2:end),6000],[Max_Torque,500],'w')
% ylim([0,500]);
filename=strcat('losses_map_',num2str(segments),'.mat');
save(filename,'losses_map','speed_map','torque_map','speed','Max_Torque');
colorbar('location','eastoutside')
xlabel('Speed [rpm]');
ylabel('Torque [Nm]');
title_string=strcat('Permanent Magnet Losses Map in Watts, Segments=',num2str(...
 ...segments));
title(title_string);

%%Print the plots
filename=strcat('C:\Users\Odyssefs\Desktop\Master Thesis\Latex_Teplate_Main_Report\...
 ...MatlabFigurer\Losses_map_',num2str(segments),'.eps');
print('-depsc',filename)



%Operating Points.m
%In this m-file the operating points map is created

%   Speed,    Current,  Angle
operating_points=...
      [500,      50,   90;
        500,     100,   90;
        500,   150,    90 ;
        500,   200,    90 ;
        500,   250,    90 ;
        500,   300,    90 ;
       1000,     50,    90 ;
       1000,   100,    90 ;
       1000,   150,    90 ;
       1000,   200,    90 ;
       1000,   250,    90 ;
       1000,   300,    90 ;
       1500,     50,    90 ;
       1500,   100,    90 ;
       1500,   150,    90 ;
       1500,   200,    90 ;
       1500,   250,    90 ;
       1500,   300,    90 ;
       2000,     50,   90  ;
       2000,   100,    90 ;
       2000,   150,    90 ;
       2000,   170,  110 ;
```

```
 2500,     50,    90 ;
 2500,   100,    90 ;
 2500,   150,   120 ;
 3000,     50,    90 ;
 3000,   100,   120 ;
 3000,   150,   130 ;
 3500,     50,   120 ;
 3500,   100,   120 ;
 3500,   150,   135 ;
 4000,     50,   130 ;
 4000,     65,   130 ;
4000,     80,   130 ;
 4000,   100,   135 ;
 4000,   120,   140 ;
 4500,     50,   140 ;
 4500,     65,   140 ;
 4500,     80,   140 ;
 4500,   100,   140 ;
 4500,   120,   140 ;
 5000,     50,   150 ;
 5000,     65,   145 ;
 5000,     80,   145 ;
 5000,   100,   140 ;
 5000,   120,   140 ;
 5500,     50,   165 ;
 5500,     65,   160 ;
 5500,     80,   155 ;
  5500,     90,   145 ;
 5500,   100,   140 ;
 5500,   110,   140 ;
 6000,     75,   170 ;
 6000,     80,   165 ;
 6000,     90,   160 ;
 6000,   100,   160 ;
 6000,   120,   150 ];

save('operating_points.mat','operating_points');
```